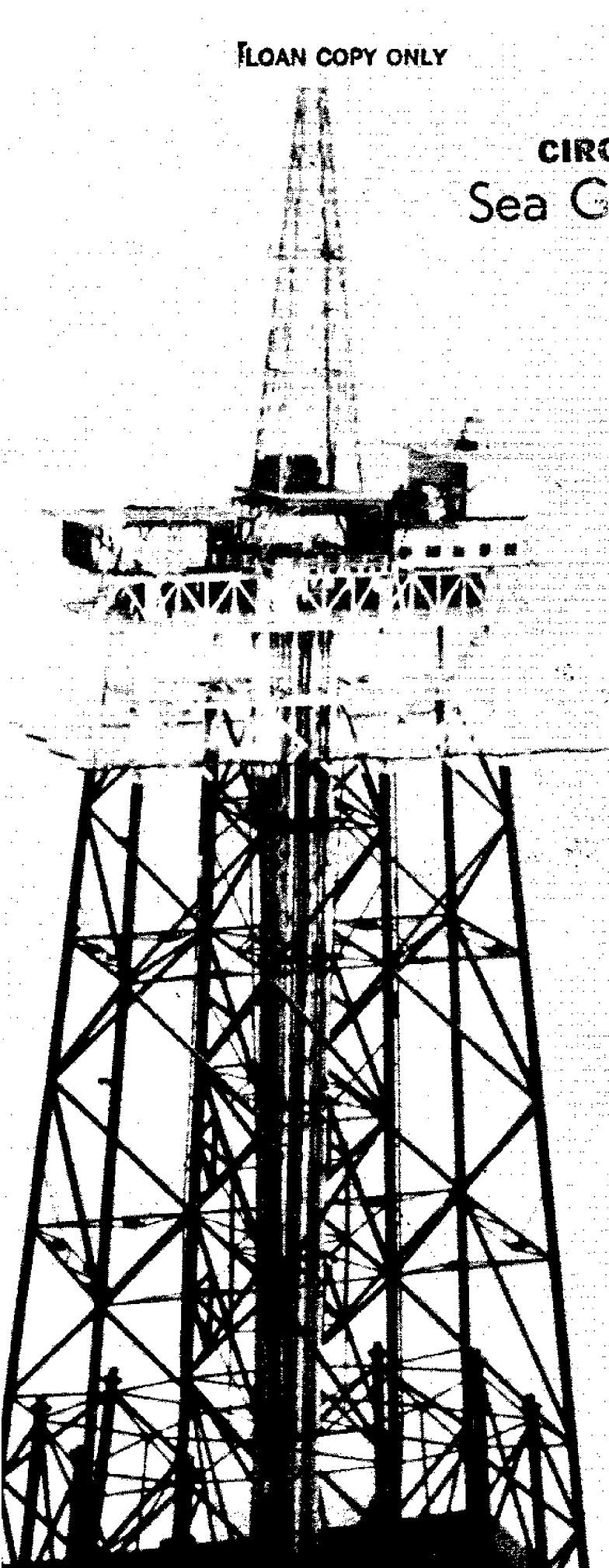


**CIRCULATING COPY**  
**Sea Grant Depository**

**Random response  
of offshore structures  
to wave  
and current forces**



**NATIONAL SEA GRANT DEPOSITORY  
PELL LIBRARY BUILDING  
URI, NARRAGANSETT BAY CAMPUS  
NARRAGANSETT, RI 02882**

**S. C. Wu  
C. C. Tung**

**A University of North Carolina  
Sea Grant Program Publication  
UNC-SG-75-22**

**September, 1975**

RANDOM RESPONSE OF OFFSHORE  
STRUCTURES TO WAVE AND CURRENT FORCES

Song C. Wu

LOAN COPY ONLY

and

Chi C. Tung

Department of Civil Engineering  
North Carolina State University  
Raleigh, N. C. 27607

This work is the result of research partially sponsored by Office of Sea Grant, NOAA, U. S. Dept. of Commerce, under Grant #04-3-158-40, the State of North Carolina, Department of Administration, North Carolina State University Center for Coastal and Marine Studies and the Department of Civil Engineering. The U. S. Government is authorized to produce and distribute reprints for governmental purposes notwithstanding any copyright that may appear hereon.

NATIONAL SEA GRANT DEPOSITORY  
PELL LIBRARY BUILDING  
URI, NARRAGANSETT BAY CAMPUS  
NARRAGANSETT, RI 02882

SEA GRANT PUBLICATION UNC-SG-75-22

September, 1975

University of North Carolina, Sea Grant Program, 1235 Burlington  
Laboratories, North Carolina State University, Raleigh, North  
Carolina 27607

## SUMMARY

Dynamic responses of offshore structures to random waves and steady current are examined. Hydrodynamic forces acting on the structures are computed according to Morison's formula. Small amplitude wave theory is invoked and the structures are assumed to respond in the linear range.

The structures are idealized as lumped mass systems for dynamic analysis purposes. Effects of fluid-structure interactions are included and the nonlinear stochastic differential equations governing structural responses are solved by the statistical equivalent linearization techniques together with the method of normal mode superposition. The phenomenon of wave-current interactions is known to change wave characteristics; its effects on structural responses are also considered.

The structural response quantities examined are the displacement, shear and bending moment. The statistic sought is the peak response which is the quantity directly used in design considerations.

Numerical results are obtained for four offshore towers, ranging in heights from 475 feet to 1075 feet, for various wave and current conditions. Results are presented graphically. It is shown that structural responses increase with increase in current speed but the effects of wave-current interactions are important only for tall slender structures. Also, the effects of current on structural response diminishes with increase in the strength of the waves.

## TABLE OF CONTENTS

	Page
LIST OF TABLES . . . . .	ii
LIST OF FIGURES . . . . .	iii
1. INTRODUCTION . . . . .	1
2. WAVES AND CURRENTS . . . . .	5
2.1 Single Wave . . . . .	5
2.2 Random Waves . . . . .	10
2.3 Currents and Wave-Current Interactions . . . . .	20
3. DYNAMIC RESPONSE OF STRUCTURES . . . . .	26
3.1 Wave and Current Forces . . . . .	26
3.2 Equations of Motion . . . . .	29
3.3 Equivalent Linearization Technique . . . . .	32
3.4 Transformation of Coordinates . . . . .	38
3.5 Normal Mode Superposition . . . . .	41
3.6 Statistics of the Linearized and Transformed System . . . . .	46
3.7 Parameters for Optimizing Damping Coefficients . . . . .	52
3.8 Peak Value Statistics . . . . .	57
4. CASE STUDIES . . . . .	61
4.1 Idealized Structural Properties and Force Parameters . . . . .	61
4.2 Results and Discussions of Computer Solution . . . . .	64
5. CONCLUSIONS AND RECOMMENDATIONS . . . . .	97
6. LIST OF REFERENCES . . . . .	98
7. APPENDICES . . . . .	102
7.1 Structural Damping Matrix . . . . .	102
7.2 Computation of Shear and Bending Moment . . . . .	106
7.3 Notation . . . . .	110

## LIST OF TABLES

	Page
4.1(a) Structural properties for Tower 1 . . . . .	65
(b) Flexibility matrix for Tower 1 . . . . .	65
4.2(a) Structural properties for Tower 2 . . . . .	66
(b) Flexibility matrix for Tower 2 . . . . .	66
4.3(a) Structural properties for Tower 3 . . . . .	67
(b) Flexibility matrix for Tower 3 . . . . .	69
4.4(a) Structural properties for Tower 4 . . . . .	68
(b) Flexibility matrix for Tower 4 . . . . .	68
4.5 Transformed structural damping matrix - Tower 1 . . . . .	69
4.6 Transformed structural damping matrix - Tower 2 . . . . .	70
4.7 Transformed structural damping matrix - Tower 3 . . . . .	71
4.8 Transformed structural damping matrix - Tower 4 . . . . .	72
4.9 Modal frequencies (rad/sec) for Towers 1, 2, 3, and 4 . .	74
4.10 Comparison of fundamental frequencies (rad/sec) for towers vibrating in water and in air . . . . .	74
4.11 Modal matrix - Tower 1 . . . . .	75
4.12 Modal matrix - Tower 2 . . . . .	75
4.13 Modal matrix - Tower 3 . . . . .	76
4.14 Modal matrix - Tower 4 . . . . .	76
4.15 Range of numerical integration for 50, 75, and 100 ft/sec wind . . . . .	78
4.16(a) Comparison of standard deviations of displacement with various modes included - Tower 1, W=50 ft/sec, $V_c = 0$ . . . . .	79
(b) Comparison of standard deviations of bending moment with various modes included - Tower 1, W=50 ft/sec, $V_c = 0$ . . . . .	79
(c) Comparison of standard deviations of shear with various modes included - Tower 1, W=50 ft/sec, $V_c = 0$ . . . . .	80

## LIST OF FIGURES

	Page
2.1 Definition sketch of wave system . . . . .	6
2.2 The influence of currents on dispersion relationship between wave number and wave frequency . . . . .	22
2.3 Frequency spectra of wave for current velocities $V_c = -4, 0, \text{ and } +4 \text{ ft/sec; } 50 \text{ ft/sec wind}$ . . . . .	24
3.1 Horizontal wave forces on a vertical circular cylinder . . .	27
3.2 Idealized tower . . . . .	30
4.1 Idealized tower used in Case Studies . . . . .	62
4.2 Peak displacements: current velocities $V_c = 0, 2, \text{ and } 4 \text{ ft/sec; } 50 \text{ ft/sec wind}$	
(a) Tower 1 . . . . .	83
(b) Tower 2 . . . . .	83
(c) Tower 3 . . . . .	84
(d) Tower 4 . . . . .	84
4.3 Peak shears: current velocities $V_c = 0, 2, \text{ and } 4 \text{ ft/sec; } 50 \text{ ft/sec wind}$	
(a) Tower 1 . . . . .	85
(b) Tower 2 . . . . .	85
(c) Tower 3 . . . . .	86
(d) Tower 4 . . . . .	86
4.4 Peak moments: current velocities $V_c = 0, 2, \text{ and } 4 \text{ ft/sec; } 50 \text{ ft/sec wind}$	
(a) Tower 1 . . . . .	87
(b) Tower 2 . . . . .	87
(c) Tower 3 . . . . .	88
(d) Tower 4 . . . . .	88
4.5 Comparison of peak deck displacements of Towers 1, 2, 3, and 4 with and without wave-current interactions considered; 50 ft/sec wind . . . . .	89
4.6 Comparison of peak base shears of Towers 1, 2, 3, and 4 with and without wave-current interactions considered; 50 ft/sec wind . . . . .	90*
4.7 Comparison of peak base moments of Towers 1, 2, 3, and 4 with and without wave-current interactions considered; 50 ft/sec wind . . . . .	91

## LIST OF FIGURES (continued)

	Page
4.8 Comparison of the ratios of peak deck displacements under wind speeds $W=50, 75,$ and $100$ ft/sec; Tower 1 . . . . .	93
4.9 Comparison of the ratios of peak base shears under wind speeds $W=50, 75,$ and $100$ ft/sec; Tower 1 . . . . .	94
4.10 Comparison of the ratios of peak base moments under wind speeds $W=50, 75,$ and $100$ ft/sec; Tower 1 . . . . .	95
7.1 Total transverse forces on an independent coordinate system . . . . .	107

## 1. INTRODUCTION

With the advent of increased activities in the ocean in recent years, more and more structures are being designed and constructed in the ocean in deeper waters. Among the various types of deep water structures, the fixed-bottom platform appears to have been widely favored by engineers. Composed of slender members, these structures are flexible and are susceptible to dynamic excitation.

The design of offshore structures requires the consideration of various forces the structures must resist. Among the forces, those due to wind, wave, current, and strong motion earthquake are of primary importance. The dynamic behavior of fixed-bottom platforms to wave action only has been studied by Harleman, Nolan and Honsinger (1963), Gaither and Billington (1964), Billington, Gaither, and Ebner (1966) for the case of deterministic waves, and by Nath and Harleman (1969), Foster (1967), Malhotra and Penzien (1970) for the case of random wind waves. The effects of earthquake on such structures have also been considered by Penzien, Kaul and Berge (1972).

In all the work cited above, wave forces exerted on members of the structure are computed according to Morison's formula. That is, forces are considered to consist of two parts: the drag force, proportional to the square of fluid particle velocity, and the inertia force, proportional to fluid particle acceleration.

In the work of Foster (1967), Malhotra and Penzien (1970), and Penzien, Kaul and Berge (1972), it was pointed out that on flexible structures the velocity and acceleration of the structure may be of the same order of magnitude as the fluid particle velocity and acceleration.



Thus, in calculating the forces from Morison's formula, the relative velocity and acceleration of the fluid particle with respect to the structure should be used. It was found that the effects of the dynamic interaction between structure and surrounding fluid and the nonlinear drag forces had considerable influence on structural response.

When current is present, fluid forces may still be evaluated according to Morison's formula (Myers, 1969). This is achieved by considering fluid particle velocity as the vector sum of current velocity and wave induced fluid particle velocity. Since the drag force is nonlinear, it cannot be regarded as simple superposition of current and wave drag forces. Consequently, dynamic response of offshore structures to combined actions of waves and current cannot be derived from those due to waves and current separately and a new formulation and derivation is required.

In considering the effects of current and waves on structural response, the phenomenon of wave-current interactions should also be considered. It is well known that when a wave encounters an externally generated current, wave characteristics undergo change. If the current is in the direction of the wave, wave amplitude decreases and wave length increases (Longuet-Higgins and Stewart, 1961); if the current opposes the wave, then the situation is reversed. In a random wave field, component waves are affected by current in a similar manner resulting in the modification of the wave spectrum (Huang et al., 1972). Subsequent to these studies, investigation was carried out to examine the effects of wave-current interactions on wave field kinematics and wave force (Tung and Huang, 1973, 1974). Results indicated that drastic changes

indeed took place in the quantities examined. Therefore, the influence of wave-current interactions on the dynamic response of the structure is also included in this study.

In carrying out the investigation of the dynamic response of offshore structures to wave and current forces and the effects of wave-current interactions on structural response, the following usual assumptions are made regarding fluid motion:

1. The fluid motion is governed by small amplitude wave theory.
2. The random gravity waves are assumed to be one-dimensional and the free surface elevation is Gaussian, stationary in time, and homogeneous in space.
3. The current is assumed to be in the direction of (or opposite to) wave propagation.
4. The current is assumed to be steady in time, non-uniform in the horizontal plane, and uniformly distributed along the depth of water.

Four offshore towers are analyzed to examine the effects of current and waves on structure response. The structural characteristics of these four towers are the same of those used by Penzien, Kaul, and Berge (1972).

The structures are idealized as lumped mass systems. Due to the nonlinear random drag force and the interactions between structure and fluid motion, the motion of structure is governed by a set of nonlinear stochastic differential equations. Solutions of nonlinear stochastic differential equations are difficult to achieve. For the set of equations considered, without the influence of current, the approximate method of statistical equivalent linearization has been employed by Malhotra and Penzien (1970). This method, with some modifications to incorporate the presence of current, will be used in this study.

For easy reference purpose, in Chapter 2, the analytical development of small amplitude wave theory, descriptions of the random sea, and the influence of wave-current interactions on wave characteristics, all relevant to subsequent determination of statistical response of offshore towers, are briefly summarized.

In Chapter 3, the differential equations governing the motion of the structure are established. The response statistics are derived by the method of equivalent linearization technique.

In Chapter 4, numerical results of the response of four structures under different wind and current conditions are computed and discussed.

In Chapter 5, conclusions and recommendations based on this study are presented.

## 2. WAVES AND CURRENTS

### 2.1 Single Wave

In this section, the theory of small amplitude single wave, upon which subsequent development of random wave theory is based, is first presented.

Consider the rectangular coordinate system shown in Figure 2.1 with the x-axis in the horizontal plane, the y-axis vertically upwards, and the origin at the mean water level. Let a single wave be propagating in the direction of the x-axis. The instantaneous vertical displacement of the free surface is specified by  $y = \eta(x, t)$ .

To determine the fluid motion in the wave field, for a first approximation, as has been commonly done (Ippen, 1966), let the fluid be incompressible, inviscid, and irrotational.

Denote  $\dot{V}_x(x, y, t)$  and  $\dot{V}_y(x, y, t)$  the fluid particle velocities in the x and y directions respectively. Irrotational flow condition requires that

$$\frac{\partial \dot{V}_x}{\partial y} = \frac{\partial \dot{V}_y}{\partial x}$$

in which the arguments x, y, and t of  $\dot{V}_x(x, y, t)$  and  $\dot{V}_y(x, y, t)$  are dropped for convenience. If the flow is irrotational, then there exists a velocity potential  $\phi(x, y, t)$  which can be defined so that

$$\left. \begin{aligned} \dot{V}_x &= \frac{\partial \phi}{\partial x} \\ \dot{V}_y &= \frac{\partial \phi}{\partial y} \end{aligned} \right\} \quad (2.1)$$

in which the arguments of  $\phi(x, y, t)$  are again dropped for convenience.

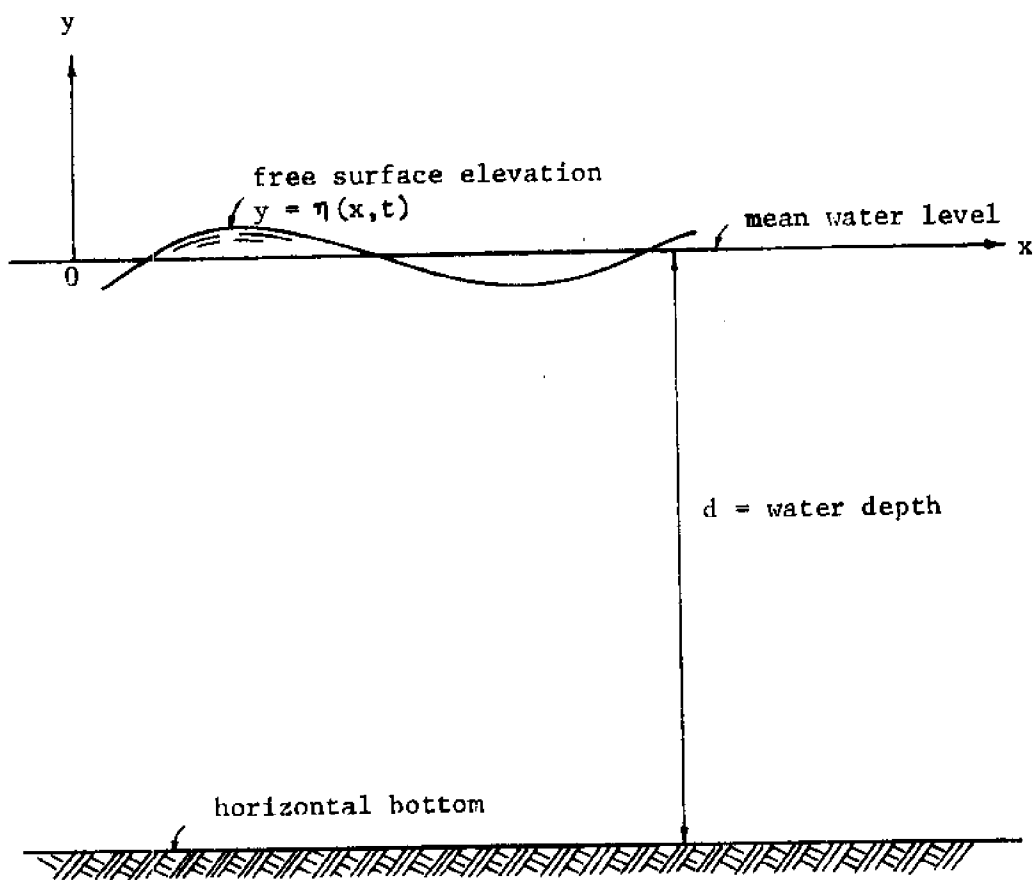


Figure 2.1. Definition sketch of wave system

Since the fluid is assumed to be incompressible, the continuity equation is

$$\frac{\partial \dot{V}_x}{\partial x} + \frac{\partial \dot{V}_y}{\partial y} = 0.$$

Combining the continuity equation with Equation (2.1), the field of flow can be represented by the Laplace's equation

$$\frac{\partial^2 \phi}{\partial x^2} + \frac{\partial^2 \phi}{\partial y^2} = 0. \quad (2.2)$$

The solution of the Laplace's equation must satisfy the boundary conditions at the free surface and at the bottom of the fluid. The boundary condition at the horizontal, fixed, and impermeable bottom requires that the normal velocity component be zero. That is

$$\dot{V}_y = 0 \quad \text{at } y = -d \quad (2.3)$$

in which  $d$  is water depth as shown in Figure 2.1.

If the position of the free surface is specified by  $y = \eta(x, t)$  at all times, then the material derivative (Ippen, 1966) of the position of a particle is its velocity. Thus a kinematic boundary condition is provided on the surface as

$$\begin{aligned} (\dot{V}_y)_\eta &= \frac{d\eta}{dt} \\ &= \frac{\partial \eta}{\partial t} + (\dot{V}_x)_\eta \frac{\partial \eta}{\partial x} \end{aligned}$$

where the subscript  $\eta$  indicates that the quantity is to be evaluated at the free surface. The arguments of  $\eta(x, t)$  are ignored here. In

irrotational motion, this kinematic boundary condition becomes

$$\left(\frac{\partial \phi}{\partial y}\right)_\eta = \frac{\partial \eta}{\partial t} + \left(\frac{\partial \phi}{\partial x}\right)_\eta \frac{\partial \eta}{\partial x}. \quad (2.4)$$

The dynamic boundary condition to be satisfied on the surface can be obtained by applying the equation of motion in the vertical direction. That is, by applying Bernoulli's equation for inviscid flow at  $y = \eta$ ,

$$\left(\frac{\partial \phi}{\partial t}\right)_\eta + g\eta + \frac{1}{2} \left[ \left(\frac{\partial \phi}{\partial x}\right)_\eta^2 + \left(\frac{\partial \phi}{\partial y}\right)_\eta^2 \right] = 0 \quad (2.5)$$

in which  $g$  is gravitational acceleration and the pressure is taken to be zero at the free surface.

If it is assumed that displacement of the free surface is small, then the nonlinear terms in Equations (2.4) and (2.5), being of the second order in comparison with the other terms, can be neglected. Furthermore, since it is assumed that  $\eta$  is very small, the boundary conditions specified at the free surface  $y = \eta$  can be considered to occur approximately at  $y = 0$ . With these approximations, Equations (2.4) and (2.5) become

$$\frac{\partial \phi}{\partial y} = \frac{\partial \eta}{\partial t} \quad \text{at } y = 0 \quad (2.6)$$

$$\frac{\partial \phi}{\partial t} + g\eta = 0 \quad \text{at } y = 0. \quad (2.7)$$

The fluid motion is specified by the Laplace's equation Equation (2.2) and the boundary conditions Equations (2.6) and (2.7). By adopting the following symbols:

$a$  = wave amplitude,

$L$  = wave length, distance between any two corresponding positions on successive waves,

$T$  = wave period, time required for motion to reoccur at a given fixed point,

$\kappa$  = wave number, defined to be equal to  $2\pi/L$ ,

and  $\omega$  = wave frequency, defined to be equal to  $2\pi/T$ ;

it may be verified that if the surface displacement is

$$\eta(x, t) = a \cos (\kappa x - \omega t), \quad (2.8)$$

then the associated velocity potential is

$$\phi(x, y, t) = \frac{a\omega}{\kappa} \frac{\cosh \kappa (d + y)}{\sinh \kappa d} \sin (\kappa x - \omega t). \quad (2.9)$$

The frequency  $\omega$  is determined by the dynamical free surface condition Equation (2.7) and is related to the wave number  $\kappa$  by the dispersive relationship

$$\omega^2 = g\kappa \tanh \kappa d. \quad (2.10)$$

Once the velocity potential  $\phi(x, y, t)$  is obtained, components of fluid particle velocities  $\dot{V}_x(x, y, t)$  and  $\dot{V}_y(x, y, t)$  can be calculated from Equation (2.1). In later derivations, components of fluid particle accelerations are also required. Consistent with the assumption of linear wave theory, by neglecting the higher order convective terms, the horizontal and vertical components of fluid particle accelerations are respectively  $\ddot{V}_x(x, y, t)$  and  $\ddot{V}_y(x, y, t)$ . Here and hereafter, overdot is used to denote differentiation with respect to time.



## 2.2 Random Waves

Waves in the real sea are quite different from the ordinary long-crested waves of permanent form as described by the deterministic mathematical wave theory in Section 2.1. This is especially true for the wind generated waves in the ocean. When these waves propagate in different directions with different amplitudes, lengths, periods, and phase angles, the resulting surface is almost always random. Therefore, detailed description of the surface waves can not be achieved in a deterministic manner in either space or time. The only alternative is to seek their properties by statistical methods.

The most important one of all the commonly used statistical measures is the wave spectrum which is the energy density function in terms of wave frequency or wave number. However, in order to utilize the general statistical theory on waves, several assumptions and their justifications are given below:

1. The wave field is assumed to be stationary and homogeneous. A random process is said to be stationary (or homogeneous) if its probability distributions are invariant under a shift of the time (or distance) scale. The duration of time that the wind acts on the water is called the wind duration. The distance over which the wind blows is called the fetch. Strictly speaking, the conditions of stationarity and homogeneity can never be satisfied since sea state obviously depends on the duration and fetch of a storm. The assumptions of stationarity and homogeneity can be justified on physical grounds that the typical wave period is much smaller than the duration of the storm, and the typical wave length is always smaller than the diameter of the storm.

2. The free surface elevation is assumed to have a Gaussian (or Normal) distribution. The Gaussian nature of the sea surface has been observed by Kinsman (1960) and can be explained by the Central Limit Theorem (Crandall and Mark, 1963). Under some general conditions, the Central Limit Theorem states that a random process will be approximately Gaussian if each of its sample functions can be considered to have been generated by the superposition of a large number of independent random sources, no single one of which contributed significantly. Thus the surface elevation might be considered approximately Gaussian when it is due to the superposition of an infinite number of random waves.

3. Since the origin of wave system is selected at the mean water level (Figure 2.1), the surface elevation will have zero mean.

If the surface elevation is stationary, homogeneous, zero-mean, and Gaussian, then a complete description of this random process can be achieved from knowledge of its auto-correlation function or its spectral density function.

The auto-correlation function  $R_{XX}(\tau)$  for a stationary process  $X(t)$  is defined as

$$R_{XX}(\tau) = E[X(t)X(t + \tau)] \quad (2.11)$$

in which  $\tau$  is the shift of time and  $E[\cdot]$  denotes the expected value (or mean) of the quantity enclosed in the bracket.

The spectral density function (or spectrum)  $S_{XX}(\omega)$  of the stationary process  $X(t)$  is the Fourier transform of the auto-correlation function  $R_{XX}(\tau)$

$$S_{XX}(\omega) = \frac{1}{2\pi} \int_{-\infty}^{\infty} R_{XX}(\tau) e^{-i\omega\tau} d\tau \quad (2.12)$$

in which  $i = (-1)^{1/2}$ . From the Fourier inversion formula, it follows that  $R_{XX}(\tau)$  can be expressed in terms of  $S_{XX}(\omega)$

$$R_{XX}(\tau) = \int_{-\infty}^{\infty} S_{XX}(\omega) e^{i\omega\tau} d\omega. \quad (2.13)$$

When  $\tau = 0$ , Equation (2.13) becomes

$$R_{XX}(0) = \int_{-\infty}^{\infty} S_{XX}(\omega) d\omega = E[X^2(t)] \quad (2.14)$$

in which  $E[X^2(t)]$  is the mean square value of  $X(t)$ .

If the surface displacement  $\eta(t)$  is considered as a function of time only, i.e., measured at one fixed point, then from Equation (2.14)

$$E[\eta^2(t)] = \int_{-\infty}^{\infty} S_{\eta\eta}(\omega) d\omega \quad (2.15)$$

so that  $S_{\eta\eta}(\omega)$  can be interpreted as the density of contributions to  $E[\eta^2(t)]$  per unit frequency interval. Since the mean energy per unit area of the wave motion is proportional to  $E[\eta^2(t)]$  (Phillips, 1966), the ordinate of the spectrum  $S_{\eta\eta}(\omega)$  is therefore a measure of the "wave energy density" per unit frequency and unit horizontal area.

The wave spectrum can be determined from actual field data (Kinsman, 1965). In this study, the spectrum for a fully developed wind-generated sea state described by the Kitaigorodskii (1962)-Pierson-Moskowitz (1964) spectrum

$$S_{\eta\eta}(\omega) = \frac{\alpha g^2}{\omega^5} \exp \left[ -\beta \left( \frac{g}{W\omega} \right)^4 \right], \quad 0 < \omega < \infty \quad (2.16)$$

is used. In Equation (2.16),  $\alpha$  and  $\beta$  are two dimensionless constants with  $\alpha = 0.0081$  and  $\beta = 0.74$ , and  $W$  is the mean wind speed. Any consistent set of units can be used in the above formula. Since this spectrum is defined only from zero to infinity, a slight modification to redefine the spectrum over the frequency interval  $(-\infty, \infty)$  can be made as

$$S_{\eta\eta}(\omega) = \frac{\alpha g^2}{2|\omega|^5} \exp \left[ -\beta \left( \frac{g}{W\omega} \right)^4 \right], \quad -\infty < \omega < \infty \quad (2.17)$$

where  $|\omega|$  is the absolute value of  $\omega$ . The points at which  $S_{\eta\eta}(\omega)$  is maximum are located at

$$\omega_0 = \pm \left( \frac{4\beta}{5} \right)^{1/4} \frac{g}{W} \quad (2.18)$$

and the maximum value of  $S_{\eta\eta}(\omega)$  at  $\omega_0$  is

$$S_{\eta\eta}(\omega_0) = \frac{\alpha W^5}{g^3} \left( \frac{4\beta}{5} \right)^{-5/4} \exp \left( \frac{-5}{4} \right).$$

There are several statistical models to represent the visible state of the random sea (Borgman, 1972). One frequently used model is obtained by a superposition of an infinite number of sinusoidal waves of different frequencies and amplitudes with random phase angles (Rice, 1945). Thus the sea surface displacement  $\eta(x, t)$  can be written as

$$\eta(x, t) = \sum_{j=1}^N a_j \cos(\kappa_j x - \omega_j t + \lambda_j) \quad (2.19)$$

in which  $N$  approaches infinity and the random phase angles  $\lambda_j$  are assumed to be uniformly distributed over the interval  $(-\pi, \pi)$  and independent from

component to component. Using the deterministic relationship between the amplitude and the energy contained in the wave at corresponding frequency (Pierson, 1955; Borgman, 1972), it is convenient to represent the above equation by the "pseudo-integral"

$$\eta(x, t) = \int_{-\infty}^{\infty} [2S_{\eta\eta}(\omega)d\omega]^{1/2} \cos(\kappa x - \omega t + \lambda). \quad (2.20)$$

It can be seen that the statistical nature of the confused sea surface is taken as arising purely from the random phase. If the model of Equation (2.20) is adopted, then the potential function, fluid particle velocity, and fluid particle acceleration of the random wave field are readily found by comparing Equation (2.20) with the results obtained from single wave in Section 2.1. That is,

$$\phi(x, y, t) = \int_{-\infty}^{\infty} [2S_{\eta\eta}(\omega)d\omega]^{1/2} \frac{\omega \cosh \kappa (y + d)}{\kappa \sinh \kappa d} \sin(\kappa x - \omega t + \lambda) \quad (2.21)$$

$$\dot{V}_x = \int_{-\infty}^{\infty} [2S_{\eta\eta}(\omega)d\omega]^{1/2} \frac{\omega \cosh \kappa (y + d)}{\sinh \kappa d} \cos(\kappa x - \omega t + \lambda) \quad (2.22)$$

$$\dot{V}_y = \int_{-\infty}^{\infty} [2S_{\eta\eta}(\omega)d\omega]^{1/2} \frac{\omega \sinh \kappa (y + d)}{\sinh \kappa d} \sin(\kappa x - \omega t + \lambda) \quad (2.23)$$

$$\ddot{V}_x = \int_{-\infty}^{\infty} [2S_{\eta\eta}(\omega)d\omega]^{1/2} \frac{\omega^2 \cosh \kappa (y + d)}{\sinh \kappa d} \sin(\kappa x - \omega t + \lambda) \quad (2.24)$$

$$\ddot{V}_y = \int_{-\infty}^{\infty} [2S_{\eta\eta}(\omega)d\omega]^{1/2} \frac{-\omega^2 \sinh \kappa (y+d)}{\sinh \kappa d} \cos (\kappa x - \omega t + \lambda). \quad (2.25)$$

These quantities are all zero-mean and they are also Gaussian due to the assumption of linear wave theory.

In Chapter 3, the cross-correlation function and the cross-spectrum of components of  $\dot{V}$  and  $\ddot{V}$  are required to calculate the input spectrum of forcing functions for dynamic analysis. The cross-correlation function  $R_{XY}(\tau)$  for two stationary processes  $X(t)$  and  $Y(t)$  is

$$R_{XY}(\tau) = E[X(t)Y(t + \tau)]. \quad (2.26)$$

The cross-spectral density function (or cross-spectrum)  $S_{XY}(\omega)$  of the two processes  $X(t)$  and  $Y(t)$  is the Fourier transform of the cross-correlation function

$$S_{XY}(\omega) = \frac{1}{2\pi} \int_{-\infty}^{\infty} R_{XY}(\tau) e^{-i\omega\tau} d\tau. \quad (2.27)$$

From the Fourier inversion formula, it follows that  $R_{XY}(\tau)$  can be expressed in terms of  $S_{XY}(\omega)$

$$R_{XY}(\tau) = \int_{-\infty}^{\infty} S_{XY}(\omega) e^{i\omega\tau} d\omega. \quad (2.28)$$

When  $\tau = 0$ , the above equation becomes

$$R_{XY}(0) = \int_{-\infty}^{\infty} S_{XY}(\omega) d\omega = E[X(t)Y(t)] = \text{Cov}(X, Y) \quad (2.29)$$

where  $\text{Cov}(X, Y)$  is the covariance of  $X$  and  $Y$ , if it is assumed that  $X$  and  $Y$  have zero means.

The general procedure of obtaining cross-spectrum for waves is given below. Let  $\dot{V}_j(x_j, y_j, t)$  denote the component of the fluid particle velocity at point  $j$ . If the component is in a direction parallel to the  $x$ -axis, then

$$\dot{V}_j(x_j, y_j, t) = \int_{-\infty}^{\infty} [2S_{\eta\eta}(\omega)d\omega]^{1/2} \frac{\omega \cosh \kappa (y_j + d)}{\sinh \kappa d} \sin(\kappa x_j - \omega t + \lambda), \quad j//x \quad (2.30)$$

where the symbol  $//$  means parallel to the corresponding coordinate axis that follows. Similarly,  $\dot{V}_k(x_k, y_k, t + \tau)$  denotes the component of fluid particle velocity at point  $k$ , but with a time lag  $\tau$ . If it is in a direction parallel to the  $y$ -axis, then

$$\dot{V}_k(x_k, y_k, t + \tau) = \int_{-\infty}^{\infty} [2S_{\eta\eta}(\omega)d\omega]^{1/2} \frac{\omega \sinh \kappa (y_k + d)}{\sinh \kappa d} \sin(\kappa y_k - \omega t - \omega\tau + \lambda), \quad k//y \quad (2.31)$$

From Equation (2.26), the cross-correlation function  $R_{\dot{V}_j \dot{V}_k}(\tau)$  can be found by taking the mean of the product of  $\dot{V}_j(x_j, y_j, t)$  and  $\dot{V}_k(x_k, y_k, t + \tau)$ . That is

$$R_{\dot{V}_j \dot{V}_k}(\tau) = E[\dot{V}_j(x_j, y_j, t) \dot{V}_k(x_k, y_k, t + \tau)], \quad \begin{array}{l} j//x \\ k//y \end{array}$$

Foster (1967) developed several simplified forms of the cross-correlation function for fluid particle velocities by considering the statistical properties of the random phase  $\lambda$ . These cross-correlation functions are listed below:

$$R_{\dot{V}_j \dot{V}_k}(\tau) = \int_{-\infty}^{\infty} S_{\eta\eta}(\omega) \frac{\omega^2 \cosh \kappa (y_j + d) \cosh \kappa (y_k + d)}{\sinh^2 \kappa d} \cos [\kappa (x_j - x_k) + \omega\tau] d\omega, \quad \begin{array}{l} j//x \\ k//x \end{array} \quad (2.32)$$

$$R_{\dot{V}_j \dot{V}_k}(\tau) = \int_{-\infty}^{\infty} S_{\eta\eta}(\omega) \frac{-\omega^2 \cosh \kappa (y_j + d) \sinh \kappa (y_k + d)}{\sinh^2 \kappa d} \sin [\kappa (x_j - x_k) + \omega\tau] d\omega, \quad \begin{array}{l} j//x \\ k//y \end{array} \quad (2.33)$$

$$R_{\dot{V}_j \dot{V}_k}(\tau) = \int_{-\infty}^{\infty} S_{\eta\eta}(\omega) \frac{\omega^2 \sinh \kappa (y_j + d) \cosh \kappa (y_k + d)}{\sinh^2 \kappa d} \sin [\kappa (x_j - x_k) + \omega\tau] d\omega, \quad \begin{array}{l} j//y \\ k//x \end{array} \quad (2.34)$$

$$R_{\dot{V}_j \dot{V}_k}(\tau) = \int_{-\infty}^{\infty} S_{\eta\eta}(\omega) \frac{\omega^2 \sinh \kappa (y_j + d) \sinh \kappa (y_k + d)}{\sinh^2 \kappa d} \cos [\kappa (x_j - x_k) + \omega\tau] d\omega, \quad \begin{array}{l} j//y \\ k//y \end{array} \quad (2.35)$$



The cross-spectral density function  $S_{\dot{V}_j \dot{V}_k}(\omega)$  corresponding to  $R_{\dot{V}_j \dot{V}_k}(\tau)$  can be obtained from Equation (2.27)

$$S_{\dot{V}_j \dot{V}_k}(\omega) = \frac{1}{2\pi} \int_{-\infty}^{\infty} R_{\dot{V}_j \dot{V}_k}(\tau) e^{-i\omega\tau} d\tau. \quad (2.36)$$

The integral on the right hand side of the above equation was carried out by Foster (1967) and the cross-spectral density functions for fluid particle velocity are given below:

$$S_{\dot{V}_j \dot{V}_k}(\omega) = S_{\eta\eta}(\omega) \frac{\omega^2 \cosh \kappa (y_j + d) \cosh \kappa (y_k + d)}{\sinh^2 \kappa d} \exp[i\kappa(x_j - x_k)], \quad \begin{array}{l} j//x \\ k//x \end{array} \quad (2.37)$$

$$S_{\dot{V}_j \dot{V}_k}(\omega) = S_{\eta\eta}(\omega) \frac{i\omega^2 \cosh \kappa (y_j + d) \sinh \kappa (y_k + d)}{\sinh^2 \kappa d} \exp[i\kappa(x_j - x_k)], \quad \begin{array}{l} j//x \\ k//y \end{array} \quad (2.38)$$

$$S_{\dot{V}_j \dot{V}_k}(\omega) = S_{\eta\eta}(\omega) \frac{-i\omega^2 \sinh \kappa (y_j + d) \cosh \kappa (y_k + d)}{\sinh^2 \kappa d} \exp[i\kappa(x_j - x_k)], \quad \begin{array}{l} j//y \\ k//x \end{array} \quad (2.39)$$

$$S_{\dot{V}_j \dot{V}_k}(\omega) = S_{\eta\eta}(\omega) \frac{\omega^2 \sinh \kappa (y_j + d) \sinh \kappa (y_k + d)}{\sinh^2 \kappa d} \exp[i\kappa(x_j - x_k)], \quad \begin{array}{l} j//y \\ k//y \end{array} \quad (2.40)$$

Since the random process  $\dot{V}(x, y, t)$  is stationary, the cross-correlation functions such as  $R_{\dot{V}\dot{V}}$ ,  $R_{\dot{V}\ddot{V}}$  and  $R_{\ddot{V}\ddot{V}}$  can be easily derived in terms of  $R_{\dot{V}\dot{V}}(\tau)$  by the relationship (Papoulis, 1965)

$$R_{\dot{V}_j \dot{V}_k}^{(n)(m)}(\tau) = (-1)^n \frac{\partial^{(n+m)}}{\partial \tau^{(n+m)}} R_{\dot{V}_j \dot{V}_k}(\tau) \quad (2.41)$$

in which  $n$  and  $m$  denote the order of derivatives. Thus,

$$R_{\dot{V}_j \ddot{V}_k}(\tau) = \frac{\partial}{\partial \tau} R_{\dot{V}_j \dot{V}_k}(\tau) \quad (2.42)$$

$$R_{\ddot{V}_j \dot{V}_k}(\tau) = -\frac{\partial}{\partial \tau} R_{\dot{V}_j \dot{V}_k}(\tau) \quad (2.43)$$

$$\text{and} \quad R_{\ddot{V}_j \ddot{V}_k}(\tau) = -\frac{\partial^2}{\partial \tau^2} R_{\dot{V}_j \dot{V}_k}(\tau) . \quad (2.44)$$

Using Equation (2.27) as the definition of Fourier transform, the cross-spectral density function of the derivatives of  $\dot{V}$  can also be obtained in terms of  $S_{\dot{V}_j \dot{V}_k}(\omega)$ . That is,

$$S_{\dot{V}_j \ddot{V}_k}(\omega) = i\omega S_{\dot{V}_j \dot{V}_k}(\omega) \quad (2.45)$$

$$S_{\ddot{V}_j \dot{V}_k}(\omega) = -i\omega S_{\dot{V}_j \dot{V}_k}(\omega) \quad (2.46)$$

$$\text{and} \quad S_{\ddot{V}_j \ddot{V}_k}(\omega) = \omega^2 S_{\dot{V}_j \dot{V}_k}(\omega) . \quad (2.47)$$

### 2.3 Currents and Wave-Current Interactions

Since currents have many effects on the ocean environment, they are of special importance to the ocean engineer. For the present study, ocean currents can contribute to drag forces which are proportional to the square of the fluid particle velocity. The American Petroleum Institute Specification (1975), which governs the design of fixed offshore platforms, recommends that due consideration be given to the possible superposition of currents and waves in some areas.

Examination of various discussions on currents (Ippen, 1966; Myers, 1969) shows that ocean currents can be classified into several groups according to the way currents are generated. They are:

1. currents related to density distribution, such as the Gulf Stream and the kuroshio,
2. tidal currents, caused by the astronomical forces of the moon and sun,
3. currents related to wind stress, caused by the effect of wind blowing over the ocean,
4. wave-induced currents, or the so-called mass-transport velocity in finite amplitude wave theory, and
5. local currents, caused by the discharged water from rivers.

Because surface waves belong to a particular group of motion in which the fluid particles are organized in such a way as to show the oscillatory surface elevation, any concurrent motion in the fluid will produce interactions; for example, wave-wave interactions (Phillips, 1960, 1966) and wave-current interactions (Taylor, 1955; Ursell, 1960); Witham, 1960, 1962; Longuet-Higgins and Stewart, 1960, 1961). From these interactions, certain

changes in wave characteristics will arise such as changes in the wave amplitude (Longuet-Higgins and Stewart, 1960, 1961) and phase speed (Longuet-Higgins and Phillips, 1962; Phillips, 1966). Thus when the wave propagates into a region of local current, the wave amplitude decreases and the wave length increases if the current and the wave are in the same direction (Longuet-Higgins and Stewart, 1961). However, if the current and the wave are in opposite directions, then wave amplitude increases and wave length decreases.

In a random wave field, influence of wave-current interactions on some statistical properties of waves has been studied by Huang et al. (1972). It was shown that in deep water the wave number  $\kappa$ , under the influence of a steady current, is related to wave frequency  $\omega$  by a general dispersion relationship (Huang et al., 1972)

$$g\kappa = \frac{4\omega^2}{\left[1 + \left(1 + \frac{V_c \omega}{g}\right)^{1/2}\right]^2} \quad (2.48)$$

in which  $V_c$  is the current velocity and  $g$  is the gravitational acceleration. It is seen from Equation (2.48) that when the current is in the direction of waves, i.e.,  $V_c > 0$ , the value of  $\kappa$  is less than that when there is no current, indicating that positive current increases the wave length. The dispersion relationship of Equation (2.48) is plotted in Figure 2.2 for different values of  $V_c$ . The dotted line indicates the theoretical limit when the group velocity of waves is equal to the negative current velocity. No wave can exist beyond this line. In fact, waves will break long before they approach this limit because the wave amplitude would be infinite at this critical velocity.

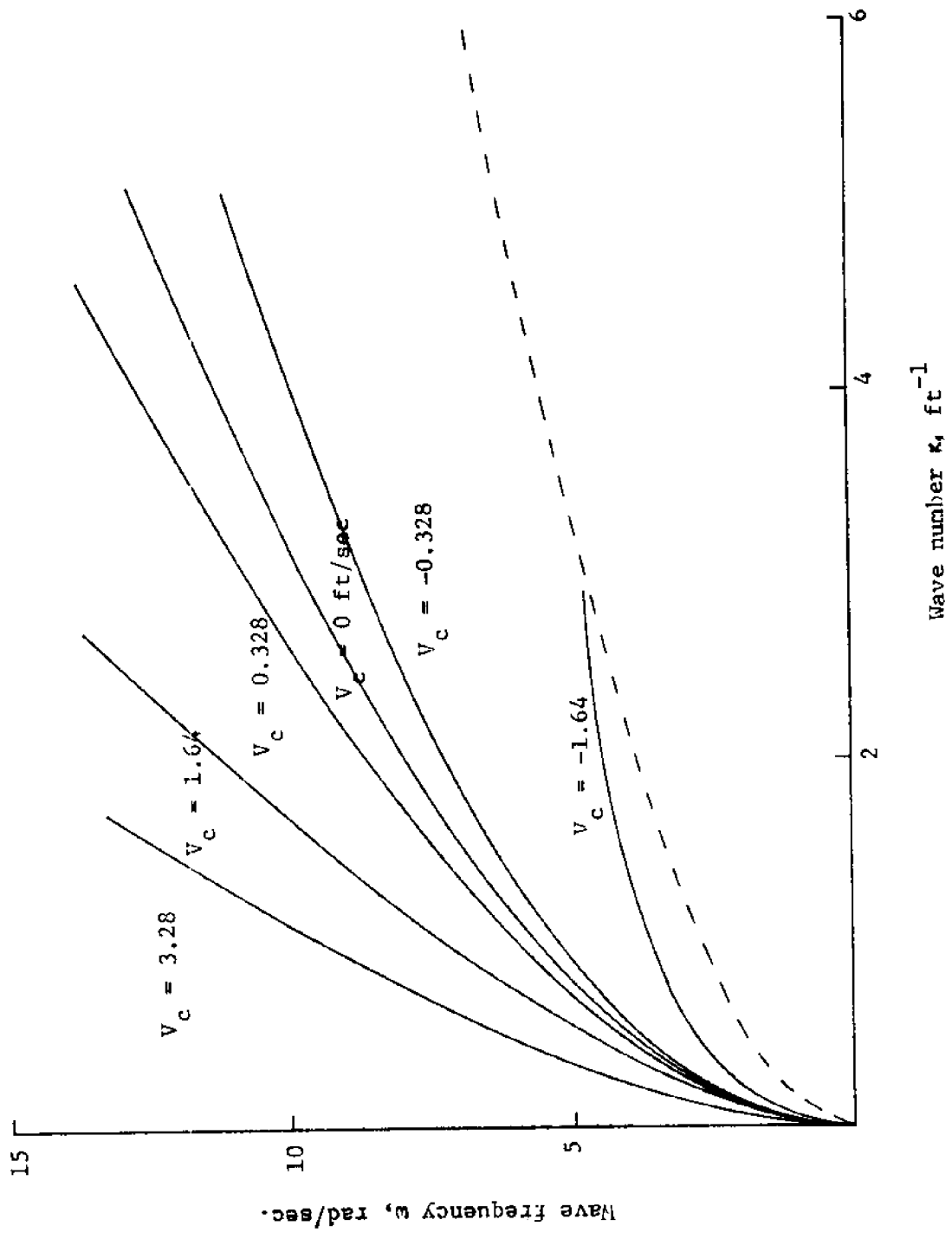


Figure 2.2. The influence of currents on dispersion relationship between wave number and wave frequency.

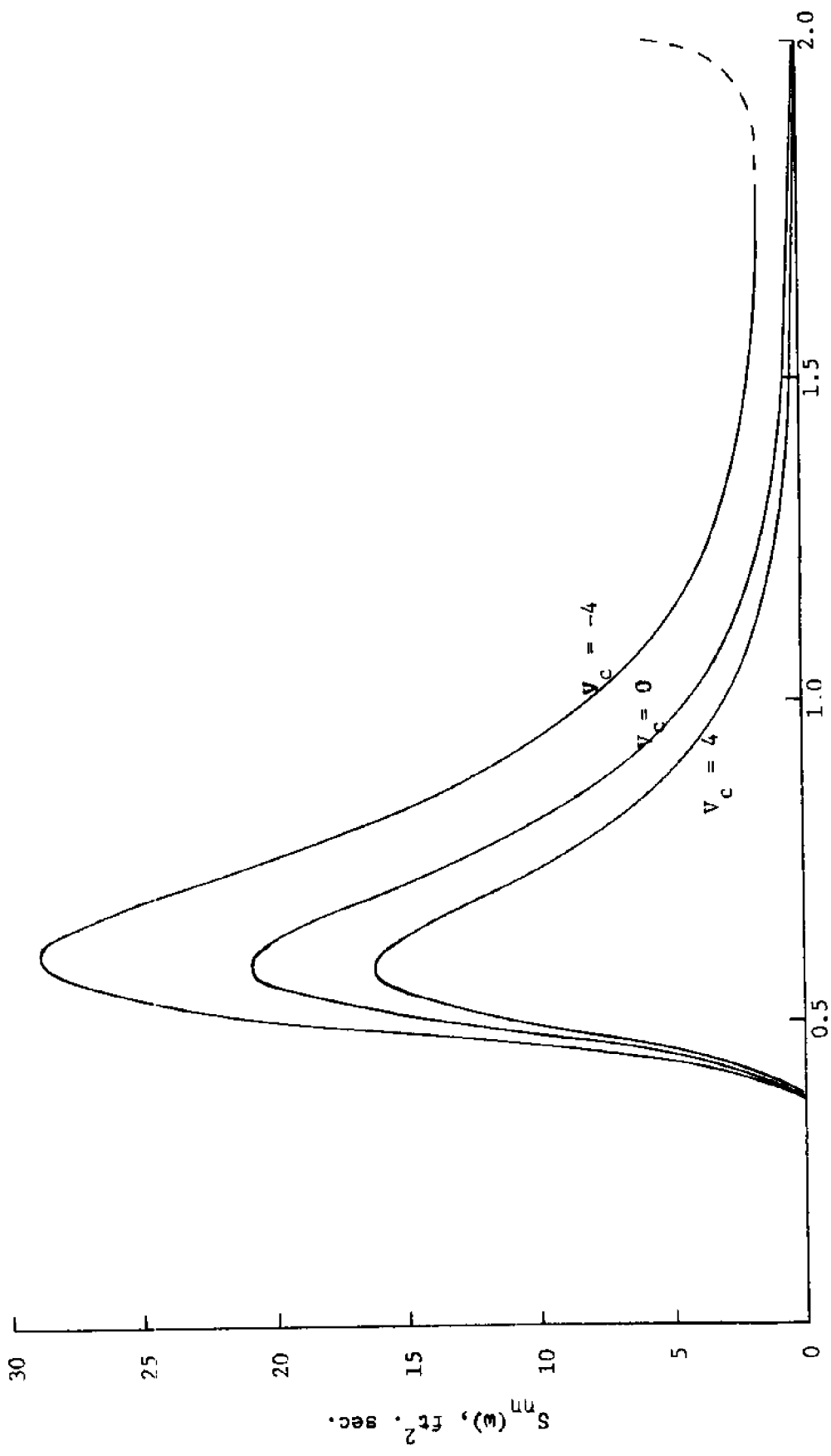
It was also shown (Huang et al., 1972) that under the action of a steady current, the frequency spectrum  $\bar{S}_{\eta\eta}(\omega)$  of surface waves of an unidirectional stationary gravity wave field in deep water can be obtained from

$$\bar{S}_{\eta\eta}(\omega) = \frac{4S_{\eta\eta}(\omega)}{\left[1 + \left(1 + \frac{4V_c\omega}{g}\right)^{1/2}\right] \left[\left(1 + \frac{4V_c\omega}{g}\right)^{1/2} + \left(1 + \frac{4V_c\omega}{g}\right)\right]} \quad (2.49)$$

in which  $S_{\eta\eta}(\omega)$  is the frequency spectrum of surface waves without the influence of current. The spectra  $\bar{S}_{\eta\eta}(\omega)$  for various values of current speed  $V_c$  are plotted in Figure 2.3 by using the Kitaigorodskii-Pierson-Moskowitz spectrum (Equation 2.17) with a mean wind speed  $W = 50$  ft/sec. Figure 2.3 shows that when the current is in the direction of the waves,  $V_c > 0$ , the surface spectrum is lowered. This is because positive current tends to lengthen the waves thus reducing the energy level of the waves. On the other hand, adverse current steepens the waves and feeds energy into the wave system; therefore, the surface wave spectrum increases in magnitude. It is noted that when current velocity is negative, there is a cut-off frequency in the surface wave spectrum. This cut-off frequency is determined by

$$1 + \frac{4V_c\omega}{g} \geq 0 \quad (2.50)$$

which is implied in Equations (2.48) and (2.49). As mentioned earlier, before this cut-off frequency is reached, waves with frequencies in the vicinity of the cut-off frequency become very steep and eventually break. Hence the spectrum should be terminated before the cut-off frequency.



Wave frequency  $\omega$ , rad/sec.

Figure 2.3. Frequency spectra of wave for current velocities  $V_c = -4, 0$ , and  $+4$  ft/sec; 50 ft/sec wind.

Since the wave spectrum is obtained from field data, therefore, actual ocean environment at the field must be observed while these wave data are being measured. If a wave spectrum is obtained without the presence of externally generated current, then Equation (2.49) should be used to modify this spectrum for consideration of possible wave-current interactions effect.



### 3. DYNAMIC RESPONSE OF STRUCTURES

#### 3.1 Wave and Current Forces

The most commonly used formula for the estimation of wave force on a vertical cylinder is the Morison formula (Morison et al., 1950). The formula states that the hydrodynamic force exerted on a vertical cylinder consists of two components. One component is the drag force which is proportional to the square of fluid particle velocity. The other component is the inertia force which is proportional to fluid particle acceleration.

Thus the wave force  $dF(t)$  on an element of a vertical cylinder of length  $ds$  (Figure 3.1) is

$$dF(t) = C_M \rho \frac{\pi D^2}{4} \ddot{V}(t) ds + \frac{1}{2} C_D \rho D \dot{V}(t) |\dot{V}(t)| ds \quad (3.1)$$

in which  $D$  is cylinder diameter,  $\rho$  is density of sea water,  $C_D$  and  $C_M$  are respectively the drag and inertia coefficient, and  $\dot{V}(t)$  and  $\ddot{V}(t)$  are respectively the horizontal components of fluid particle velocity and acceleration of wave - at the point under consideration and in the direction of wave propagation. The usual assumption that the presence of the structure does not alter the wave field is made in this study.

The appropriate use of Morison's formula depends primarily on the choice of the numerical values of drag and inertia coefficients. These empirical coefficients are estimated from laboratory and field investigations. Methods for estimating  $C_D$  and  $C_M$  by either deterministic or statistical approach are presented in the work by Borgman (1972). Although there are considerable scatters among published results (Wilson

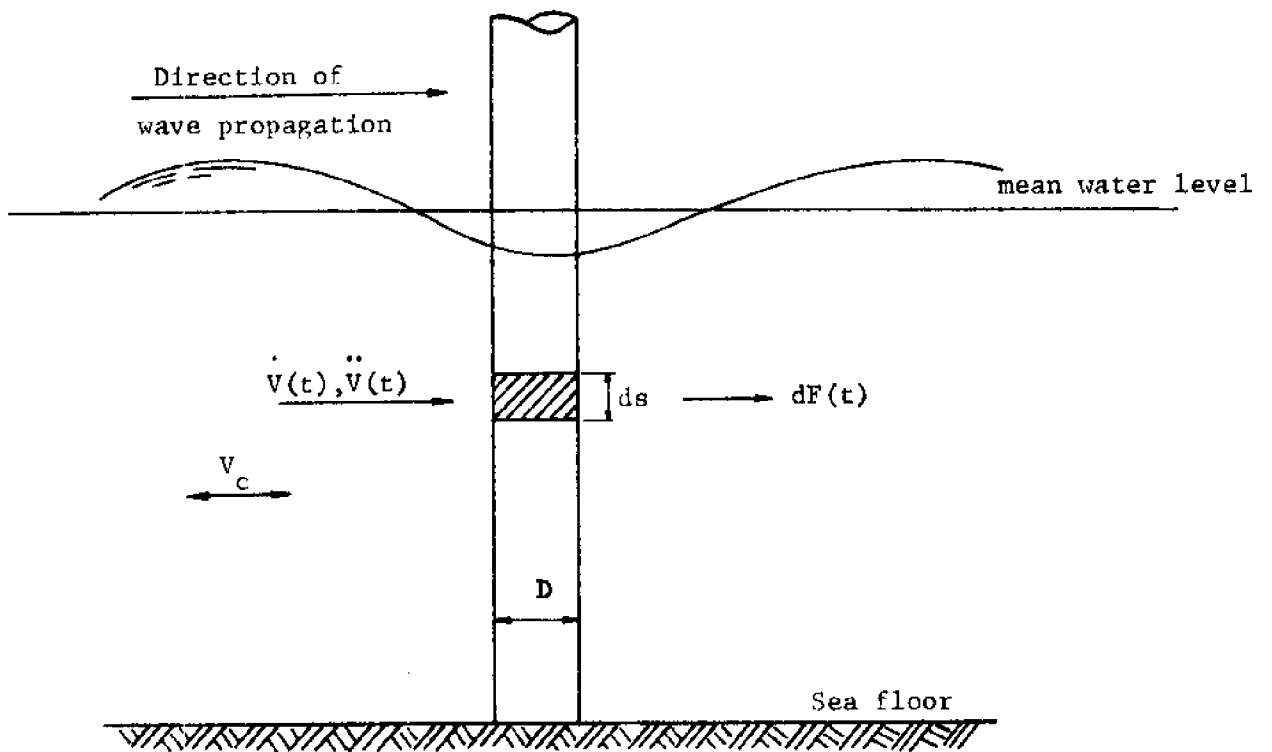


Figure 3.1. Horizontal wave forces on a vertical circular cylinder.

and Reid, 1963, Myers, 1969; Trasher and Aagaard, 1970; Dean and Aagaard, 1970; Wheeler, 1970; Evans, 1970) for drag and inertia coefficients,  $C_D$  and  $C_M$  are normally considered constants having values in the ranges  $1.0 \leq C_D \leq 1.4$  and  $1.4 \leq C_M \leq 2.0$  (Wiegel, 1964). To be consistent with the previous study (Penzien, Kaul and Berge, 1972),  $C_D$  and  $C_M$  are assumed constant and the values of 1.4 and 2.0 are selected respectively.

In the presence of a steady current, the Morison formula can be modified by including the contribution of current on drag force (Wiegel, 1964; Borgman, 1972). That is

$$dF(t) = C_M \rho \frac{\pi D^2}{4} \ddot{V}(t) ds + \frac{1}{2} C_D \rho D (\dot{V}(t) + V_c) |(\dot{V}(t) + V_c)| ds \quad (3.2)$$

where  $V_c$  is the velocity of steady current. In Equation (3.2) it is assumed that values of  $C_D$  and  $C_M$  do not change in the presence of a steady current.

From Equation (3.2) it is seen that in the presence of a current, the drag force can not be considered simply as the sum of drag force due to current

$$\frac{1}{2} C_D \rho D V_c |V_c| ds$$

and drag force due to waves

$$\frac{1}{2} C_D \rho D \dot{V}(t) |\dot{V}(t)| ds .$$

Furthermore, when the phenomenon of wave-current interactions is considered, the fluid particle velocity  $\dot{V}(t)$  and acceleration  $\ddot{V}(t)$  should be modified accordingly.

### 3.2 Equations of Motion

The offshore tower is a continuous structure with an infinite number of degrees of freedom. For dynamic analysis purpose, it is convenient and usually adequate, to represent such a structure with a lumped mass model consisting of discrete masses located at selected nodal points. Figure 3.2 shows such an idealized model of an offshore tower. The dynamic equations of motion for this model can be written in matrix form as

$$[M]\{\ddot{U}(t)\} + [C]\{\dot{U}(t)\} + [K]\{U(t)\} = \{F(t)\} \quad (3.3)$$

in which  $[M]$  is the diagonal matrix of masses lumped at nodal points,  $[C]$  and  $[K]$  are the structural damping and stiffness matrices, respectively.  $\{\ddot{U}(t)\}$ ,  $\{\dot{U}(t)\}$ , and  $\{U(t)\}$  are column vectors of nodal accelerations, velocities, and displacements, respectively, and  $\{F(t)\}$  is a column vector of forcing functions acting on the nodal points. In this study, it is assumed that the waves travel in the positive  $x$  direction. All structural and loading variations in the  $z$  direction are therefore neglected in Equation (3.3). Thus, the number of degrees of freedom at each node is reduced to three; namely, translational displacements in the horizontal  $x$  direction and in the vertical  $y$  direction, and rotational displacement about the  $z$ -axis.

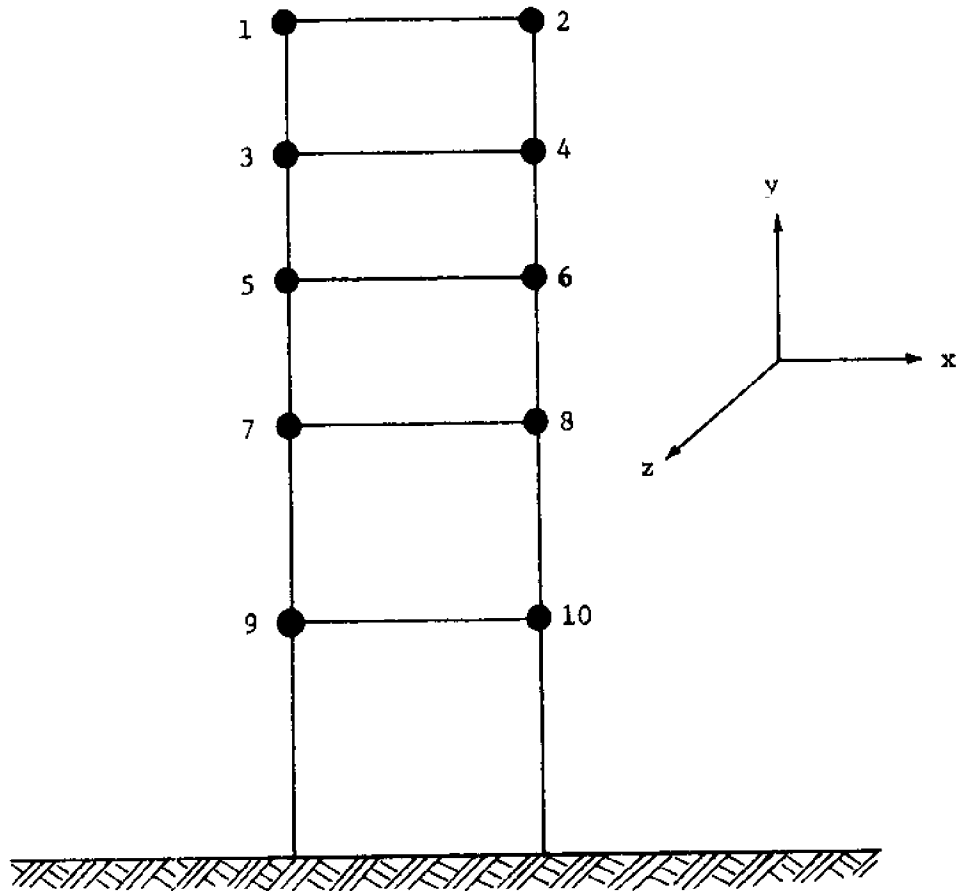


Figure 3.2. Idealized tower.

The forces considered in Equation (3.3) are those due to wave and current only. With the effect of fluid structure interaction included, the drag force, according to Morison's formula, can be expressed as

$$\frac{1}{2} C_D \rho [A_p] \{(\dot{V} + v_c - \dot{U}) | (\dot{V} + v_c - \dot{U})|\} . \quad (3.4)$$

Here and hereafter in this dissertation, the argument  $t$  of these time dependent quantities is dropped for convenience, except when a time dependent quantity first appears. In Equation (3.4) the elements of the diagonal matrix  $[A_p]$  represent the projected areas of structural members lumped at nodal points and perpendicular to motion of fluid.

By considering the effect of fluid structure interactions the inertia forces of the lumped masses moving in accelerating fluid may be divided into three parts (Chakrabarti, 1971):

1. The inertia forces of the lumped masses due to their own movements

$$[M]\{\ddot{U}\} \quad (3.5)$$

2. The inertia forces induced on the lumped masses by the masses of the fluid displaced by the lumped masses

$$\rho [V]\{\ddot{V}\} \quad (3.6)$$

where the elements of the diagonal matrix  $[V]$  represent the enclosed volumes of structural members lumped at nodal points, and  $\{\ddot{V}\}$  are fluid particle accelerations at nodal points.

3. The inertia forces due to added mass (Myers, 1969) based on relative acceleration between the lumped masses and surrounding fluid

$$C_M \rho [\Psi] \{\ddot{V} - \ddot{U}\} - \rho [\Psi] \{\ddot{V} - \ddot{U}\}, \text{ i.e.,}$$

$$(C_M - 1) \rho [\Psi] \{\ddot{V} - \ddot{U}\} . \quad (3.7)$$

Therefore, the total forces  $\{F(t)\}$  due to waves and currents on the lumped masses, in  $x$ -direction, can be calculated by combining Equations (3.4), (3.6), and (3.7). Substituting  $\{F(t)\}$  into Equation (3.3), the equations of motion become

$$\begin{aligned} [M]\{\ddot{U}\} + [C]\{\dot{U}\} + [K]\{U\} &= \rho [\Psi] \{\ddot{V}\} + (C_M - 1) \rho [\Psi] \{\ddot{V} - \ddot{U}\} \\ &+ \frac{1}{2} C_D \rho [A_p] \{(\dot{V} + v_c - \dot{U}) | (\dot{V} + v_c - \dot{U}) | \} \end{aligned} \quad (3.8)$$

In Equation (3.8), the fluid particle velocities and accelerations should be those at the instantaneous deflected position of the structure. However, for frequency components of the input forces near the fundamental frequency of the structure system, i.e., for small wave number  $\kappa$  the wave length  $L$  will be large, the wave particle velocities  $\dot{V}$  and accelerations  $\ddot{V}$  may be evaluated at the original undeflected structural coordinate with reasonable accuracy.

### 3.3 Equivalent Linearization Technique

By introducing  $\{\dot{r}(t)\} = \{\dot{V}(t)\} - \{\dot{U}(t)\}$ , the relative velocities between fluid particle velocities corresponding to wave motion and velocities of structural nodal points, the equations of motion (Equation (3.8)) are changed to

$$\begin{aligned}
[M_s]\{\dot{r}(t)\} + [C]\{\dot{r}(t)\} + \frac{1}{2} C_D \rho [A_p] \{(\dot{r}(t) + v_c) | (\dot{r}(t) + v_c) |\} \\
+ [K]\{r(t)\} = \{f(t)\} \quad (3.9)
\end{aligned}$$

in which  $[M_s] = [M] + (C_M - 1)\rho [V]$  is a diagonal matrix of the sum of structural and added masses, and  $\{f(t)\} = ([M] - \rho [V])\{\ddot{V}\} + [C]\{\dot{V}\} + [K]\{V\}$  is an effective forcing function which is independent of  $\{r\}$ .

Equation (3.9) is a set of nonlinear stochastic differential equations. These equations may be linearized through an equivalent linearization technique (Krylor and Bogoliubov, 1943; Lin, 1967). The essence of this technique, employed by Malhotra and Penzien (1970), is to replace the nonlinear term  $\frac{1}{2} C_D \rho [A_p] \{(\dot{r} + v_c) | (\dot{r} + v_c) |\}$  by a linear term by altering damping coefficients in an "optimal" manner. With the presence of currents in this study, this technique can still be applied. However, some modifications are necessary.

Let the linearized form of the  $i^{\text{th}}$  element of  $\{(\dot{r} + v_c) | (\dot{r} + v_c) |\}$  i.e.,  $(\dot{r}_i + v_c) | (\dot{r}_i + v_c) |$  be  $a_i \dot{r}_i + b_i$ . Then the error  $E_i$  introduced by this approximation is given by

$$E_i = (\dot{r}_i + v_c) | (\dot{r}_i + v_c) | - (a_i \dot{r}_i + b_i) . \quad (3.10)$$

In order to minimize the error  $E_i$  in the mean square sense, it requires that

$$E\left[\frac{\partial E_i^2}{\partial a_i}\right] = 0 \quad \text{and} \quad E\left[\frac{\partial E_i^2}{\partial b_i}\right] = 0 . \quad (3.11)$$



Substitution of Equation (3.10) into Equation (3.11) yields

$$2E[a_1 \dot{r}_1 - \dot{r}_1 (\dot{r}_1 + v_c) | (\dot{r}_1 + v_c) | + b_1 \dot{r}_1] = 0$$

and 
$$2E[b_1 + a_1 \dot{r}_1 - (\dot{r}_1 + v_c) | (\dot{r}_1 + v_c) |] = 0 .$$

From these two equations  $a_1$  and  $b_1$  can be obtained

$$a_1 = \frac{E[\dot{r}_1 (\dot{r}_1 + v_c) | (\dot{r}_1 + v_c) |] - b_1 E[\dot{r}_1]}{E[\dot{r}_1^2]} \quad (3.12)$$

$$b_1 = -a_1 E[\dot{r}_1] + E[(\dot{r}_1 + v_c) | (\dot{r}_1 + v_c) |] . \quad (3.13)$$

The vector  $\{(\dot{r} + v_c) | (\dot{r} + v_c) |\}$  in Equation (3.9) can now be replaced by the vector  $[a]\{\dot{r}\} + \{b\}$ . Elements of the diagonal matrix  $[a]$  and the vector  $\{b\}$  are those in Equations (3.12) and (3.13) respectively. When the damping terms of coefficients of  $\{\dot{r}\}$  in Equation (3.9) are combined, an optimal damping matrix  $[\underline{C}]$  is formed,

$$[\underline{C}] = [C] + \frac{1}{2} C_D^p [A_p][a] \quad (3.14)$$

in which the coefficients of  $[\underline{C}]$  are given by

$$c_{ij} = \begin{cases} c_{ij} & i \neq j \\ c_{ii} + \frac{1}{2} C_D^p A_{p_i} \frac{E[\dot{r}_1 (\dot{r}_1 + v_c) | (\dot{r}_1 + v_c) |] - b_1 E[\dot{r}_1]}{E[\dot{r}_1^2]} & i = j . \end{cases} \quad (3.15)$$

The linearized version of the equations of motion in Equation (3.9) thus becomes

$$[M_s]\{\ddot{r}\} + [C]\{\dot{r}\} + [K]\{r\} = \{f(t)\} - \frac{1}{2} C_{D\rho}[A_p]\{b\} . \quad (3.16)$$

It is seen from Equations (3.12), (3.13) and (3.15) that the elements of the matrix  $[C]$  and the vector  $\{b\}$  depend on the statistics of the solution  $\{\dot{r}\}$ . In the following, explicit expression of  $[C]$  in terms of the statistics of  $\{\dot{r}\}$  is given.

It is well known that the sum of a number of zero mean Gaussian processes is also zero mean Gaussian. Therefore, as seen from Equation (3.9), the input forcing function  $\{f(t)\}$  is a zero mean Gaussian process. It is noted from Equation (3.16) that the response vector  $\{r\}$  consists of two parts, one due to the constant force  $\frac{1}{2} C_{D\rho}[A_p]\{b\}$ , and the other due to the input zero mean Gaussian process  $\{f(t)\}$ . That is

$$\{r(t)\} = \{r_c(t)\} + \{r_f(t)\} \quad (3.17)$$

in which  $\{r_c(t)\}$  represents the response vector due to the constant force  $\frac{1}{2} C_{D\rho}[A_p]\{b\}$  and  $\{r_f(t)\}$  the response vector due to  $\{f(t)\}$ . Taking derivatives of Equation (3.17) with respect to time  $t$  gives

$$\{\dot{r}(t)\} = \{\dot{r}_f(t)\} . \quad (3.18)$$

The expected values of  $\{r\}$  and  $\{\dot{r}\}$  are obtained from Equations (3.17) and (3.18) respectively. Since the input  $\{f(t)\}$  is a zero mean Gaussian process, the linearized output process  $\{r_f(t)\}$  is also a zero mean Gaussian process. Hence it is concluded from Equation (3.18) that the

relative velocity vector  $\{\dot{r}\}$  is a zero mean Gaussian process. The probability density function for  $\dot{r}_i$ , the  $i^{\text{th}}$  element of  $\{\dot{r}\}$ , is

$$P(\dot{r}_i) = \frac{1}{(2\pi)^{1/2} \sigma_{\dot{r}_i}} \exp \left[ -\frac{1}{2} \left( \frac{\dot{r}_i}{\sigma_{\dot{r}_i}} \right)^2 \right] \quad (3.19)$$

in which  $\sigma_{\dot{r}_i}$  is the standard deviation of  $\dot{r}_i$ .

With the probability density function of  $\dot{r}_i$  known, it is possible to evaluate the expected values of the terms shown in Equations (3.12) and (3.13). For example,

$$\begin{aligned} E[\dot{r}_i (\dot{r}_i + v_c) | (\dot{r}_i + v_c) |] &= \frac{1}{(2\pi)^{1/2} \sigma_{\dot{r}_i}} \int_{-\infty}^{\infty} \dot{r}_i (\dot{r}_i + v_c) \\ &\quad | (\dot{r}_i + v_c) | \exp \left[ -\frac{1}{2} \left( \frac{\dot{r}_i}{\sigma_{\dot{r}_i}} \right)^2 \right] d\dot{r}_i . \end{aligned} \quad (3.20)$$

After the integration on right side of Equation (3.20) is carried out, the expected value is obtained as

$$\begin{aligned} E[\dot{r}_i (\dot{r}_i + v_c) | (\dot{r}_i + v_c) |] &= \left( \frac{8}{\pi} \right)^{1/2} \sigma_{\dot{r}_i}^2 \left\{ \sigma_{\dot{r}_i} \exp \left[ -\frac{1}{2} \left( \frac{v_c}{\sigma_{\dot{r}_i}} \right)^2 \right] \right. \\ &\quad \left. + (2\pi)^{1/2} v_c \operatorname{erf} \left( \frac{v_c}{\sigma_{\dot{r}_i}} \right) \right\} \quad (3.21) \end{aligned}$$

in which  $\operatorname{erf}(\cdot)$  is the error function defined by

$$\operatorname{erf}(u) = (2/\pi)^{-1/2} \int_0^u \exp \left( -\frac{1}{2} v^2 \right) dv. \quad (3.22)$$

$$\text{Similarly, } E[(\dot{r}_i + v_c) | (\dot{r}_i + v_c) |] = 2 \{ (2\pi)^{-1/2} \sigma_{r_i} v_c \exp[-\frac{1}{2} (\frac{v_c}{\sigma_{r_i}})^2] + (\sigma_{r_i}^2 + v_c^2) \text{erf}(\frac{v_c}{\sigma_{r_i}}) \} .$$

(3.23)

The optimized damping coefficients  $[C]$  in Equation (3.15) can now be expressed in terms of  $\sigma_{r_i}$  by substitution of Equation (3.21) and noting that  $E[\dot{r}_i] = 0$  and  $E[\dot{r}_i^2] = \sigma_{r_i}^2$

$$C_{ij} = \begin{cases} C_{ij} & i \neq j \\ C_{ii} + C_D \rho A_{p_i} \{ (\frac{2}{\pi})^{1/2} \sigma_{r_i} \exp[-\frac{1}{2} (\frac{v_c}{\sigma_{r_i}})^2] + 2v_c \text{erf}(\frac{v_c}{\sigma_{r_i}}) \} & i = j \end{cases}$$

(3.24)

Similarly, substituting Equation (3.23) into Equation (3.13) gives

$$b_i = 2 \{ (2\pi)^{-1/2} \sigma_{r_i} v_c \exp[-\frac{1}{2} (\frac{v_c}{\sigma_{r_i}})^2] + (\sigma_{r_i}^2 + v_c^2) \text{erf}(\frac{v_c}{\sigma_{r_i}}) \} .$$

(3.25)

Since values of  $\sigma_{r_i}$  can only be calculated from the solution of Equation (3.16), an iterative procedure is necessary for the solution of the linearized equations of motion. The iterative procedure can be carried out by first substituting trial values of  $\sigma_{r_i}$  (denoted by  $^1\sigma_{r_i}$ )

in Equation (3.24) to get the first trial damping matrix  ${}^1[\hat{C}]$ . The equations of motion can then be solved and the modified  ${}^2_{r_1}\sigma$  and  ${}^2[\hat{C}]$  are obtained to complete the first cycle of iteration. This process may be continued until convergence is achieved after N cycles, i.e., the iteration process may be terminated when

$${}^{N+1}[\hat{C}] \cong {}^N[\hat{C}] \quad (3.26)$$

For those case studies examined in Chapter 4, the rate of convergence is fast and only very few iteration cycles are needed.

Substituting back the previously defined relation  $\{\dot{r}\} = \{\dot{V}\} - \{\dot{U}\}$  in Equation (3.16) to determine the structural response, one obtains

$$[M_s]\{\ddot{U}\} + [\hat{C}]\{\dot{U}\} + [K]\{U\} = C_M^o [V]\{\ddot{V}\} + [\bar{C}]\{\dot{V}\} + \frac{1}{2} C_D^o [A_p]\{b\} \quad (3.27)$$

in which  $[\bar{C}]$  is defined as

$$[\bar{C}] = [\hat{C}] - [C] . \quad (3.28)$$

### 3.4 Transformation of Coordinates

Most structural systems are subject to constraints which may result from relationships among forces, or result from relationships among displacements, i.e., kinematical constraints. Members of structure are generally not equally flexible with respect to all axes, hence in systems it is sometimes appropriate to neglect certain deflections which are

small when compared with others. Thus, constraints may be introduced because of certain idealizations which may be made for convenience of analysis. In performing numerical dynamic analysis, it is important to reduce analysis costs by reducing the number of dynamic degrees of freedom. Two general approaches have been used effectively to reduce the dynamic degrees of freedom (Clough and Penzien, 1975). The simplest is based on the assumption that inertia forces are associated with only certain selected degrees of freedom of the original idealization; the remaining degrees of freedom are not explicitly involved in the dynamic analysis and can be condensed from the dynamic formulation. In the second approach, the number of dynamic degrees of freedom is limited by assuming that the displacements of the structure are combined in selected patterns, the amplitudes of which become the generalized coordinates of the dynamic analysis.

To illustrate how independent degrees of freedom are selected from constraint requirements in this study, consider the idealized offshore tower shown in Figure 3.1. Since the orientation of the flow is assumed in the direction of the x-axis, the analysis can be treated as two-dimensional and only the horizontal displacement  $U(t)$  at each nodal point is the quantity of interest. This is because the wave forces are different at the nodes on each floor level and consequently should be computed separately. If the axial deformation such as the relative elongation between nodes 1 and 2 is neglected, then the equation of constraint  $U_1 - U_2 = 0$  is introduced. Thus in solving the linearized set of differential equations Equation (3.27), the dependent displacements  $\{U(t)\}$  at nodal points are first used to estimate wave forces. Then a transformation from

the  $N$  ( $N = 10$  in this example) dependent displacements  $\{U(t)\}$  to the  $L$  ( $L = 50$  in this example) independent displacements  $\{X(t)\}$  is made. That is

$$\{U(t)\} = [A] \{X(t)\}$$

$$\begin{matrix} N \times 1 & N \times L & L \times 1 \end{matrix} \qquad (3.29)$$

where  $[A]$  is the transformation matrix with  $N$  rows and  $L$  columns. In this example (Figure 3.1), there are ten dependent horizontal displacements  $\{U\}$  at nodal points and five independent horizontal displacements  $\{X\}$  at floor levels. Equation (3.29) thus becomes

$$\begin{Bmatrix} U_1 \\ U_2 \\ U_3 \\ U_4 \\ U_5 \\ U_6 \\ U_7 \\ U_8 \\ U_9 \\ U_{10} \end{Bmatrix} = \begin{bmatrix} 1 & 0 & 0 & 0 & 0 \\ 1 & 0 & 0 & 0 & 0 \\ 0 & 1 & 0 & 0 & 0 \\ 0 & 1 & 0 & 0 & 0 \\ 0 & 0 & 1 & 0 & 0 \\ 0 & 0 & 1 & 0 & 0 \\ 0 & 0 & 0 & 1 & 0 \\ 0 & 0 & 0 & 1 & 0 \\ 0 & 0 & 0 & 0 & 1 \\ 0 & 0 & 0 & 0 & 1 \end{bmatrix} \begin{Bmatrix} X_1 \\ X_2 \\ X_3 \\ X_4 \\ X_5 \end{Bmatrix} \qquad (3.30)$$

Substituting Equation (3.29) and its corresponding derivatives into Equation (3.27), and premultiplying Equation (3.27) by  $[A]^T$  (transpose of  $[A]$ ), results in

$$[M^a]\{\ddot{X}(t)\} + [C^a]\{\dot{X}(t)\} + [K^a]\{X(t)\} = \{P^a(t)\} \quad (3.31)$$

in which

$$[M^a] = [A]^T [M_g] [A] \quad (3.32)$$

$$\begin{aligned} [C^a] &= [A]^T [C] [A] \\ &= [A]^T [C] [A] + [A]^T [\bar{C}] [A] \end{aligned} \quad (3.33)$$

$$[K^a] = [A]^T [K] [A] \quad (3.34)$$

and

$$\{P^a(t)\} = [A]^T (C_M \rho [\Psi] \{\ddot{V}\} + [\bar{C}] \{\dot{V}\} + \frac{1}{2} C_D \rho [A_p] \{b\}) \quad (3.35)$$

Thus, N equations of motion in Equation (3.27) corresponding to the N dependent displacements  $\{U\}$  have been reduced to L equations of motion in Equation (3.31) corresponding to the L independent displacements  $\{X\}$ .

### 3.5 Normal Mode Superposition

After the transformed set of equations of motion Equation (3.31) is obtained, the method of normal mode superposition can be used to calculate the response and response statistics of the structure. The response of the structure is given by

$$\{X(t)\} = [\psi] \{Y(t)\} \quad (3.36)$$

in which  $\{X(t)\}$  is the independent displacement vector of the structure,



$\{Y(t)\}$  is the generalized modal coordinate vector, and  $[\psi]$  is the modal matrix obtained from the undamped and homogeneous form of Equation (3.31) by the following equations for eigenvalues and eigenvectors.

$$[K^a][\psi] = [M^a][\psi][\omega_n^2] \quad (3.37)$$

where  $[\omega_n^2]$  is a diagonal matrix of all eigenvalues  $\omega_n^2$  ( $n = 1$  to  $L$ ).  $[\psi]$  is a square matrix containing all eigenvectors such that the  $n^{\text{th}}$  column is the set of modal displacements for the  $n^{\text{th}}$  mode corresponding to the eigenvalue  $\omega_n^2$ . Hence the element  $\psi_{ij}$  represents the  $i^{\text{th}}$  modal displacement in the  $j^{\text{th}}$  normal mode.

By substituting Equation (3.36) into Equation (3.31), premultiplying Equation (3.31) by  $[\psi]^T$  (transpose of  $[\psi]$ ), and using the orthogonality properties of normal modes, the equations of motion can be expressed in terms of the generalized modal coordinate vector  $\{Y(t)\}$  as

$$[M^*]\{\ddot{Y}(t)\} + [C_o]\{\dot{Y}(t)\} + [K^*]\{Y(t)\} = \{P^*(t)\} \quad (3.38)$$

$$\text{in which } [M^*] = [\psi]^T [M^a] [\psi]$$

$$= \text{generalized mass matrix} \quad (3.39)$$

$$[K^*] = [\psi]^T [K^a] [\psi] = [\omega_n^2] [M^*]$$

$$= \text{generalized stiffness matrix} \quad (3.40)$$

$$[C_o] = [\psi]^T [C^a] [\psi]$$

$$= \text{coupled damping matrix} \quad (3.41)$$

$$\begin{aligned} \{P^*(t)\} &= [\psi]^T \{P^a(t)\} \\ &= \text{generalized fluid force vector.} \end{aligned} \quad (3.42)$$

Both the generalized mass matrix and stiffness matrix are diagonal matrices due to the orthogonality properties of normal modes. The original structural damping matrix  $[C]$  in Equation (3.3) is selected to satisfy the orthogonality condition for a structure vibrating in air (Wilson and Penzien, 1972). Detailed derivation of the structural damping matrix  $[C]$  from specified modal damping ratios is provided in Appendix 7.1. It should be noted that the damping matrix  $[C_o]$  is not a diagonal matrix, since  $C_{ij}$  are evaluated through the optimized Equation (3.24). The coupling between damping in the various modes due to off-diagonal terms of  $[C_o]$  must be removed to have an uncoupled set of equations of motion. The procedure used to obtain an optimized diagonal damping matrix  $[C^*]$  is similar to that used to obtain  $[C]$  in Section 3.3. That is, let

$$[C_o]\{\dot{Y}\} = [C^*]\{\dot{Y}\} + \{E'\} \quad (3.43)$$

in which  $[C^*]$  is a diagonal damping matrix and  $\{E'\}$  is an error vector. To minimize the mean square value of each term in  $\{E'\}$ , it requires

$$E \left[ \frac{\partial E_j'^2}{\partial C_{jj}^*} \right] = 2E \left[ \left( \sum_{k=1}^L C_{ojk} \dot{Y}_k - C_{jj}^* \dot{Y}_j \right) (-\dot{Y}_j) \right] = 0$$

from which the coefficients of  $[C^*]$  are obtained

$$C_{jj}^* = \sum_{k=1}^L C_{ojk} \frac{E[\dot{Y}_j \dot{Y}_k]}{E[\dot{Y}_j^2]} \quad (3.44)$$

It can be seen that the above optimization also requires iteration, since the mean products of the generalized response quantities  $\dot{Y}_j$  and  $\dot{Y}_k$  must first be determined, which in turn depend on the solution of the structural system. Therefore, the iterative procedure for the determination of  $C_{jj}^*$  is similar to that for  $C_{jj}$ .

The error vector  $\{E'\}$  can now be dropped from Equation (3.43) so that the coupled damping matrix  $[C_o]$  can be replaced by the diagonal matrix  $[C^*]$  in Equation (3.38)

$$[M^*]\{\ddot{Y}\} + [C^*]\{\dot{Y}\} + [K^*]\{Y\} = \{P^*\} \quad (3.45)$$

which is a set of uncoupled linear differential equations and can be written in the standard form as

$$\ddot{Y}_k + 2\xi_k \omega_k \dot{Y}_k + \omega_k^2 Y_k = \frac{P_k^*}{M_k^*} \quad k = 1, 2, \dots, L \quad (3.46)$$

in which

$$M_k^* = \{\psi_k\}^T [M^a] \{\psi_k\} \quad (3.47)$$

$$\begin{aligned}
P_k^* &= \{\psi_k\}^T \{P^a\} \\
&= \{\psi_k\}^T [A]^T (C_M^o [V] \{\ddot{V}\} + [\bar{C}] \{\dot{V}\} + \frac{1}{2} C_D^o [A_p] \{b\}) \quad (3.48)
\end{aligned}$$

$$\xi_k = \frac{C_{kk}^*}{2M_k^* \omega_k} \quad (3.49)$$

and  $\omega_k$  is the natural circular frequency of the  $k^{\text{th}}$  mode.

Generally, the solution of Equation (3.46) can be obtained by the use of an impulse response function together with the Duhamel integral in the time domain, or by the use of a complex frequency response function together with the Fourier integral in the frequency domain (Crandall and Mark, 1963).

The solution by the Duhamel integral is of the form

$$Y_k(t) = \int_{-\infty}^{\infty} P_k^*(t-\tau) h_k(\tau) d\tau \quad k = 1, 2, \dots, L \quad (3.50)$$

in which

$$h_k(t) = \frac{1}{M_k^* \omega_{dk}} \exp(-\xi_k \omega_k t) \sin(\omega_{dk} t) \quad (3.51)$$

is the unit impulse response function for the  $k^{\text{th}}$  mode and

$$\omega_{dk} = \omega_k (1 - \xi_k^2)^{1/2} \quad (3.52)$$

is the damped natural circular frequency of the  $k^{\text{th}}$  mode.

The solution by the complex frequency response function approach is of the form

$$Y_k(t) = (2\pi)^{-1} \int_{-\infty}^{\infty} H_k(\omega) e^{i\omega t} d\omega \int_{-\infty}^{\infty} P_k^*(\tau) e^{-i\omega\tau} d\tau \quad (3.53)$$

where

$$H_k(\omega) = \frac{1}{M_k^* (\omega_k^2 - \omega^2 + 2i\xi_k \omega_k \omega)} \quad (3.54)$$

is the complex frequency response function, or the transfer function of the system for the  $k^{\text{th}}$  mode.

It has been shown that  $h_k(t)$  and  $H_k(\omega)$  are related by

$$H_k(\omega) = \int_{-\infty}^{\infty} h_k(t) e^{-i\omega t} dt . \quad (3.55)$$

Once  $Y_k(t)$ ,  $k = 1, 2, \dots, L$  are determined, the independent displacement vector  $\{X\}$  can be found from Equation (3.36) or by combining modal contributions from selected first few modes.

### 3.6 Statistics of the Linearized and Transformed System

Since the stationary Gaussian nature of the input force in Equation (3.27) does not change through linear transformations of coordinate, the output of the linearized and transformed Equation (3.31) is also a stationary Gaussian process. The desired statistics of some responses, such as displacement, shear, and moment, can be obtained through the evaluation of their variances and mean values, respectively, for Gaussian processes.

For general application purpose, let  $Z(t)$  represent some response quantities of interest, e.g., displacement, shear, and moment at some location. The general response function  $Z(t)$  at certain location can be described by the generalized coordinate  $Y_k(t)$  through some known coefficients  $B_k$ ,  $k = 1, 2, \dots, L$ . That is

$$Z(t) = \sum_{k=1}^L B_k Y_k(t) \quad (3.56)$$

For example, if  $Z_i(t)$  represents the independent displacement  $X_i(t)$  at node  $i$ , then it can be seen from Equation (3.36) that

$$Z_i(t) = \sum_{k=1}^L \psi_{ik} Y_k(t) . \quad (3.57)$$

Hence the coefficients  $B_k$  in Equation (3.56) are equal to  $\psi_{ik}$  of the modal matrix  $[\psi]$  in this case.

The auto-correlation function  $R_{ZZ}(\tau)$  for the stationary process  $Z(t)$  is

$$\begin{aligned} R_{ZZ}(\tau) &= E[Z(t)Z(t + \tau)] \\ &= \sum_{r=1}^L \sum_{s=1}^L B_r B_s E[Y_r(t)Y_s(t + \tau)] . \end{aligned} \quad (3.58)$$

Substitution of Equation (3.50) into the above equation gives

$$R_{ZZ}(\tau) = \sum_{r=1}^L \sum_{s=1}^L B_r B_s E \left[ \int_{-\infty}^{\infty} \int_{-\infty}^{\infty} P_r^*(t - \theta_1) P_s^*(t + \tau - \theta_2) h_r(\theta_1) h_s(\theta_2) d\theta_1 d\theta_2 \right] \quad (3.59)$$

where  $\theta_1$ ,  $\theta_2$ , and  $\tau$  are dummy time variables. Next, interchanging the order of integration and expectation in Equation (3.59) and using the fact that for the two stationary processes,  $P_r^*(t)$  and  $P_s^*(t)$ ,  $E[P_r^*(t - \theta_1) P_s^*(t + \tau - \theta_2)]$  is just the cross-correlation function  $R_{P_r^* P_s^*}(\tau - \theta_2 + \theta_1)$  with a time lag of  $\tau - \theta_2 + \theta_1$ , one obtains

$$R_{ZZ}(\tau) = \sum_{r=1}^L \sum_{s=1}^L B_r B_s \int_{-\infty}^{\infty} \int_{-\infty}^{\infty} h_r(\theta_1) h_s(\theta_2) R_{P_r^* P_s^*}(\tau - \theta_2 + \theta_1) d\theta_1 d\theta_2 \quad (3.60)$$

The spectral density function  $S_{ZZ}(\omega)$  of the process  $Z(t)$  is the Fourier transform of  $R_{ZZ}(\tau)$ . That is,

$$S_{ZZ}(\omega) = (2\pi)^{-1} \sum_{r=1}^L \sum_{s=1}^L B_r B_s \int_{-\infty}^{\infty} e^{-i\omega\tau} d\tau \int_{-\infty}^{\infty} \int_{-\infty}^{\infty} h_r(\theta_1) h_s(\theta_2) R_{P_r^* P_s^*}(\tau - \theta_2 + \theta_1) d\theta_1 d\theta_2 \quad (3.61)$$

By using the known relation between  $h_k(t)$  and  $H_k(\omega)$  in Equation (3.55),

the above equation becomes

$$S_{ZZ}(\omega) = \sum_{r=1}^L \sum_{s=1}^L B_r B_s \bar{H}_r(\omega) H_s(\omega) S_{P_r^* P_s^*}(\omega) \quad (3.62)$$

where  $\bar{H}_r(\omega)$  is the complex conjugate of  $H_r(\omega)$ .

To calculate  $R_{ZZ}(\tau)$  and  $S_{ZZ}(\omega)$ , the cross-correlation function  $R_{P_r^* P_s^*}(\tau)$  and the cross-spectrum  $S_{P_r^* P_s^*}(\omega)$  should first be determined from the forcing function in Equation (3.48). That is,

$$P_r^*(t) = \{\psi_r\}^T \{P^a(t)\} \quad (3.63)$$

$$P_s^*(t + \tau) = \{P^a(t + \tau)\} \{\psi_s\} \quad (3.64)$$

where  $\{\psi_r\}$  is the column vector corresponding to the  $r^{\text{th}}$  mode shape.

By definition,

$$\begin{aligned} R_{P_r^* P_s^*}(\tau) &= E[P_r^*(t) P_s^*(t + \tau)] \\ &= \{\psi_r\}^T E[\{P^a(t)\} \{P^a(t + \tau)\}^T] \{\psi_s\} \end{aligned} \quad (3.65)$$

$$\text{or} \quad R_{P_r^* P_s^*}(\tau) = \{\psi_r\}^T [R_{P^a P^a}(\tau)] \{\psi_s\} \quad (3.66)$$

The forcing function  $\{P^a\}$  is given in Equation (3.35). Therefore, the matrix  $[R_{P^a P^a}(\tau)]$  in the above equation is expressed as

$$[R_{P^a P^a}(\tau)] = E[\{P^a(t)\} \{P^a(t + \tau)\}^T]$$



$$\begin{aligned}
&= [A]^T (C_M^\rho [\Psi] [R_{\dot{V}\dot{V}}(\tau)] C_M^\rho [\Psi]^T + [\bar{C}] [R_{\dot{V}\dot{V}}(\tau)] [\bar{C}]^T \\
&\quad + C_M^\rho [\Psi] [R_{\ddot{V}\ddot{V}}(\tau)] [\bar{C}]^T + [\bar{C}] [R_{\ddot{V}\ddot{V}}(\tau)] C_M^\rho [\Psi]^T \\
&\quad + \frac{1}{2} C_D^\rho [A_p] \{b\} \{b\}^T \frac{1}{2} C_D^\rho [A_p]^T) [A]. \quad (3.67)
\end{aligned}$$

After taking the Fourier transform of Equation (3.66), the cross spectral density function of the forces is given by

$$S_{P^*P^*}(\omega) = \{\psi_r\}^T [S_{P^*P^*}(\omega)] \{\psi_s\} \quad (3.68)$$

in which  $[S_{P^*P^*}(\omega)]$  can be obtained similarly by taking the Fourier transform of Equation (3.67)

$$\begin{aligned}
[S_{P^*P^*}(\omega)] &= [A]^T (C_M^\rho [\Psi] [S_{\dot{V}\dot{V}}(\omega)] C_M^\rho [\Psi]^T + [\bar{C}] [S_{\dot{V}\dot{V}}(\omega)] [\bar{C}]^T \\
&\quad + C_M^\rho [\Psi] [S_{\ddot{V}\ddot{V}}(\omega)] [\bar{C}]^T + [\bar{C}] [S_{\ddot{V}\ddot{V}}(\omega)] C_M^\rho [\Psi]^T \\
&\quad + \frac{1}{2} C_D^\rho [A_p] \{b\} \{b\}^T \frac{1}{2} C_D^\rho [A_p] \delta(\omega)) [A] \quad (3.69)
\end{aligned}$$

where  $\delta(\omega)$  is the Dirac delta function defined by

$$\int_{-\infty}^{\infty} f(\omega) \delta(\omega) d\omega = f(0) \quad (3.70)$$

In Equations (3.67) and (3.69), values of the cross-correlation functions and cross spectral density functions for fluid particle velocities, such as  $R_{VV}(\tau)$  and  $S_{VV}(\omega)$ , are given in Equations (2.32) to (2.35) and Equations (2.37) to (2.40), respectively. Those cross-correlation terms for fluid particle accelerations, such as  $R_{VV}(\tau)$  and  $S_{VV}(\omega)$ , can be expressed in terms of  $R_{VV}(\tau)$  and  $S_{VV}(\omega)$  as indicated in Equations (2.42) to (2.47).

When the expressions of  $R_{ZZ}(\tau)$  and  $S_{ZZ}(\omega)$  are determined, the mean square value of the response quantity  $Z(t)$  can be found from either

$$E[Z^2(t)] = R_{ZZ}(0) \quad (3.71)$$

or

$$E[Z^2(t)] = \int_{-\infty}^{\infty} S_{ZZ}(\omega) d\omega . \quad (3.72)$$

To find the variance of  $Z(t)$ , i.e.,

$$\sigma_Z^2 = E[Z^2(t)] - E^2[Z(t)], \quad (3.73)$$

it is necessary to determine the expected value  $E[Z(t)]$  of  $Z(t)$ .  $E[Z(t)]$  can be obtained by taking expected values of both sides of Equation (3.56).

$$E[Z(t)] = \sum_{k=1}^L B_k E[Y_k(t)] \quad (3.74)$$

in which  $E[Y_k(t)]$  can be found by taking expected values on both sides

of Equation (3.46). It is noted that in Section 3.3, the relative velocity is defined as  $\dot{r} = \dot{V} - \dot{U}$ , which implies the relation  $E[\dot{U}] = E[\dot{V}] - E[\dot{r}]$ . It has been shown that  $E[\dot{V}] = 0$  and  $E[\dot{r}] = 0$ , therefore  $E[\dot{U}]$  and consequently  $E[\ddot{U}]$  are all equal to zero. Since the vector  $\{Y\}$  is derived through linear transformations of Equations (3.36) and (3.29), it follows that  $E[\dot{Y}] = 0$  and  $E[\ddot{Y}] = 0$ . Considering the above statements and taking the means of Equation (3.46), one obtains

$$E[Y_k(t)] = \frac{1}{M_k^* \omega_k^2} \{\psi_k\}^T [A]^T \frac{1}{2} C_D \rho [A_p] \{b\} . \quad (3.75)$$

### 3.7 Parameters for Optimizing Damping Coefficients

Sections 3.3 to 3.6 formally conclude the discussion of the method of solution of the nonlinear differential equations Equation (3.8) by means of the equivalent linearization technique. However, it is recalled that in the solution procedure, the response quantity  $\sigma_{r_i}$  must be evaluated to determine  $[\zeta]$  and  $\{b\}$  as shown in Equations (3.24) and (3.25). Both  $[\zeta]$  and  $\{b\}$  appear in Equation (3.27) which is the linearized version of Equation (3.8) governing structural responses. Also, the solution of the linearized Equation (3.27) by the normal mode superposition method requires the replacement of the coupled damping matrix  $[C_o]$  in Equation (3.38) by the diagonal damping matrix  $[C^*]$  which depends on knowledge of the response quantities  $E[\dot{Y}_j(t)\dot{Y}_k(t)]$  as indicated in Equation (3.49). Both the quantities  $\sigma_{r_i}$  and  $E[\dot{Y}_j(t)\dot{Y}_k(t)]$  may be derived in much the same manner that statistics of

response quantity  $Z(t)$  is obtained, although the detailed results differ. These derivations are briefly explained in the following.

It is seen from Equation (3.50) that the cross-correlation function  $R_{Y_j Y_k}(\tau)$  of the generalized coordinate  $Y_j(t)$  and  $Y_k(t)$  is

$$\begin{aligned} R_{Y_j Y_k}(\tau) &= \int_{-\infty}^{\infty} \int_{-\infty}^{\infty} E[P_j^*(t - \theta_1)P_k^*(t + \tau - \theta_2)h_j(\theta_1)h_k(\theta_2)]d\theta_1 d\theta_2 \\ &= \int_{-\infty}^{\infty} \int_{-\infty}^{\infty} h_j(\theta_1)h_k(\theta_2)R_{P_j^* P_k^*}(\tau - \theta_2 + \theta_1)d\theta_1 d\theta_2 . \end{aligned} \quad (3.76)$$

The cross-spectrum  $S_{Y_j Y_k}(\omega)$  of the process  $Y_j(t)$  and  $Y_k(t)$  is the Fourier transform of the above equation

$$S_{Y_j Y_k}(\omega) = \bar{H}_j(\omega)H_k(\omega)S_{P_j^* P_k^*}(\omega) \quad (3.77)$$

in which  $S_{P_j^* P_k^*}(\omega)$  is given by Equation (3.68).

By adopting the known relations in Equations (2.44) and (2.47),  $R_{\dot{Y}_j \dot{Y}_k}(\tau)$  and  $S_{\dot{Y}_j \dot{Y}_k}(\omega)$  of the process  $\dot{Y}_j(t)$  and  $\dot{Y}_k(t)$  are respectively

$$R_{\dot{Y}_j \dot{Y}_k}(\tau) = -\frac{\partial^2}{\partial \tau^2} R_{Y_j Y_k}(\tau) \quad (3.78)$$

and

$$S_{\dot{Y}_j \dot{Y}_k}(\omega) = \omega^2 S_{Y_j Y_k}(\omega) . \quad (3.79)$$

Thus, the quantity  $E[\dot{Y}_j(t)\dot{Y}_k(t)]$  can be evaluated by

$$E[\dot{Y}_j(t)\dot{Y}_k(t)] = R_{\dot{Y}_j\dot{Y}_k}(0) = \int_{-\infty}^{\infty} \omega^2 S_{Y_j Y_k}(\omega) d\omega \quad (3.80)$$

To evaluate the response quantity  $\sigma_{\dot{r}_1}$ , it is necessary to use the definition of relative velocity

$$\dot{r}_j(t) = \dot{V}_j(t) - \dot{U}_j(t) \quad (3.81)$$

The auto-correlation function  $R_{\dot{r}_j\dot{r}_j}(\tau)$  of the relative velocity is therefore given by

$$\begin{aligned} R_{\dot{r}_j\dot{r}_j}(\tau) &= E[\dot{r}_j(t)\dot{r}_j(t+\tau)] \\ &= R_{\dot{V}_j\dot{V}_j}(\tau) + R_{\dot{U}_j\dot{U}_j}(\tau) - R_{\dot{U}_j\dot{V}_j}(\tau) - R_{\dot{V}_j\dot{U}_j}(\tau) \end{aligned} \quad (3.82)$$

in which  $R_{\dot{V}_j\dot{V}_j}(\tau)$  is given by Equations (2.32) to (2.35).  $R_{\dot{U}_j\dot{U}_j}(\tau)$  can be evaluated from Equations (3.29) and (3.36). That is

$$\{\dot{U}\} = [A]\{\dot{X}\} = [A][\psi]\{\dot{Y}\} = [W]\{\dot{Y}\} \quad (3.83)$$

or

$$\dot{U}_j(t) = \sum_{k=1}^L W_{jk} \dot{Y}_k(t) \quad (3.84)$$

Hence

$$R_{\dot{U}_j\dot{U}_j}(\tau) = \sum_{i=1}^L \sum_{k=1}^L W_{ji} W_{jk} R_{\dot{Y}_k\dot{Y}_i}(\tau) \quad (3.85)$$

in which  $[W] = [A][\psi]$  is a matrix with coefficients similar to  $B_k$  of Equation (3.56).

The last two terms of Equation (3.82) can be written respectively as

$$R_{\dot{U}_j \dot{V}_j}(\tau) = \sum_{k=1}^L W_{jk} E[\dot{Y}_k(t) \dot{V}_j(t + \tau)] = \sum_{k=1}^L W_{jk} R_{\dot{Y}_k \dot{V}_j}(\tau) \quad (3.86)$$

and

$$R_{\dot{V}_j \dot{U}_j}(\tau) = \sum_{k=1}^L W_{jk} E[\dot{V}_j(t) \dot{Y}_k(t + \tau)] = \sum_{k=1}^L W_{jk} R_{\dot{V}_j \dot{Y}_k}(\tau) \quad (3.87)$$

Thus, Equation (3.82) becomes

$$\begin{aligned} R_{\dot{r}_j \dot{r}_j}(\tau) &= R_{\dot{V}_j \dot{V}_j}(\tau) + \sum_{i=1}^L \sum_{k=1}^L W_{ji} W_{jk} R_{\dot{Y}_k \dot{Y}_i}(\tau) \\ &\quad - \sum_{k=1}^L W_{jk} [R_{\dot{Y}_k \dot{V}_j}(\tau) + R_{\dot{V}_j \dot{Y}_k}(\tau)] \end{aligned} \quad (3.88)$$

in which

$$R_{\dot{V}_j \dot{Y}_k}(\tau) = R_{\dot{Y}_k \dot{V}_j}(-\tau) \quad (3.89)$$

$$R_{\dot{Y}_k \dot{V}_j}(\tau) = -\frac{\partial}{\partial \tau} R_{\dot{Y}_k \dot{V}_j}(\tau) \quad (3.90)$$

$$\begin{aligned}
\text{and } R_{\dot{Y}_k \dot{V}_j}(\tau) &= E \left[ \int_{-\infty}^{\infty} h_k(\theta) P_k^*(t - \theta) d\theta \dot{V}_j(t + \tau) \right] \\
&= E \left[ \int_{-\infty}^{\infty} h_k(\theta) \{\psi_k\}^T [A]^T (C_M^p [V]) \{\dot{V}(t - \theta)\} \right. \\
&\quad \left. + [\bar{C}] \{\dot{V}(t - \theta)\} + \frac{1}{2} C_D^p [A_p] \{b\} \dot{V}_j(t + \tau) d\theta \right] \\
&= \int_{-\infty}^{\infty} h_k(\theta) \{\psi_k\}^T [A]^T (C_M^p [V]) \{R_{\dot{V}_j}(\tau + \theta)\} \\
&\quad + [\bar{C}] \{R_{\dot{V}_j}(\tau + \theta)\} d\theta . \quad (3.91)
\end{aligned}$$

By taking the Fourier transform of Equations (3.88) to (3.91), the corresponding spectral density functions are readily found

$$\begin{aligned}
S_{\dot{r}_j \dot{r}_j}(\omega) &= S_{\dot{V}_j \dot{V}_j}(\omega) + \sum_{i=1}^L \sum_{k=1}^L W_{ji} W_{jk} S_{\dot{Y}_k \dot{Y}_i}(\omega) \\
&\quad - \sum_{k=1}^L W_{jk} [S_{\dot{Y}_k \dot{V}_j}(\omega) + S_{\dot{V}_j \dot{Y}_k}(\omega)] \quad (3.92)
\end{aligned}$$

in which

$$S_{\dot{V}_j \dot{Y}_k}(\omega) = \bar{S}_{\dot{Y}_k \dot{V}_j}(\omega) \quad (3.93)$$

$$S_{\dot{Y}_k \dot{V}_j}(\omega) = -i\omega S_{\dot{Y}_k \dot{V}_j}(\omega) \quad (3.94)$$

$$\text{and } S_{Y_k \dot{V}_j}(\omega) = \bar{H}_k(\omega) \{\psi_k\} [A]^T (C_M^{\rho} [V] \{S_{\dot{V}_j}(\omega)\} + [\bar{C}] \{S_{\dot{V}_j}(\omega)\}) \quad (3.95)$$

where  $\bar{S}_{Y_k \dot{V}_j}(\omega)$  is the complex conjugate of  $S_{Y_k \dot{V}_j}(\omega)$ .

Since  $E[\dot{r}] = 0$ , the variance of the relative velocity is simply

$$\sigma_{\dot{r}_j}^2 = E[\dot{r}_j^2] = R_{\dot{r}_j \dot{r}_j}(0) = \int_{-\infty}^{\infty} S_{\dot{r}_j \dot{r}_j}(\omega) d\omega \quad (3.96)$$

### 3.8 Peak Value Statistics

The analysis procedures of this study for the response of offshore structures have been, so far, in deriving expressions of the mean, correlation function, spectrum, and variance of structural responses such as the displacement, shear, and bending moment. These statistical properties provide all the information required to describe a Gaussian process. It is now shown how this information can be used to answer various questions of practical importance such as: What maximum displacements, shear forces, and bending moments are likely to occur in the structure? How frequently is a quantity of interest likely to exceed a prescribed value? Some mathematical expressions which assist in answering these questions are given below.

Consider a stationary random function  $Z$  which has a Gaussian probability distribution with mean  $E[Z]$  and standard deviation  $\sigma_Z$ . It is convenient to define the variable  $\bar{\eta} = (Z - E[Z])/\sigma_Z$ . In this case the



probability density function of  $\bar{\eta}$  is

$$P(\bar{\eta}) = (2\pi)^{-1/2} \exp\left(-\frac{1}{2} \bar{\eta}^2\right). \quad (3.97)$$

The cumulative probability distribution function,  $Q(\eta')$ , will be defined as the probability of the function not exceeding some value  $\eta'$ . That is

$$Q(\eta') = \int_{-\infty}^{\eta'} P(\bar{\eta}) d\bar{\eta}. \quad (3.98)$$

It was shown (Rice, 1945) that, for a prescribed period  $T$ , the expected number of times that a peak (or largest, extreme) value  $\bar{\eta}_{\max}$  is intercepted with positive slope is

$$N(\bar{\eta}_{\max}) = \nu T \exp\left(-\frac{1}{2} \bar{\eta}_{\max}^2\right) \quad (3.99)$$

where  $\nu$  is given by

$$\nu = \frac{1}{2\pi} \left[ \frac{\int_{-\infty}^{\infty} \omega^2 S_{ZZ}(\omega) d\omega}{\int_{-\infty}^{\infty} S_{ZZ}(\omega) d\omega} \right]^{1/2} \quad (3.100)$$

When  $\bar{\eta}_{\max}$  is large, the occurrence of such interceptions constitutes a rare event. Therefore, the Poission distribution may be used to estimate the probability that there are given numbers of interceptions larger than some value  $\bar{\eta}_{\max}$  during the same period  $T$  (Davenport, 1964).

For this distribution, the probability of getting exactly  $r$  interceptions is

$$\exp(-N) \frac{N^r}{r!} \quad r = 0, 1, \dots \quad (3.101)$$

where  $N$  is the expected or the average number of interceptions in the duration  $T$ . The probability that there are no interceptions (*i.e.*,  $r = 0$ ) is also the probability that the largest value must be less than  $\bar{n}_{\max}$ . Thus it is seen from Equations (3.98) and (3.101) that

$$Q(\bar{n}_{\max}) = \exp[-N(\bar{n}_{\max})] \quad (3.102)$$

and upon substitution of Equation (3.99), the probability density function for the peak value  $\bar{n}_{\max}$  is

$$\begin{aligned} P(\bar{n}_{\max}) &= \frac{d}{d\bar{n}_{\max}} Q(\bar{n}_{\max}) \\ &= \frac{d}{d\bar{n}_{\max}} \exp[-vT \exp(-\frac{1}{2} \bar{n}_{\max}^2)] \quad (3.103) \end{aligned}$$

which can be used to evaluate the mean and variance of  $\bar{n}_{\max}$ . That is

$$\begin{aligned} E[\bar{n}_{\max}] &= \int_{-\infty}^{\infty} \bar{n}_{\max} P(\bar{n}_{\max}) d\bar{n}_{\max} \\ E[\bar{n}_{\max}^2] &= \int_{-\infty}^{\infty} \bar{n}_{\max}^2 P(\bar{n}_{\max}) d\bar{n}_{\max} \end{aligned}$$

and

$$\sigma_{\bar{\eta}_{\max}}^2 = E[\bar{\eta}_{\max}^2] - E^2[\bar{\eta}_{\max}] .$$

The above statistical quantities were found (Davenport, 1964; Cartwright and Longuet-Higgins, 1956) to have the following expressions.

$$E[\bar{\eta}_{\max}] = (2 \log_e \nu T)^{1/2} + 0.5772(2 \log_e \nu T)^{-1/2} \quad (3.104)$$

$$\sigma_{\bar{\eta}_{\max}} = \pi(6)^{-1/2} (2 \log_e \nu T)^{-1/2} . \quad (3.105)$$

It is noticed that the distribution of the peak values is related to the product  $\nu T$ . When the value of  $\nu T$  becomes large,  $\sigma_{\bar{\eta}_{\max}}$  becomes small, therefore, a narrow distribution results. Usually the storm duration in the ocean is very long, thus for most practical problems, it is sufficient to assume the mean peak value of structural response as the peak (or largest) value of structural response and ignore the variability. Hence the actual peak value, when referred to the true origin of  $Z$ , can then be written as

$$Z_{\text{peak}} = E[Z] + \sigma_Z [(2 \log_e \nu T)^{1/2} + 0.5772(2 \log_e \nu T)^{-1/2}] . \quad (3.106)$$

## 4. CASE STUDIES

### 4.1 Idealized Structural Properties and Force Parameters

In this chapter, four offshore towers with individual heights of 475, 675, 875, and 1075 feet corresponding to water depth of 400, 600, 800, and 1000 feet respectively are analyzed by using the method developed in chapter 3. These towers were previously examined by Penzien et al., (1972). The structural details are therefore not given here and only the pertinent properties of the idealized structures of these towers are presented.

All four towers are idealized as two-dimensional structures as shown in Figure 4.1. Since the orientation of the flow is assumed in the direction of the x-axis, the analysis can be treated as two-dimensional on the x-y plane. The origin of the structure and fluid system is selected at the mean water level with the y-axis vertically upward. A lumped mass model with a reduced coordinate system is used in the dynamic analysis. This model has one dynamic degree of freedom at each framing level along the x-axis. For such a lumped mass model, the proper value of mass must be assigned to each degree of freedom. The procedure used is equivalent to partitioning the structure at mid-framing levels, computing all of the masses contained within that range, and assigning the total mass to the degree of freedom encircled by the range. The total dynamic lumped mass includes the mass of structure and equipment, enclosed water in flooded members, and added hydrodynamic mass.

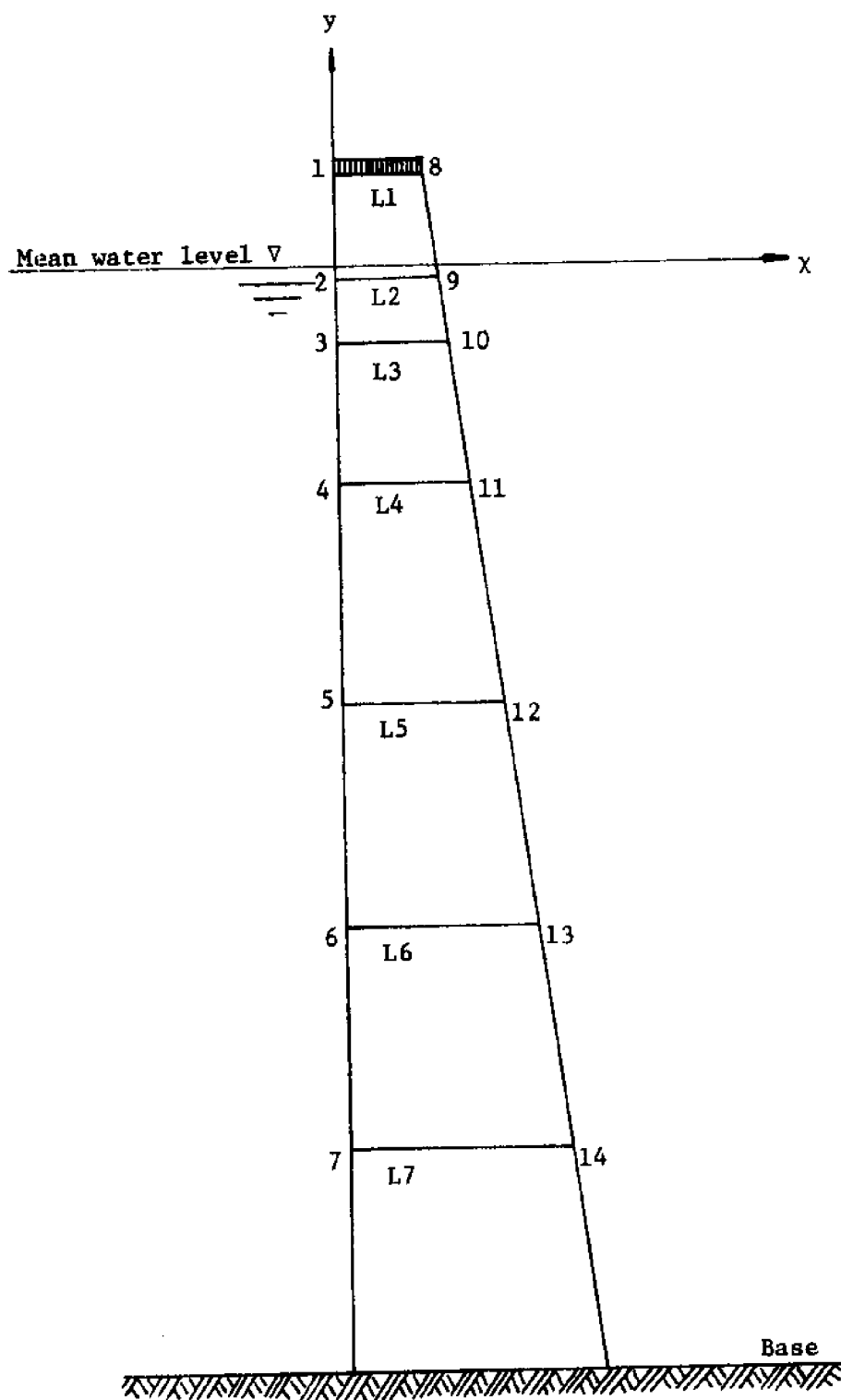


Figure 4.1. Idealized tower used in case studies

The flexibility matrix is determined by applying a series of unit lateral loads to the original structure at the levels for which dynamic degrees of freedom have been specified. The full set of lateral displacements obtained separately for unit loads at levels  $i = 1, 2, \dots, L$  yields an  $L \times L$  flexibility matrix, which when inverted gives the corresponding  $L \times L$  stiffness matrix. In the following case studies, the structural data given by Penzien et al., (1972) are based on a structure with lumped masses at the seven levels (i.e.,  $L = 7$  in Eq. (3.29)) instead of at the fourteen nodal points ( $N = 14$ ). This means that the given mass and flexibility matrices are the transformed matrices,  $[A]^T [M] [A]$  and  $[k^a]^{-1}$  respectively, with dimensions  $7 \times 7$  as indicated by the relationship in Equations (3.32) and (3.34). For the kind of numbering sequence of the idealized tower shown in Figure 4.1, the transformation matrix  $[A]$  in Equation (3.29) is a  $14 \times 7$  matrix of the form

$$[A] = \begin{bmatrix} [I] \\ -[I] \end{bmatrix} \quad (4.1)$$

where the submatrix  $[I]$  is a  $7 \times 7$  identity matrix.

Although the masses are given at the seven levels, the wave forces should be computed at each of the fourteen nodal points—two locations at each level, since the wave forces are different at the two nodes, even though they are at the same level. In the following computation, the drag coefficient  $C_D$  and inertia coefficient  $C_M$  are assumed to be 1.4 and 2.0 respectively, and the density of sea water  $\rho$  is  $2.0 \times 10^{-3}$  kip. sec<sup>2</sup>/ft<sup>4</sup>. The wave force parameters,  $C_M \rho V$  and  $\frac{1}{2} C_D \rho A_p$ , are accordingly evaluated at nodal points before the transformation to independent coordinates is performed.

The numbering sequence of the floor level is from top to bottom. For example, the third level L3 connects node 3 and node 10 as shown in Figure 4.1. General information on structural properties and wave force parameters for the four towers considered are summarized in Tables 4.1 (a), 4.2 (a), 4.3 (a), and 4.4 (a). Units used in these tables are:  $x$  and  $y$  in feet, mass  $M$  at each level in  $\text{kip} \cdot \text{sec}^2/\text{ft}$ ,  $C_M \rho V$  in  $\text{kip} \cdot \text{sec}^2/\text{ft}$ , and  $\frac{1}{2} C_D \rho A_p$  in  $\text{kip} \cdot \text{sec}^2/\text{ft}^2$ . Because node 1 and node 8 are above the mean water level, their enclosed volumes and projected areas need not be calculated and values of  $C_M \rho V$  and  $\frac{1}{2} C_D \rho A_p$  are set to zero for these nodes. The flexibility matrices  $[K^a]^{-1}$  for these towers are also included in Tables 4.1(b), 4.2(b), 4.3(b), and 4.4(b). Tables 4.1 to 4.4 are reproduced from those previously used by Penzien et al., (1972).

#### 4.2 Results and Discussions of Computer Solution

From the information on structural mass and flexibility matrices  $[A]^T [M] [A]$  and  $[K^a]^{-1}$ , the eigenvalues and eigenvectors of the undamped free vibrating structure in air can be determined. These free vibration modal frequencies and mode shapes are used to generate the transformed damping matrix  $[A]^T [C] [A]$ , by assigning modal damping ratios of 0.05 for all seven modes of the tower standing in air. The technique of numerical evaluation of an orthogonal damping matrix (Wilson and Penzien, 1972) is provided in Appendix 7.1. Listed in Tables 4.5 to 4.8 are the generated transformed structural damping matrices for Towers 1 to 4, respectively.

Table 4.1(a). Structural properties for Tower 1 (Height = 475 ft.)

Level	y	M	Node	x	$C_M^{pV}$	$\frac{1}{2}C_D^{pA}$	Node	x	$C_M^{pV}$	$\frac{1}{2}C_D^{pA}$
1	75	330	1	0	0	0	8	80	0	0
2	-10	101	2	0	78.4	12.4	9	88.7	41	4.1
3	-75	89.2	3	0	73.6	10.7	10	98.1	41	3.4
4	-140	105	4	0	82.8	11.1	11	107.5	50	3.9
5	-205	126	5	0	104	11.5	12	116.8	71.6	4.3
6	-270	151	6	0	124	12.3	13	126.2	91.8	5.0
7	-335	256	7	0	253	23.3	14	135.5	222	9.2

Table 4.1(b). Flexibility matrix for Tower 1

$[k^a]^{-1} =$

288	207	149	101	60	29.8	9.4
189	140	97.5	61.5	32.3	11.3	
	136	96	62	34.7	12.7	
		97	64	36.8	14.1	
			67.5	40.3	15.4	
				43.9	18.0	
					18.3	

Sym.

$\times 10^{-6} \text{ ft/kip}$







Table 4.4(a). Structural properties for Tower 4 (Height = 1075 ft.)

Level	y	M	Node	x	$C_M^{PV}$	$\frac{1}{2}C_D^{PA}$	Node	x	$C_M^{PV}$	$\frac{1}{2}C_D^{PA}$
1	75	330	1	0	0	0	8	80	0	0
2	-10	101	2	0	79.9	17.4	9	88.7	35.1	3.1
3	-75	146	3	0	123	22.9	10	98.1	64.5	4.3
4	-205	383	4	0	284	37.6	11	116.8	187	9.3
5	-400	537	5	0	437	51.3	12	145	320	13.5
6	-600	665	6	0	550	54	13	174	431	15.8
7	-800	1197	7	0	957	63.8	14	203	838	24.5

Table 4.4(b). Flexibility matrix for Tower 4

$[k]^{-1} =$

756	622	531	374	210	98.2	30.8
568	491	357	209	102	33.6	35.8
464	344	207	105	40.1	46.5	53.2
321	205	203	118	126	58.8	
Sym.						

$\times 10^{-6}$  ft/kip

Table 4.5. Transformed structural damping matrix --- Tower 1

$$[A]^T [C] [A] = \begin{bmatrix} 172.73 & -85.23 & -18.01 & -9.22 & 0.63 & 1.24 & 4.05 \\ & 198.07 & 64.13 & 12.95 & 9.87 & 0.49 & 2.07 \\ & & 192.33 & -63.73 & -11.06 & -7.23 & -1.49 \\ & & & 215.21 & -73.46 & -11.05 & -7.72 \\ & & & & 250.11 & -88.47 & -8.35 \\ & & & & & 295.30 & -109.91 \\ & & & & & & 463.62 \end{bmatrix} \frac{\text{kip} \cdot \text{sec}}{\text{ft.}}$$

Sym.

Table 4.6. Transformed structural damping matrix --- Tower 2

155.05	-78.46	-20.14	-15.00	1.03	1.90	1.82
186.76	-63.32	-19.37	-8.80	-0.51	-0.29	
192.19	-74.35	-14.77	-3.22	0.31		
225.10	-68.29	-13.26	-1.11			
269.83	-93.95	-10.64				
	331.23	-88.13				
		563.92				

Sym.

$[A]^T [C] [A] =$

$\frac{\text{kip} \cdot \text{sec}}{\text{ft.}}$

Table 4.7. Transformed structural damping matrix -- Tower 3

$$[A]^T [C] [A] = \begin{bmatrix} 152.43 & -79.01 & -30.43 & -13.00 & 0.54 & 3.53 & 2.07 \\ 188.35 & 208.30 & -75.53 & -19.24 & -2.00 & -0.77 & 0.94 \\ 268.21 & -73.81 & -7.16 & -2.40 & 0.84 \\ 323.52 & -88.39 & -13.90 & -4.10 \\ 353.43 & -126.18 & -13.11 \\ 572.57 \end{bmatrix} \frac{\text{kip} \cdot \text{sec}}{\text{ft.}}$$

Sym.

Table 4.8. Transformed structural damping matrix -- Tower 4

	151.13	-80.00	-32.04	-14.65	0.05	3.08	2.40
		189.44	-76.46	-19.08	-5.50	0.93	0.59
			209.51	-74.28	-8.80	-3.64	0.70
				263.54	-95.30	-13.71	-3.12
					307.35	-109.45	-17.83
						362.13	-127.88
							547.37

Sym.

$\frac{\text{kip} \cdot \text{sec}}{\text{ft.}}$

The modal frequencies and mode shapes of the undamped freely vibrating structure in water are determined using the relation

$$[k^a] [\psi] = [M^a] [\psi] [\omega_n^2]$$

in which  $[k^a]$  is obtained from the inverse of the given structural flexibility matrix, and the evaluation of  $[M^a]$  is given by Equation (3.32).

The modal frequencies computed for each tower standing in water are given in Table 4.9. For comparison, the fundamental frequencies of each tower standing in air and in water are listed in Table 4.10, which agrees with results obtained by Penzien et al. (1972). The modal matrices for each tower vibrating in water are given in Tables 4.11, 4.12, 4.13, and 4.14 respectively.

All relevant characteristics of structures having been obtained, it is possible now to calculate the structural response to any specified wave surface spectrum and superimposed currents. The Kitaigorodskii-Pierson-Moskowitz spectrum for surface wave elevation is selected for this study. It is noted from Equation (2.17) that this spectrum, in fully developed wind-generated seas, is a function of the mean wind velocity only. In this study, three different mean wind velocities at 50, 75, and 100 ft/sec are chosen to calculate the structural responses of each tower. Also, for each wind velocity, the structural responses of each tower are calculated with the presence of a steady and uniform current varying from 0 ft/sec (no current) to 4 ft/sec by increment of 1 ft/sec.

The required statistics of the structural response may be obtained by either of the following two methods. The first uses the autocorrelation



Table 4.9. Modal frequencies (rad/sec) for Towers 1,2,3, and 4

Mode	Tower 1	Tower 2	Tower 3	Tower 4
1	2.593	1.851	1.421	1.155
2	6.074	3.958	2.905	2.201
3	10.547	7.273	5.321	3.663
4	14.325	9.829	6.815	5.174
5	17.964	11.019	8.407	6.532
6	21.129	14.630	10.439	10.546
7	24.357	22.050	18.777	18.914

Table 4.10. Comparison of fundamental frequencies (rad/sec) for towers vibrating in water and in air

	Tower 1	Tower 2	Tower 3	Tower 4
In water	2.593	1.851	1.421	1.155
In air	2.813	2.086	1.644	1.369

Table 4.11. Modal matrix — Tower 1

$$[\psi] = \begin{bmatrix} .6500 & -.3759 & .2938 & .2020 & -.1299 & .0676 & -.0482 \\ .5194 & -.0023 & -.3021 & -.5112 & .5926 & -.4657 & .3665 \\ .4070 & .2726 & -.5561 & -.4595 & -.0214 & .5075 & -.6340 \\ .2993 & .4610 & -.4365 & .1569 & -.6231 & .0979 & .5444 \\ .1968 & .5393 & -.0357 & .5410 & .1076 & -.5062 & -.3528 \\ .1099 & .4704 & .3922 & .1283 & .4170 & .4781 & .1939 \\ .0400 & .2445 & .4093 & -.3911 & -.2403 & -.1630 & -.0537 \end{bmatrix}$$

Table 4.12. Modal matrix — Tower 2

$$[\psi] = \begin{bmatrix} .5945 & -.5746 & -.4013 & -.2862 & .0923 & .2215 & .6346 \\ .5048 & -.2268 & .1135 & .2825 & -.1155 & -.7590 & -.5492 \\ .4344 & .0241 & .4088 & .5070 & -.1871 & -.3715 & .8091 \\ .3652 & .2458 & .5581 & .4618 & -.1276 & .4809 & -.1991 \\ .2327 & .5427 & .2403 & -.5260 & .3251 & -.0739 & .0120 \\ .1217 & .4916 & -.4810 & .1070 & -.4734 & .0062 & -.0009 \\ .0271 & .1458 & -.2417 & .2826 & .7727 & .0004 & .0010 \end{bmatrix}$$

Table 4.13. Modal matrix -- Tower 3

$$[\psi] = \begin{bmatrix} .5761 & -.6153 & -.5577 & -.2989 & .1832 & -.3610 & -.1453 \\ .5110 & -.3663 & -.1051 & .0541 & -.1228 & .4851 & .8804 \\ .4606 & -.1774 & .2103 & .2733 & -.2669 & .7423 & -.4506 \\ .3600 & .1734 & .6146 & .4039 & -.1465 & -.2770 & .0281 \\ .2174 & .4640 & .0447 & -.5176 & .5480 & .0733 & -.0013 \\ .1298 & .4319 & -.4021 & -.0495 & -.6517 & -.0346 & -.0003 \\ .0325 & .1542 & -.3037 & .6321 & .3657 & .0117 & .0001 \end{bmatrix}$$

Table 4.14. Modal matrix -- Tower 4

$$[\psi] = \begin{bmatrix} .5418 & -.6253 & .6033 & -.5025 & .4088 & .3694 & -.1440 \\ .4942 & -.4416 & .2902 & -.1086 & -.0282 & -.4868 & .8804 \\ .4570 & -.3029 & .0682 & .1582 & -.3303 & -.7464 & -.4510 \\ .3822 & -.0345 & -.3322 & .5529 & -.5573 & .2610 & .0287 \\ .2737 & .2742 & -.4817 & .0933 & .5720 & -.0359 & -.0036 \\ .1660 & .4023 & -.0218 & -.5746 & -.2859 & .0067 & .0016 \\ .0692 & .2899 & .4520 & .2571 & .0591 & -.0010 & -.0001 \end{bmatrix}$$

function  $R_{ZZ}(\tau)$  through the time domain as indicated in Equation (3.71). The second uses the response spectrum  $S_{ZZ}(\omega)$  through integration in the frequency domain as indicated in Equation (3.72). These two different approaches give identical results for specific mean square values. Since the frequency domain approach is computationally more convenient, it is used in this study.

It is recalled that two types of iteration are required in the procedure. One type of iteration arises in the computation of the optimal damping coefficients of  $[\zeta]$  which requires the evaluation of the quantity  $\sigma_{\dot{y}_i}$  at each nodal point. The other type of iteration is for the computation of the optimal diagonal damping coefficients of  $[C^*]$  which requires the evaluation of the quantity  $E[\dot{Y}_j \dot{Y}_k]$  of the generalized coordinates. In the main computer program, the quantity  $\sigma_{\dot{y}_i}$  and  $E[\dot{Y}_j \dot{Y}_k]$  are assigned initial values of unity to begin the iteration. Subsequent revisions of coefficients of  $[\zeta]$  and  $[C^*]$  are performed by using Equations (3.24) and (3.44) respectively. In each cycle of iteration, imbalance ratios of consecutive terms such as  $|(c_{jj}^{n+1} - c_{jj}^n)/c_{jj}^n|$  and  $|(c_{jj}^{*n+1} - c_{jj}^{*n})/c_{jj}^{*n}|$  are formed. When all these imbalance ratios are less than some specified tolerance limit, chosen to be 0.05 in this study, the process of iteration is terminated.

It is noted from Equation (3.72) that the mean square value of structural response theoretically requires integration of the corresponding response spectrum over the frequency range  $-\infty < \omega < \infty$ . However, for numerical integration purpose, a finite frequency domain with cut-off points must be used since most response spectra become extremely small at moderate frequencies, beyond which the energy content

is insignificant. For the three wind speeds considered, the cut-off frequencies  $\omega_{\text{begin}}$  and  $\omega_{\text{end}}$  are shown in Table 4.15. The numerical integration is by means of the trapezoidal rule, and the length and number of subintervals for each wind speed are also shown in Table 4.15.

Table 4.15. Range of numerical integration for 50, 75, and 100 ft/sec wind

Wind ft/sec	$\omega_{\text{begin}}$ rad/sec	$\omega_{\text{end}}$ rad/sec	$\Delta\omega$ rad/sec	No of intervals
50	0.20	1.50	0.050	26
75	0.20	1.00	0.025	32
100	0.15	0.75	0.020	30

For the idealized seven-degree-of-freedom tower analyzed, there are seven mode shapes which correspond to the seven modal frequencies to characterize the dynamic response of the tower. However, the more mode shapes used in the response analysis, the more computer time is required. It is important that reasonable number of modes be used to adequately describe the response without spending too much computer time. To determine the number of modes necessary for desired accuracy without undue computer expense, Tower 1 is selected as a test example. Table 4.16(a) shows the effect of including the first one, two, three, four, five, six, and seven modes of vibration on the standard deviations of

Table 4.16(a). Comparison of standard deviations of displacement with various modes included - Tower 1,  $W = 50$  ft/sec,  $V_c = 0$

No. of mode included	Standard deviations of displacement ( $10^{-1}$ ft) at level						
	1	2	3	4	5	6	7
1	.620	.495	.388	.286	.188	.105	.038
2	.603	.495	.401	.307	.213	.127	.050
3	.594	.505	.419	.321	.214	.114	.037
4	.589	.518	.430	.317	.201	.111	.046
5	.586	.528	.430	.307	.202	.118	.043
6	.586	.532	.427	.307	.207	.114	.044
7	.586	.533	.423	.310	.205	.115	.044

Table 4.16(b). Comparison of standard deviations of bending moment with various modes included - Tower 1,  $W = 50$  ft/sec,  $V_c = 0$

No. of mode included	Standard deviations of moment ( $10^{-3}$ kip · ft) at level						
	1	2	3	4	5	6	7
1	11.7	24.1	39.0	56.1	74.9	94.9	94.9
2	10.1	21.2	35.2	52.1	72.0	94.5	119.1
3	7.1	17.1	31.8	51.3	74.0	96.6	116.9
4	4.3	14.7	32.2	53.5	74.2	93.9	117.3
5	2.4	14.6	33.7	53.1	72.6	94.8	116.7
6	1.8	15.1	33.8	52.3	73.4	94.4	117.0
7	1.5	15.6	33.2	52.6	73.1	94.4	116.8

Table 4.16(c). Comparison of standard deviations of shear force with various modes included - Tower 1,  $W = 50$  ft/sec,  $V_c = 0$

No. of mode included	Standard deviations of shear ( $10^4$ kip) at level						
	1	2	3	4	5	6	7
1	1.38	1.91	2.29	2.62	2.89	3.08	3.20
2	1.18	1.71	2.16	2.61	3.08	3.47	3.82
3	.83	1.54	2.28	3.01	3.50	3.52	3.13
4	.50	1.62	2.70	3.29	3.20	3.06	3.63
5	.29	1.89	2.96	3.00	3.03	3.43	3.41
6	.21	2.08	2.88	2.87	3.27	3.25	3.50
7	.17	2.21	2.73	2.99	3.17	3.30	3.48

displacement at each level--for Tower 1 under 50 ft/sec wind and zero current velocity. Tables 4.16(b) and 4.16(c) give respectively the standard deviations of bending moment and shear of the same tower using one to seven modes.

It is seen from these tables that the tower responds essentially in the first mode to the random forces. However, the relative importance of higher modes is also observed for bending moment and shear. This is due to the fact that computations of bending moment and shear involve the differentiations of the expressions for dynamic deflection (Biggs, 1964). In this investigation the first five modes are used in the dynamic response analysis. Convergence of the iteration process is achieved in one to three cycles by using the first five modes. The computer run time depends on the height of tower and the velocities of wind and current. It takes approximately 1/2 to 1 minute central processor unit time on an IBM 370/165 computer to obtain the response quantities of a tower under one wind and current condition.

The structural response quantities obtained are the means, standard deviations, and peak values of displacement, shear, and bending moment. Since the designer is more interested in the peak value (maximum response) that might occur during a storm among other statistics, only the peak values are presented in the following figures. The peak values of displacement, shear, and bending moment are computed according to Equation (3.106) with an assumed 4 hour storm duration. That is,  
$$T = (4)(60)^2 \text{ seconds.}$$

The results presented first are the structural responses calculated without considering the wave-current interactions effect. The structural



responses obtained with the effect of wave-current interactions included are presented and compared at the end of this section.

For a mean wind speed of 50 ft/sec, Figures 4.2(a) to 4.2(d) show respectively the peak displacement responses of the Towers 1 to 4, with the current velocity  $V_c$  of 0, 2, and 4 ft/sec as the parameter. While it is unusual that current velocity would reach values as high as 4 ft/sec, for the purpose of parametric study  $V_c = 4$  ft/sec is included. Since wave-current interactions are not included in the analysis, these figures give only the cases of positive current velocity. The cases of negative current velocity ( $V_c < 0$ ) are merely the mirror image of those presented curves associated with positive current velocity ( $V_c > 0$ ).

Under the same wind speed of 50 ft/sec, the distributions of peak total transverse shear for Towers 1, 2, 3, and 4 are shown in Figures 4.3(a), 4.3(b), 4.3(c), and 4.4(d) respectively. The distributions of peak total overturning moment for the four towers are shown in Figures 4.4(a), 4.4(b), 4.4(c), and 4.4(d). These responses are calculated according to the method given in Appendix 7.2 for computation of total transverse shear and bending moment. Three cases, with different current velocities  $V_c = 0, 2, \text{ and } 4$  ft/sec, are shown in each figure.

These figures (Figures 4.2, 4.3, and 4.4) indicate, as expected, that peak responses increase with increase in current speed, not linearly but in an accelerated manner. This is more vividly seen if the responses are plotted against current speed. Thus, in Figures 4.5, 4.6, and 4.7 the peak deck displacement, peak base shear, and peak base moment for wind

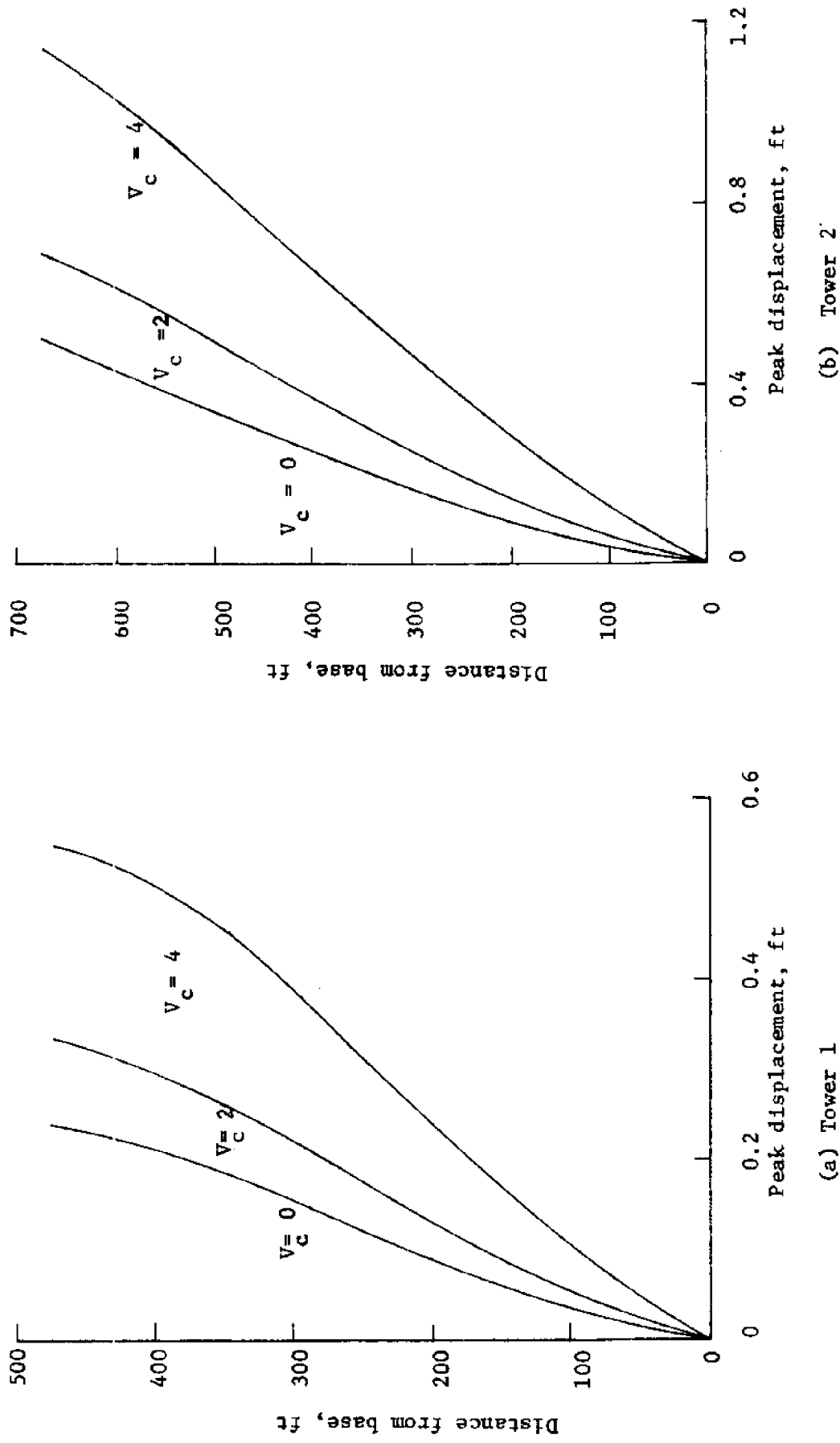
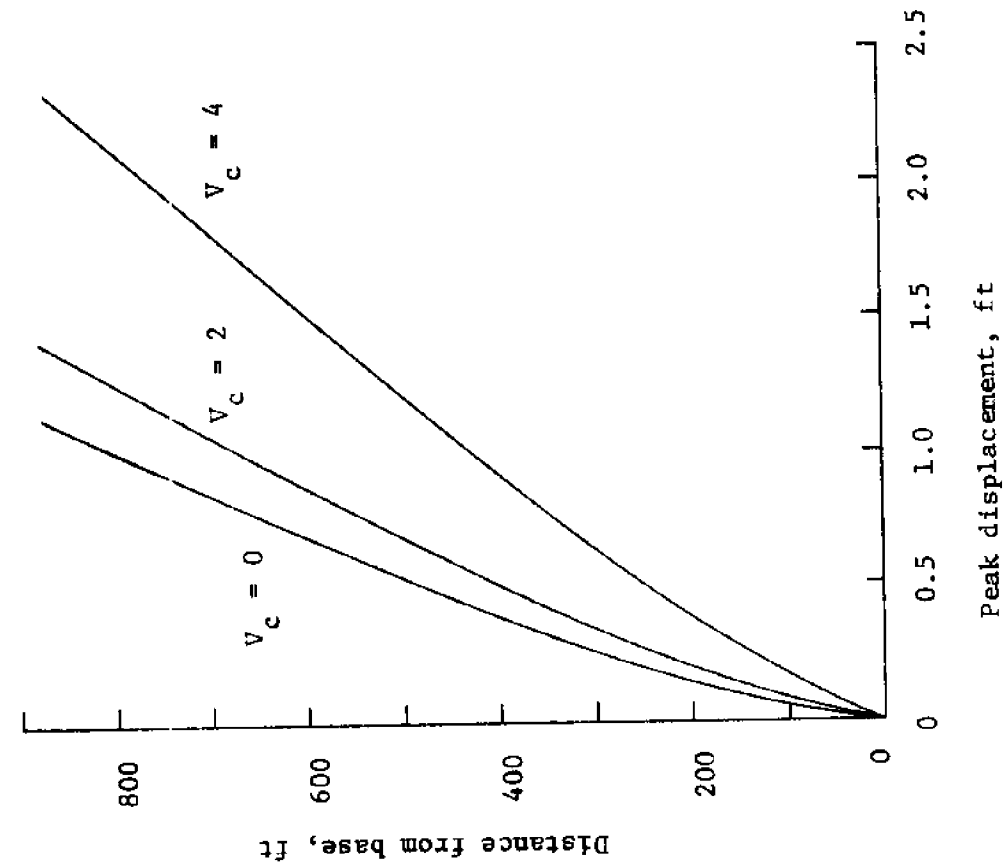
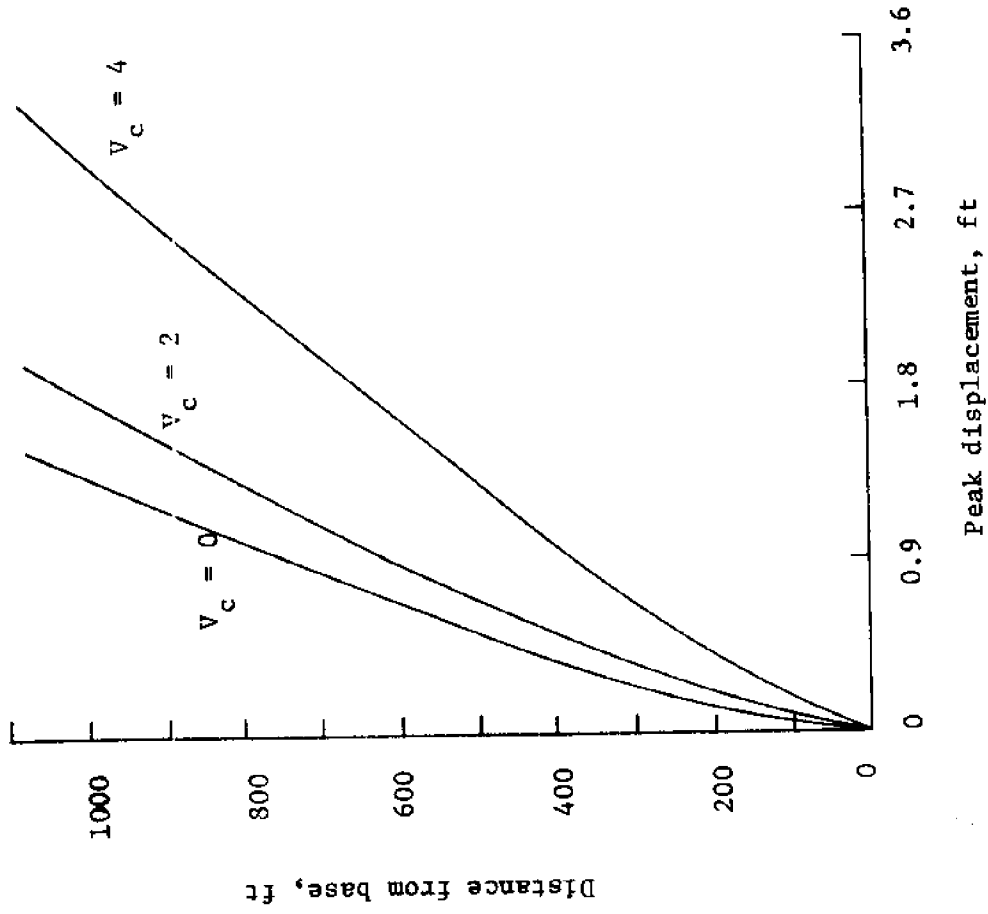


Figure 4.2. Peak displacements: current velocities  $V_c = 0, 2, \text{ and } 4 \text{ ft/sec}$ ;  $50 \text{ ft/sec}$  wind

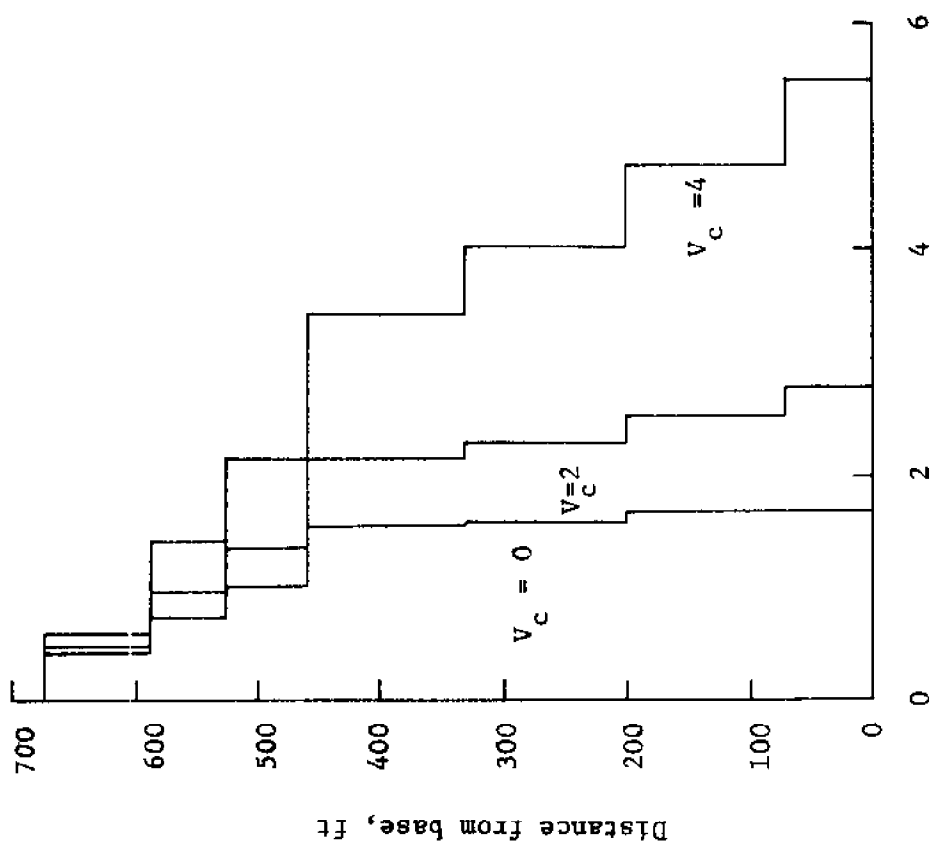


(c) Tower 3

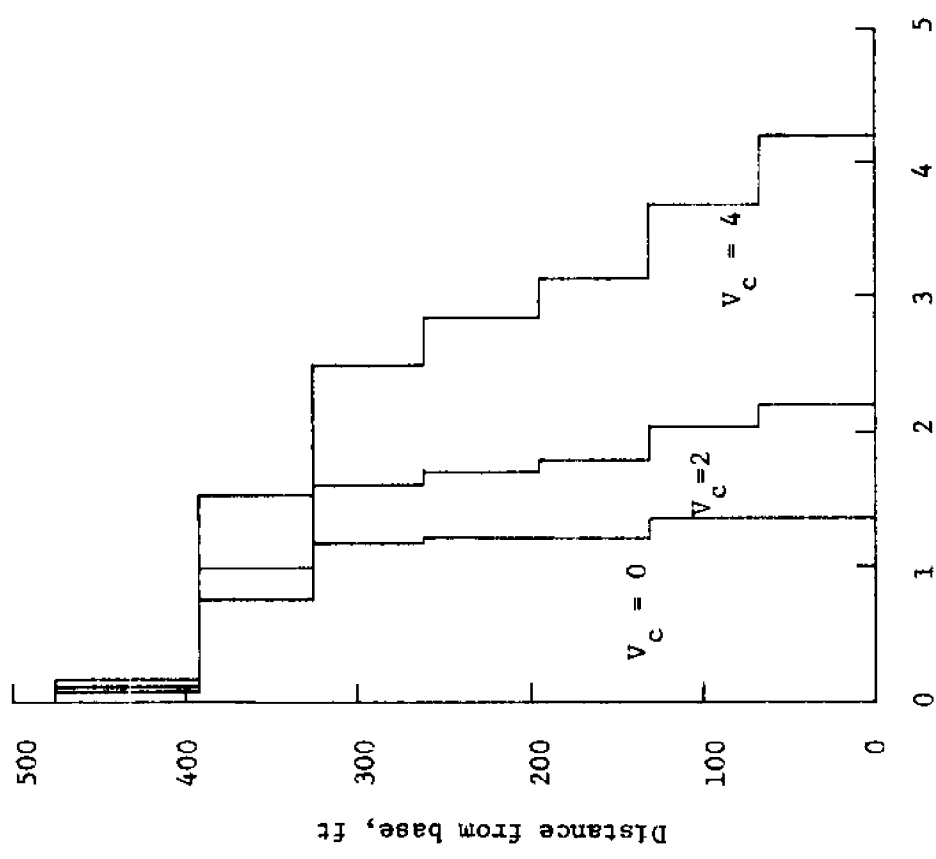


(d) Tower 4

Figure 4.2. Peak displacements: current velocities  $V_c = 0, 2,$  and  $4$  ft/sec;  $50$  ft/sec wind



(a) Tower 1  
Peak shear,  $10^3$  kip



(b) Tower 2  
Peak shear,  $10^3$  kip

Figure 4.3. Peak shears: current velocities  $V_c = 0, 2,$  and  $4$  ft/sec;  $50$  ft/sec wind

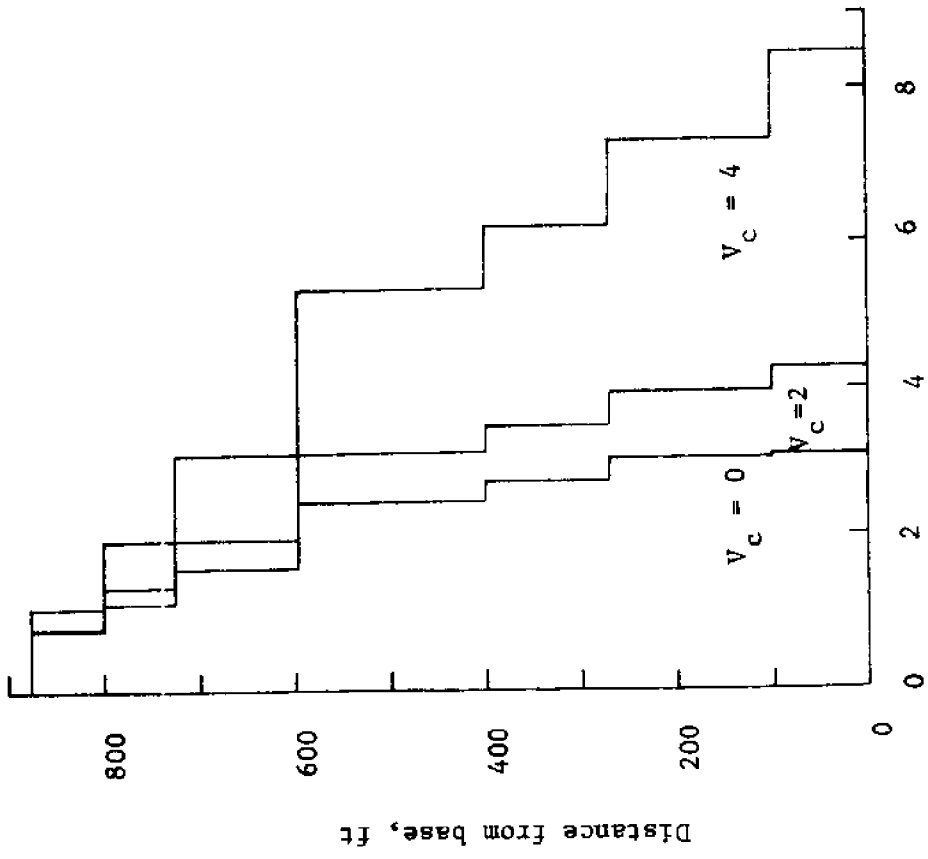
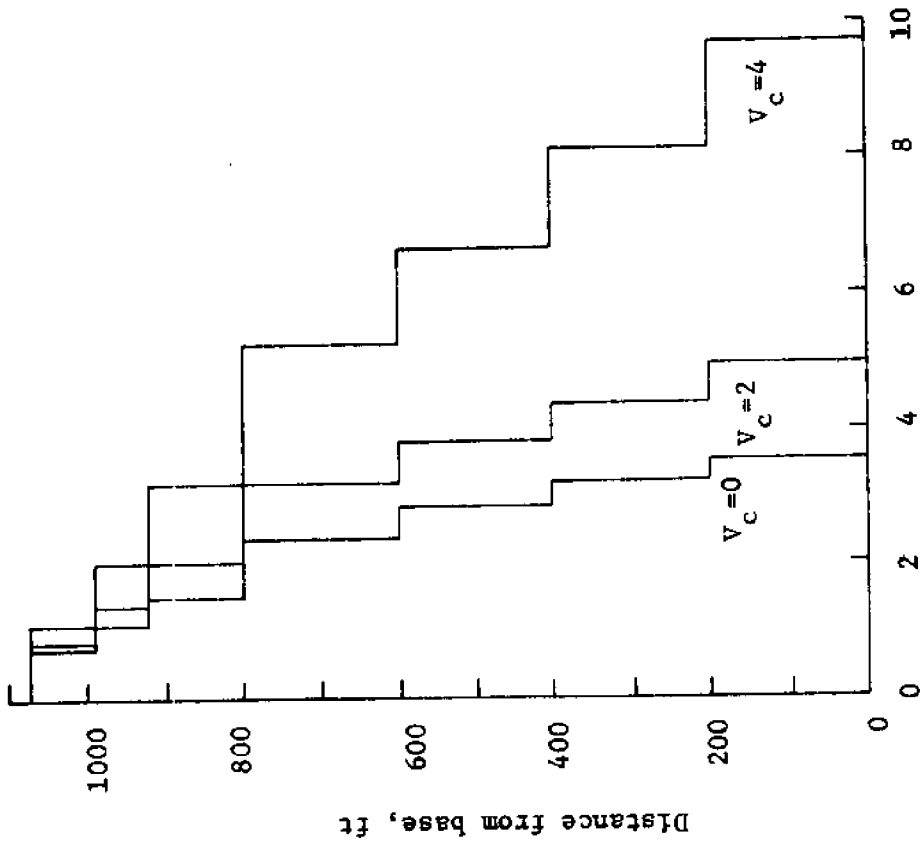
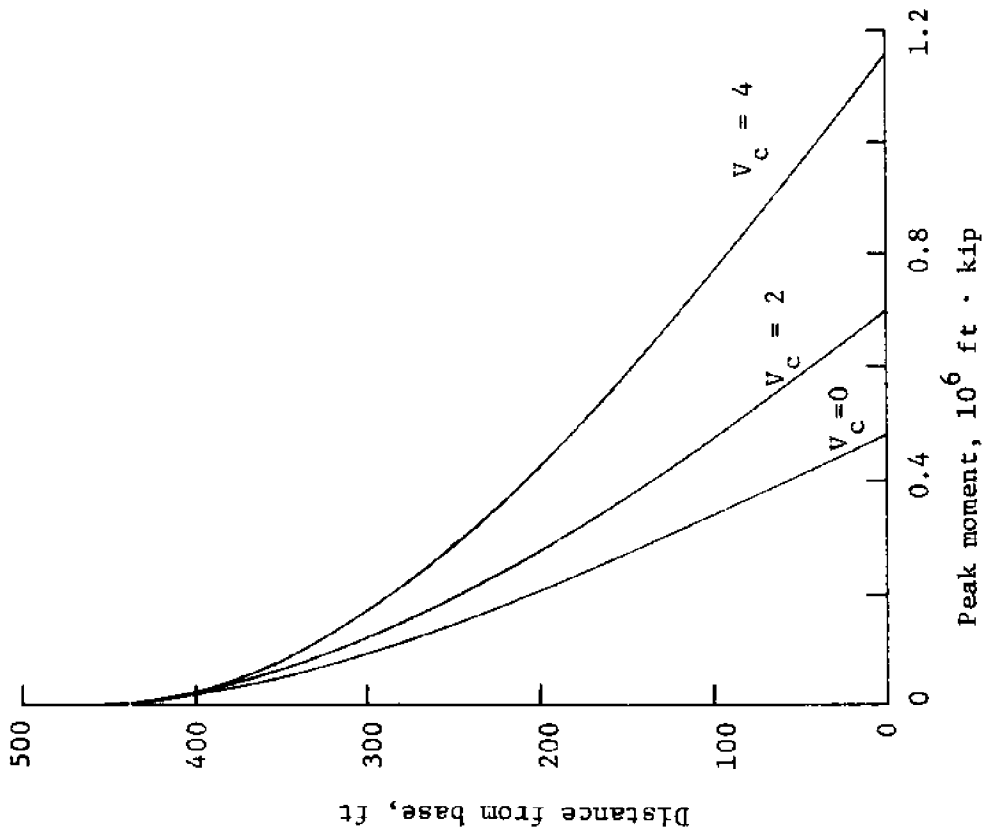
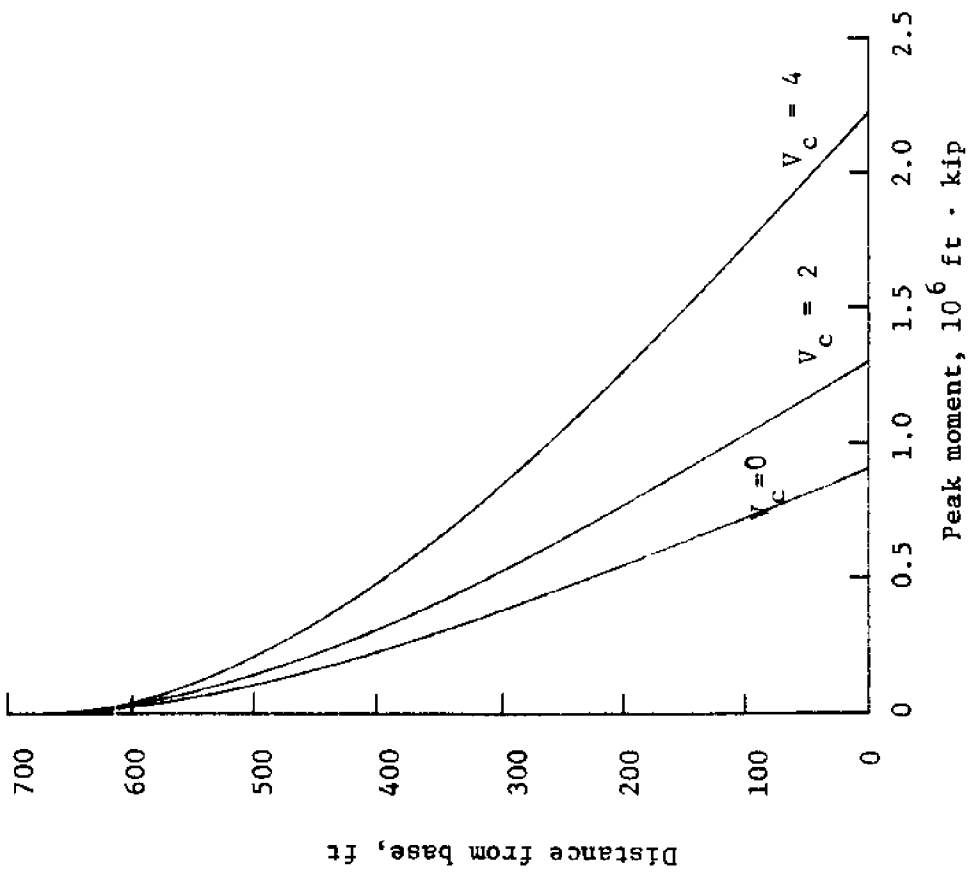


Figure 4.3. Peak shears: current velocities  $V_c = 0, 2, \text{ and } 4$  ft/sec; 50 ft/sec wind

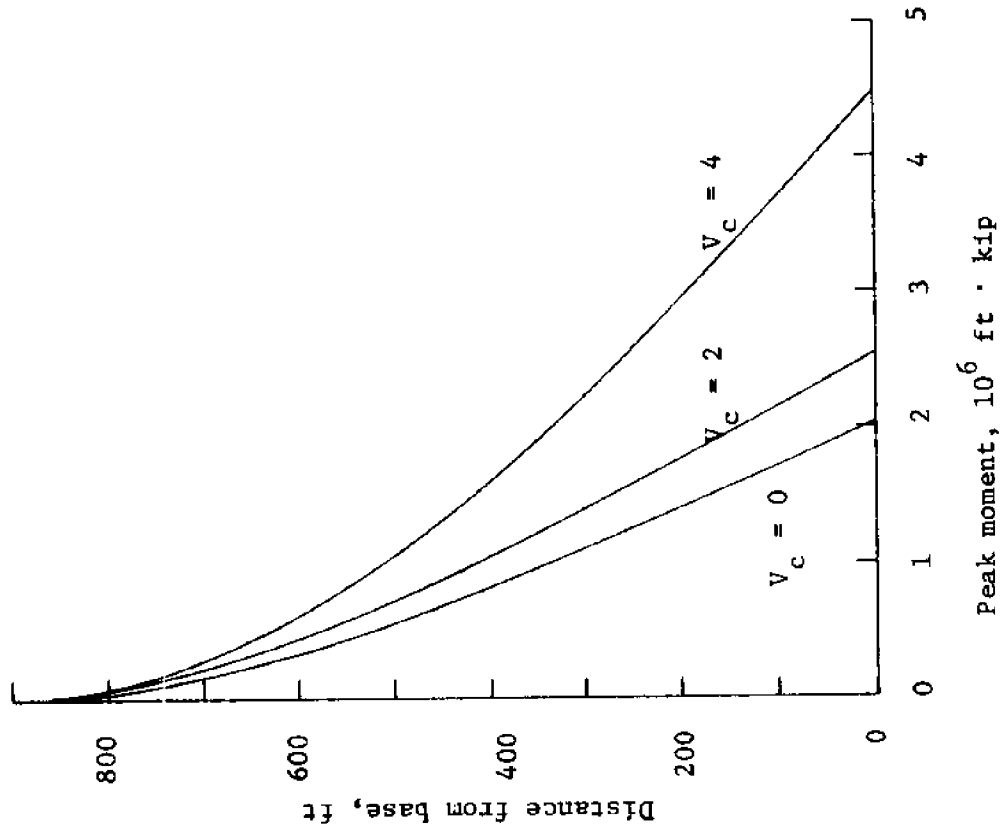


(a) Tower 1

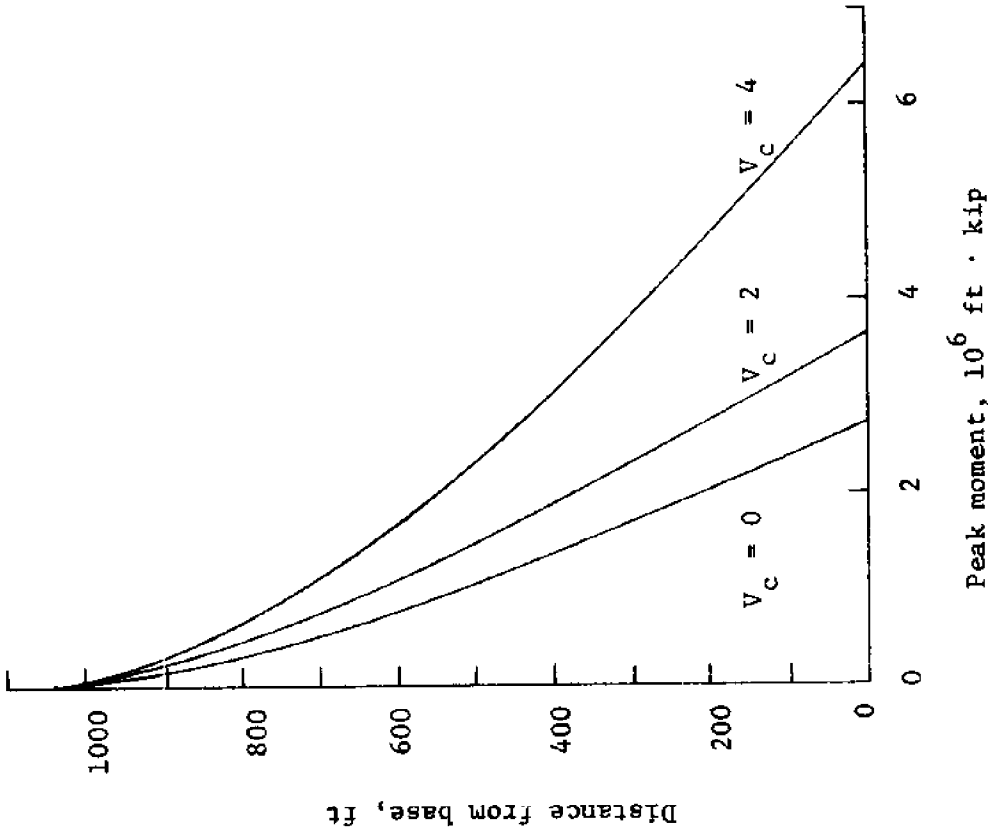


(b) Tower 2

Figure 4.4. Peak moments: current velocities  $V_c = 0, 2, \text{ and } 4$  ft/sec; 50 ft/sec wind



(c) Tower 3



(d) Tower 4

Figure 4.4. Peak moments: current velocities  $V_c = 0, 2, \text{ and } 4$  ft/sec; 50 ft/sec wind

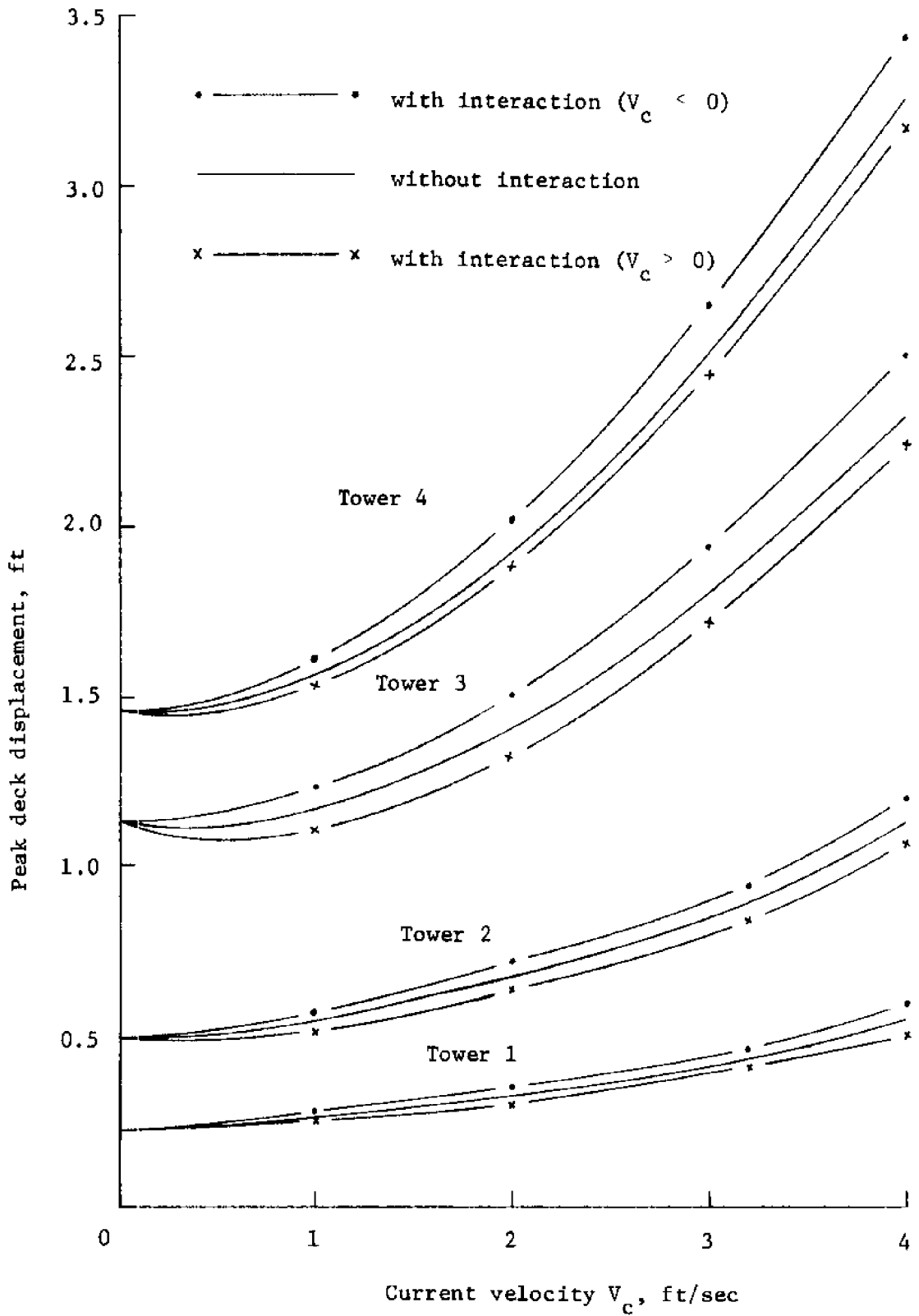


Figure 4.5. Comparison of peak deck displacements of Towers 1,2,3, and 4, with and without wave-current interactions considered; 50 ft/sec wind



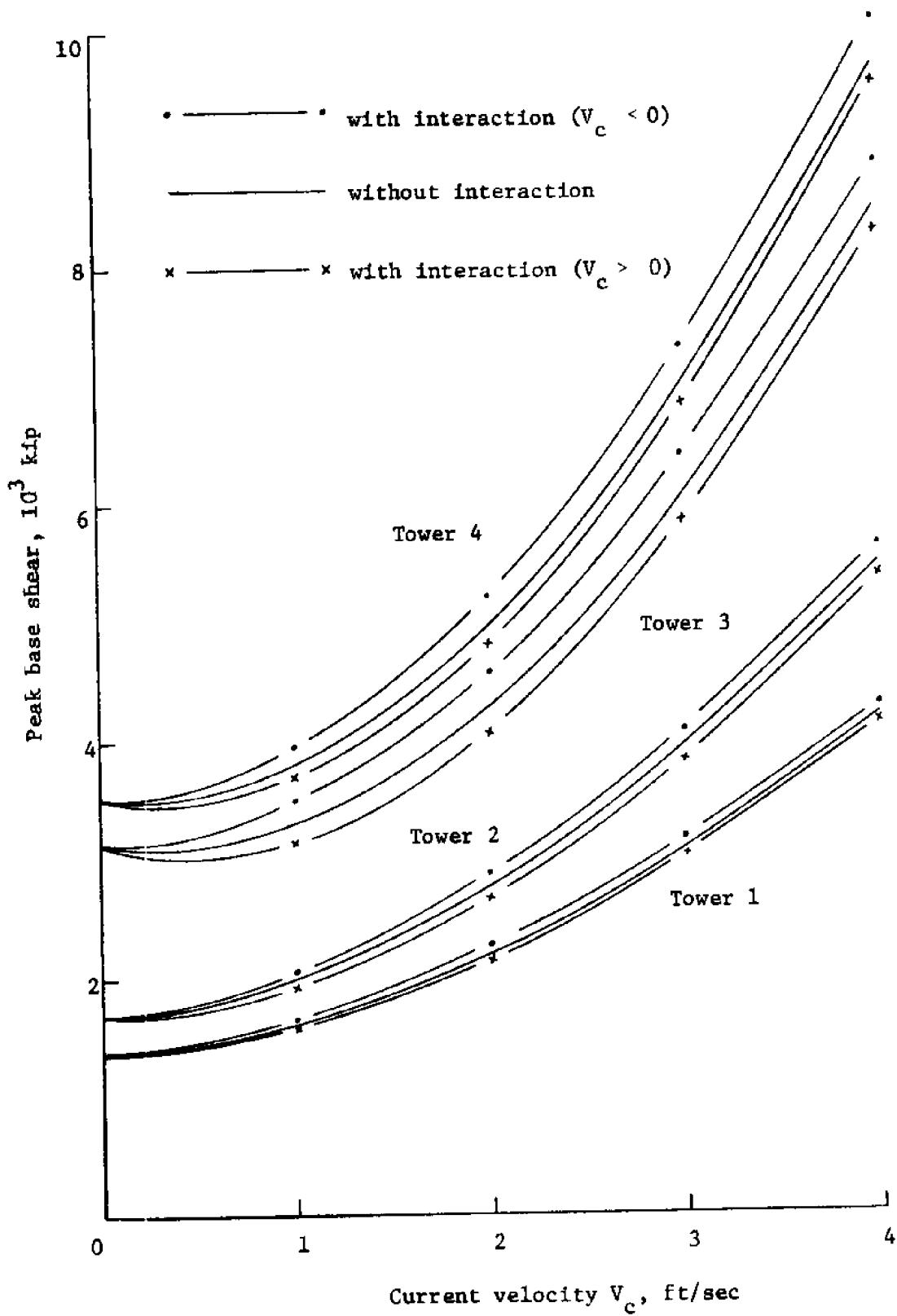


Figure 4.6. Comparison of peak base shears of Towers 1, 2, 3, and 4, with and without wave-current interactions considered; 50 ft/sec wind

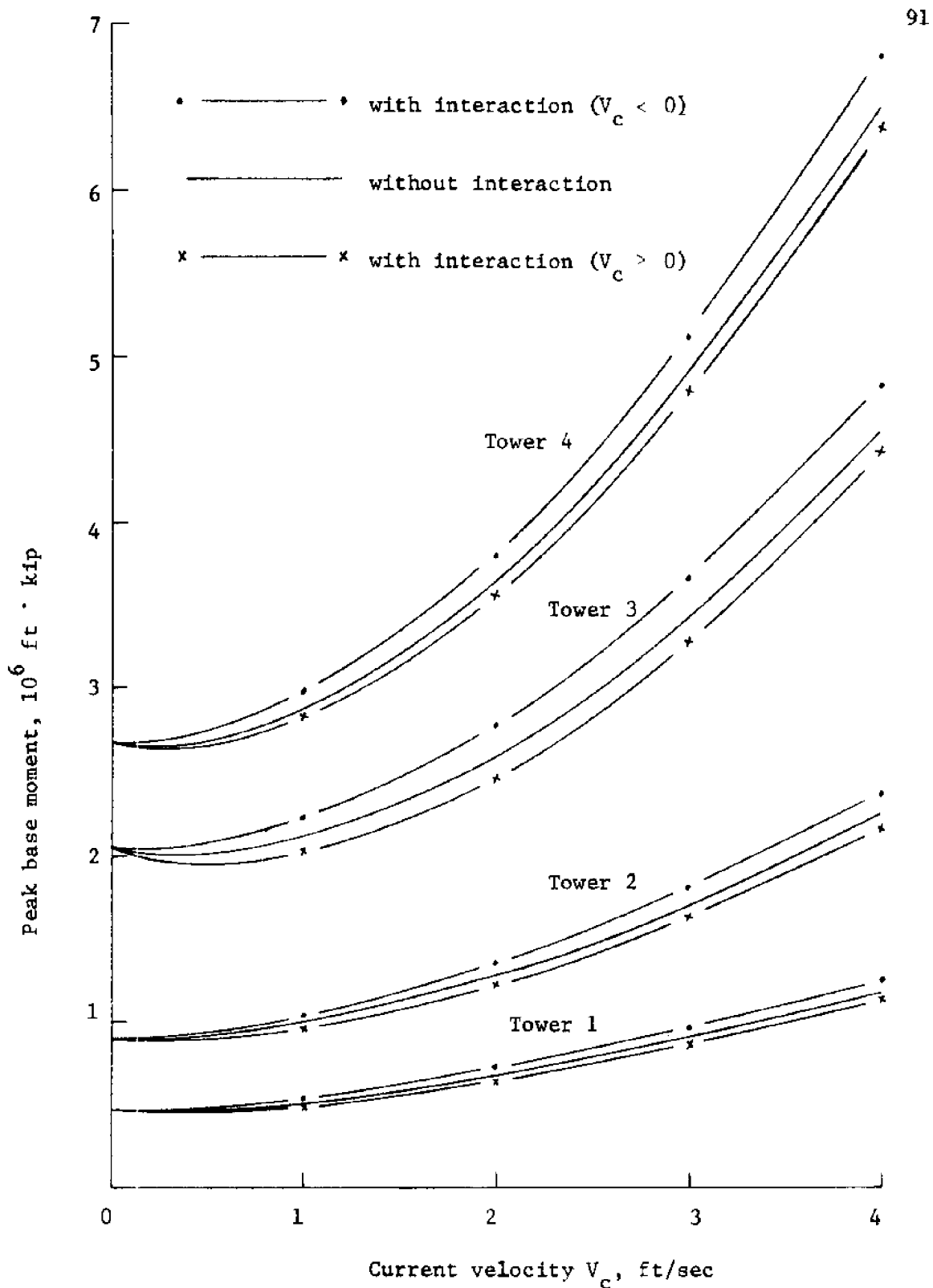


Figure 4.7. Comparison of peak base moments of Towers 1, 2, 3, and 4, with and without wave-current interactions considered; 50 ft/sec

speed  $W = 50$  ft/sec are plotted. The nonlinear characteristics of the response quantities as functions of current speed are clearly noted. It is also seen that the current effects are more important for tall and slender towers than short and rigid towers.

The peak responses of each tower are also computed for mean wind speeds of 75 and 100 ft/sec. The complete results for these two wind speeds are consistent to the results for the 50 ft/sec wind speed case and are therefore not given. Some partial results, however, are presented here so that effects of wind speed on structural responses can be examined. To achieve this purpose, it is convenient to introduce a ratio factor. This ratio factor is defined as the ratio of the peak response at any current velocity to the peak response which would result when no current ( $V_c = 0$ ) exists. Figure 4.8 shows the ratios for the peak deck displacement under wind speeds of 50, 75, and 100 ft/sec, respectively. Similarly, the ratios for the responses of peak base shear and peak base moment are shown in Figures 4.9 and 4.10. It is seen from these figures that the influence of current on structural response diminishes as the wind speed increases.

The results shown above are all calculated without considering wave-current interactions. To study the effect of wave-current interactions on structural response, the peak deck displacement, peak base shear, and peak base moment are again plotted against current speed in Figures 4.5, 4.6, and 4.7 along with the case when wave-current interactions effects are ignored. It is noted that  $V_c > 0$  means

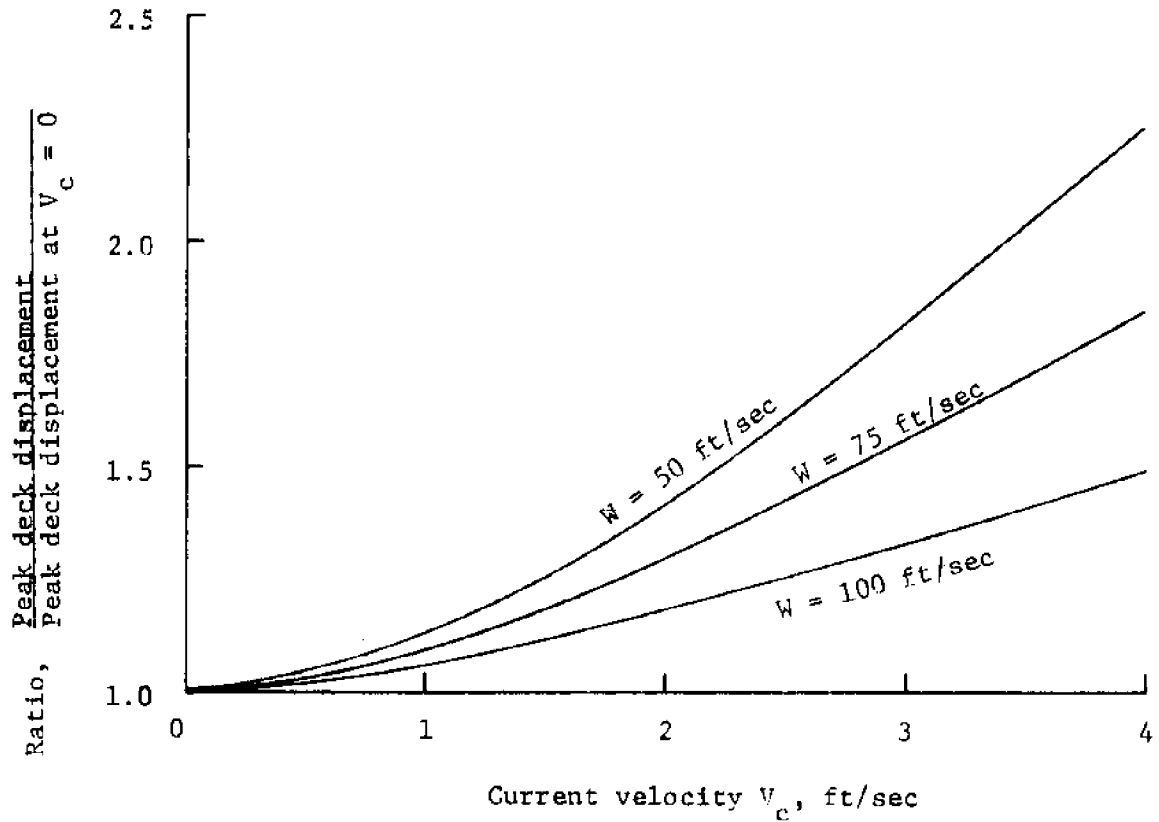


Figure 4.8. Comparison of the ratios of peak deck displacements under wind speeds  $W = 50, 75,$  and  $100$  ft/sec; Tower 1

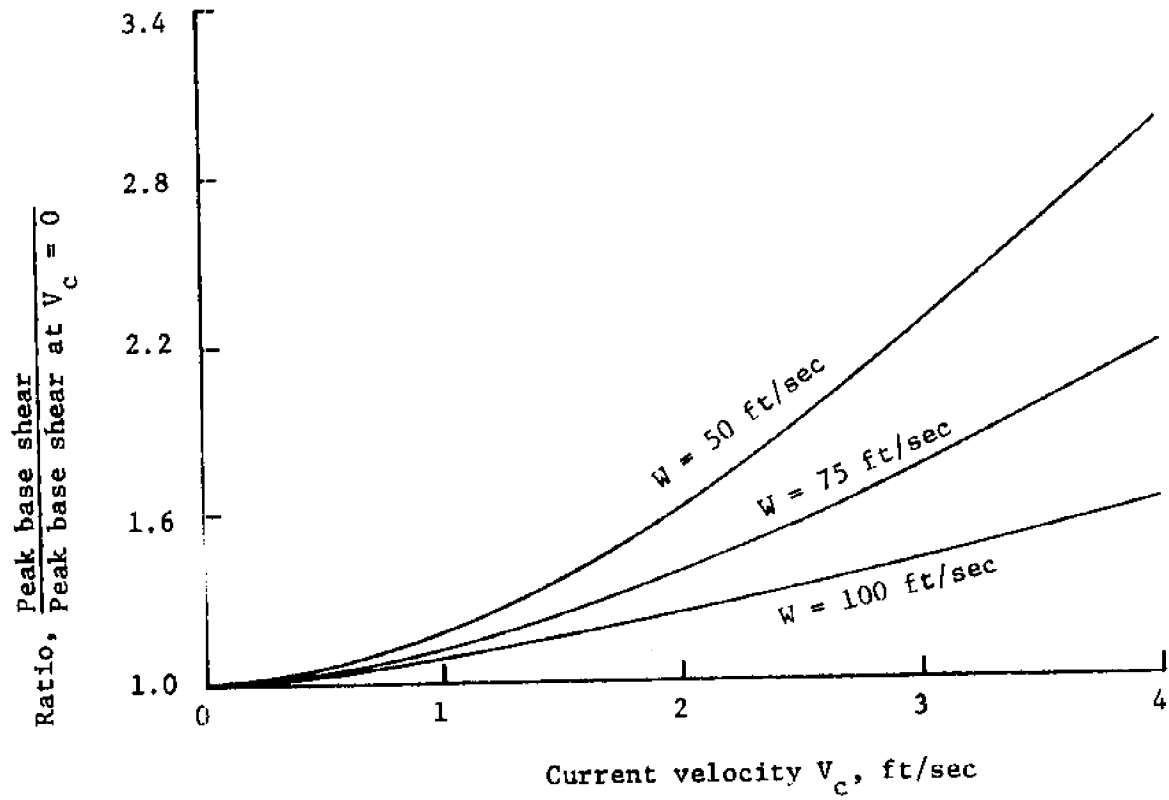


Figure 4.9. Comparison of the ratios of peak base shears under wind speeds  $W = 50, 75,$  and  $100$  ft/sec; Tower 1

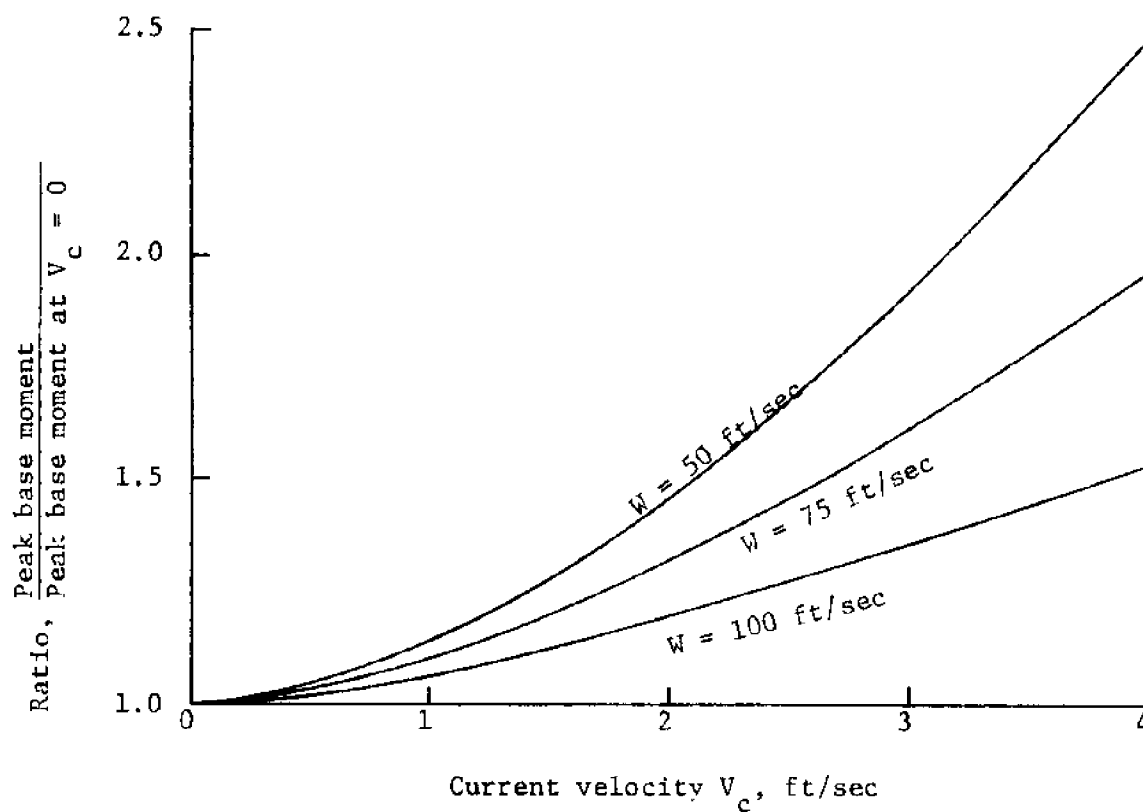


Figure 4.10. Comparison of the ratios of peak base moments under wind speed  $W = 50, 75,$  and  $100 \text{ ft/sec}$ ; Tower 1

current is in the direction of wave propagation, and  $V_c < 0$  means current is opposite to the waves. As would be expected, for a given absolute value of current velocity, the response in the presence of positive current velocity ( $V_c > 0$ ) is smaller than the response when the current velocity is negative ( $V_c < 0$ ). However, the influence of wave-current interactions on structural response is seen to be rather slight, especially when the structure is rigid. This is due to the fact that the fundamental frequencies of the towers studied are much larger than the predominant wave frequencies.

## 5. CONCLUSIONS AND RECOMMENDATIONS

In this study, the dynamic response of offshore structures to combined action of random waves and steady currents is formulated, the equivalent linearization technique is used, and the response characteristics of four towers are examined for various wind speed and current strength with and without the wave-current interactions phenomenon considered. It is noted in the formulation and development of the solution method that, due to the nonlinear nature of drag forces, the drag forces of current cannot be simply added to those of waves. Hence the manner in which currents affect the dynamic response of structures cannot be simply obtained but must resort to numerical case studies. Based on the numerical results, it may be concluded that:

1. The influence of current on structural responses is significant, especially when the structure is tall and flexible; however, the effect is smaller when the wind speed becomes larger.

2. The effect of wave-current interactions on structural response is not very important for the type of towers examined in this study.

It should be noted that the current is assumed to be uniformly distributed along water depth and in deep water. In the future research, it will be a major undertaking to consider the current nonuniformly distributed along the depth of water.



## 6. LIST OF REFERENCES

- American Petroleum Institute. 1975. API recommended practice for planning, designing, and constructing fixed offshore platforms. API RP2A, 6th edition.
- Biggs, J.M. 1964. Introduction to Structural Dynamics, McGraw-Hill, Inc., New York.
- Billington, D.P., Gaither, W.S. and Ebner, A.M. 1966. Analysis of four-legged tower for dynamic loads. J. of the Eng. Mech. Div. Proc. ASCE, Vol. 92, No. EM2, 61-73.
- Borgman, L.E. 1972. Statistical models for ocean waves and wave forces. Adv. in Hydrosiences, 8.
- Cartwright, D.E. and Longuet-Higgins, M.S. 1956. Statistical distribution of the maxima of a random function. Proc. Roy. Soc. A. Vol. 237, 212-232.
- Chakrabarti, S.K. 1971. Discussion, nondeterministic analysis of offshore structures. J. of the Eng. Mech. Div. Proc. ASCE, Vol. 97, No. EM3, 1028-1029.
- Clough, R.W. and Penzien, J. 1975. Dynamics of Structures. McGraw-Hill, Inc., New York.
- Crandall, S.H. and Mark, W.D. 1963. Random Vibration in Mechanical Systems, Academic Press, New York.
- Davenport, A.G. 1964. Note on the distribution of the largest value of a random function with application to gust loading. Proc. Inst. Civil Engrs, Vol. 28, 187-196.
- Dean, R.G. and Aagaard, P.M. 1970. Wave forces: Data analysis and engineering calculation method. J. Petrol. Technol. 22, 368-375.
- Evans, D.C. 1970. Analysis of wave force data. J. Petro. Technol. 22, 339-346.
- Foster, E.T. 1967. Statistical prediction of wave-induced responses in deep-ocean tower structures. College of Eng., Tech. Report HEL-9-14, Univ. of California, Berkeley.
- Gaither, W.S. and Billington, D.P. 1964. The dynamic response of offshore structures to time dependent forces. Conf. on Coastal Eng. Vol. 9, 453-471.
- Harleman, D.R.F., Nolan, W.C. and Honsinger, V.C. 1963. Dynamic analysis of offshore structures. Proc. of 8th Conf. on Coastal Eng. 482-499.

## REFERENCES (continued)

- Huang, N.E., Chen, D.T., Tung, C.C. and Smith, J.R. 1972. Interactions between steady non-uniform currents and gravity waves with applications for current measurements. *J. Phy. Oceanography* 2, 420-431.
- Ippen, A.T. 1966. *Estuary and Coastline Hydrodynamics*. McGraw-Hill, Inc., New York.
- Kinsman, B. 1960. Surface waves at short fetches and low wind speed-- a field study. Chesapeake Bay Inst., The Johns Hopkins Univ., Tech. Report No. 19.
- Kinsman, B. 1965. *Wind Waves*. Prentice-Hall, Inc., Englewood Cliffs, New Jersey.
- Kitaigorodskii, S.A. 1962. Applications of the theory of similarity to the analysis of wind-generated wave motion as a stochastic process. *Bull. Acad. Sci. USSR, Geophys. Ser. 1*, 105-107.
- Krylov, N. and Bogoliubov, N. 1947. *Introduction to Nonlinear Mechanics: approximate asymptotic methods*. Vol. 11. Princeton Univ. Press.
- Lin, Y.K. 1967. *Probabilistic Theory of Structural Dynamics*. McGraw-Hill, Inc., New York, 283-289.
- Longuet-Higgins, M.S. and Phillips, O.M. 1962. Phase velocity effects in tertiary wave interactions. *J. Fluid Mech.* 12, 333-336.
- Longuet-Higgins, M.S. and Stewart, R.W. 1960. Changes in the form of short gravity waves on long waves and tidal currents. *J. Fluid Mech.* 8, 565-583.
- Longuet-Higgins, M.S. and Stewart, R.W. 1961. The changes in amplitude of short gravity waves on steady non-uniform currents. *J. Fluid Mech.* 10, 529-549.
- Malhotra, A.K. and Penzien, J. 1970. Nondeterministic analysis of offshore structures. *J. of the Eng. Mech. Div. Proc. ASCE*, Vol. 96, No. EM6.
- Morison, J.R., O'Brien, M.P., Johnson, J.W. and Schaaf, S.A. 1950. The force exerted by surface waves on piles. *Trans. ASCE* 119, 149-154.
- Myers, J.J., Holm, C.H. and McAllister, R.F. 1960. *Handbook of Ocean and Underwater Engineering*. McGraw-Hill, Inc., New York.
- Nath, J.H. and Harleman, D.R.F. 1969. Dynamics of fixed towers in deep water random waves. *J. of the Waterways and Harbors Div. Proc. ASCE*, Vol. 95, No. WW4, 539-556.

## REFERENCES (continued)

- Papoulis, A. 1965. Probability, Random Variables, and Stochastic Processes. McGraw-Hill, Inc., New York.
- Penzien, J., Kaul, M.K. and Berge, B. 1972. Stochastic response of offshore towers to random sea waves and strong motion earthquakes. Computers and Structures, Vol. 2, 733-755.
- Phillips, O.M. 1960. On the dynamics of unsteady gravity waves of finite amplitude, Part I. J. Fluid Mech. 9, 426-434.
- Phillips, O.M. 1966. The Dynamics of the Upper Ocean. Cambridge Univ. Press, England.
- Pierson, W.J., Jr. 1955. Wind-generated gravity waves. Adv. Geophys. 2, 93-178.
- Pierson, W.J., Jr. and Moskowitz, L.A. 1964. A proposed spectral form for fully developed wind seas based on the similarity theory of S.A. Kitaigorodskii. J. Geophys. Res. 69, 5181-5190.
- Rice, S.O. 1945. Mathematical analysis of random noise, Part III, Bell System Tech. J. 24, 46-156.
- Taylor, G.I. 1955. The action of a surface current used as breakwater. Proc. Roy. Soc. A. Vol. 231, 466-478.
- Trasher, I.W. and Aagaard, P.M. 1970. Measured wave force data on offshore platforms. J. Petro. Technol. 22, 339-346.
- Tung, C.C. and Huang, N.E. 1973. Combined effects of current and waves on fluid force. Ocean Eng. 2, 183-193.
- Tung, C.C. and Huang, N.E. 1973. Influence of wave-current interactions on fluid force. Ocean Eng. 2, 207-218.
- Tung, C.C. and Huang, N.E. 1974. Influence of current on statistical properties of waves. J. of the Waterways, Harbors and Coastal Eng. Div. Proc. ASCE, Vol. 100, No. WW4.
- Ursell, F. 1960. Steady wave patterns on a non-uniform steady fluid flow. J. Fluid Mech. 9, 333-346.
- Wheeler, J.D. 1970. Method for calculating forces produced by irregular waves. J. Petro. Technol. 22, 359-367.
- Whitham, G.B. 1960. A note on group velocity. J. Fluid Mech. 9, 347-352.

## REFERENCES (Continued)

- Whitham, G.B. 1962. Mass, momentum and energy flux in water waves. *J. Fluid Mech.* 12, 135-147.
- Wiegel, R.L. 1964. *Oceanographical Engineering*. Prentice-Hall, Inc., Englewood Cliffs, New Jersey.
- Wilson, B.W. and Reid, R.O. 1963. A discussion of: Wave force coefficients for offshore pipelines. *J. Proc. ASCE*, 61-65.
- Wilson, E.L. and Penzien, J. 1972. Evaluation of orthogonal damping matrices. *International J. for Numerical Methods in Eng.* Vol. 4, 5-10.

## 7 APPENDICES

## 7.1 Structural Damping Matrix

The damping matrix for a structure vibrating in air is generally not known in explicit form. If a numerical analysis with an optimization procedure as explained in Sec. 3.5 is to be made, actual damping coefficients must in some way be determined. In the usual formulation of modal analysis, the damping matrix [C] of Equation (3.3) is selected so that it can be uncoupled in the same way through the generalized coordinate transformation as the mass [M] and stiffness [K] matrices. In order to be sure that the damping coefficients are reasonable, it is advisable to relate these to the percentage of critical damping in each mode. This relation may be established by the following procedure which is originally developed by Wilson and Penzien (1972).

For lumped mass systems the general dynamic equations of motion are

$$[M] \{\ddot{U}\} + [C] \{\dot{U}\} + [k] \{U\} = \{F(t)\} \quad (7.1)$$

where [M], [C], and [K] are the NxN structural mass, damping, and stiffness matrices, respectively, and where {U} and {F(t)} are the corresponding Nx1 displacement and force vectors.

The undamped free vibration mode shapes and frequencies are obtained by solving the equations

$$[K] [\psi'] = [M] [\psi'] [\omega_r^2] \quad (7.2)$$

where  $[\psi']$  is the  $N \times N$  mode shape matrix and  $[\omega_r^2]$  is a  $N \times N$  diagonal frequency matrix containing the squared frequencies  $\omega_r^2$ ,  $r = 1, 2, \dots, N$ .

Introducing the generalized coordinate as  $\{U\} = [\psi'] \{Y\}$ , and assuming the damping matrix to possess the same orthogonality property as does the mass and stiffness matrices, i.e.,

$$\{\psi'_r\}^T [C] \{\psi'_s\} = 0, \quad r \neq s \quad (7.3)$$

where  $\{\psi'_r\}$  and  $\{\psi'_s\}$  are the mode shape vectors of  $r$  and  $s$ , respectively, one can obtain the following uncoupled equations of motion as

$$[M'] \{\ddot{Y}\} + [C'] \{\dot{Y}\} + [K'] \{Y\} = \{F'(t)\} \quad (7.4)$$

where  $[M']$ ,  $[C']$ , and  $[k']$  are the generalized diagonal mass, damping, and stiffness matrices, respectively, and where  $\{F'(t)\}$  is the generalized force vector. The individual terms in these matrices are given by the relations

$$\left. \begin{aligned} M'_r &= \{\psi'_r\}^T [M] \{\psi'_r\} \\ C'_r &= \{\psi'_r\}^T [C] \{\psi'_r\} = 2M'_r \omega_r \zeta_r \\ K'_r &= \{\psi'_r\}^T [k] \{\psi'_r\} = M'_r \omega_r^2 \\ F'_r &= \{\psi'_r\}^T \{F\} \end{aligned} \right\} r=1,2,\dots,N \quad (7.5)$$

where  $\zeta_r$  is the damping ratio of the  $r^{\text{th}}$  mode of vibration,

To establish a numerical damping matrix with assigned damping ratios, first consider the generalized damping matrix  $[C']$  as defined by the second part of Equation (7.5). After simple matrix manipulation, one obtains the relation

$$[C] = [\psi']^{T-1} [C'] [\psi']^{-1} \quad (7.6)$$

where  $[\psi']^{T-1}$  is the inverse of  $[\psi']^T$  and  $[\psi']^{-1}$  is the inverse of  $[\psi']$ . Using the first part of Equation (7.5), it can be shown that

$$[\psi']^{T-1} = [M] [\psi'] [M']^{-1}$$

$$[\psi']^{-1} = [M']^{-1} [\psi]^T [M]$$

Substituting the above equations into Equation (7.6) yields

$$[C] = [M] [\psi'] [M']^{-1} [C'] [M']^{-1} [\psi']^T [M] \quad (7.7)$$

$$\text{or } [C] = [\theta] [\beta] [\theta]^T \quad (7.8)$$

$$\text{where } [\theta] = [M] [\psi'] \quad (7.9)$$

$$\text{and } [\beta] = [M']^{-1} [C'] [M']^{-1} \quad (7.10)$$

It can be seen from Equation (7.5) that the terms of the diagonal matrix  $[\beta]$  are given by

$$\beta_r = \frac{2\zeta_r \omega_r}{M_r'} \quad (7.11)$$

An alternate form of Equation (7.8) is a summation of modal damping matrices  $[C_r]$ , i.e.,

$$[C] = \sum_{r=1}^N [C_r] \quad (7.12)$$

where  $[C_r]$  is a matrix which produces damping in mode  $r$  only and may be calculated directly from the relation

$$[C_r] = \beta_r \{ \theta_r \} \{ \theta_r \}^T. \quad (7.13)$$

Thus, each modal damping ratio  $\zeta_r$  provides an independent contribution to the damping matrix  $[C]$ . Since each of the damping matrices  $[C_r]$  in Equation (7.12) produces damping in a given mode and zero damping in all other modes, the advantage of this procedure is that arbitrary modal damping can be assigned directly. The modal damping ratios should be estimated based on the known physical properties of the system. For steel structures, these ratios are very low, varying from 0.01 to 0.02.



## 7.2 Computation of Shear and Bending Moment

The statistics of displacements at nodal points are usually the first quantities determined from the dynamic analysis presented in Chapter 3. It is convenient to establish a  $N \times N$  force and displacement relation matrix  $[\mu_{QX}]$  so that a  $N \times 1$  internal member force vector  $\{Q\}$  can be related to the  $N \times 1$  displacement vector  $\{X\}$ .

$$\{Q(t)\} = [\mu_{QX}] \{X(t)\} \quad (7.14)$$

The autocorrelation function of the process  $Q$  is defined as

$$[R_{QQ}(\tau)] = E[\{Q(t)\} \cdot \{Q(t + \tau)\}^T] \quad (7.15)$$

Substitution of Equation (7.14) into the above equation gives

$$[R_{QQ}(\tau)] = [\mu_{QX}] [R_{XX}(\tau)] [\mu_{QX}]^T \quad (7.16)$$

Since  $[\mu_{QX}]$  is a matrix of constant elements, Fourier transform of both sides of Equation (7.16) gives

$$[S_{QQ}(\omega)] = [\mu_{QX}] [S_{XX}(\omega)] [\mu_{QX}]^T. \quad (7.17)$$

Thus, the response spectrum of member force is related to the response spectrum of the displacement. The statistics of member force can be obtained in the same way as the general response function  $Z(t)$  are obtained as described in Section 3.6.

An example is given here to demonstrate the construction of the matrix  $[\mu_{QX}]$ . Figure 7.1 shows a transformed independent coordinate system

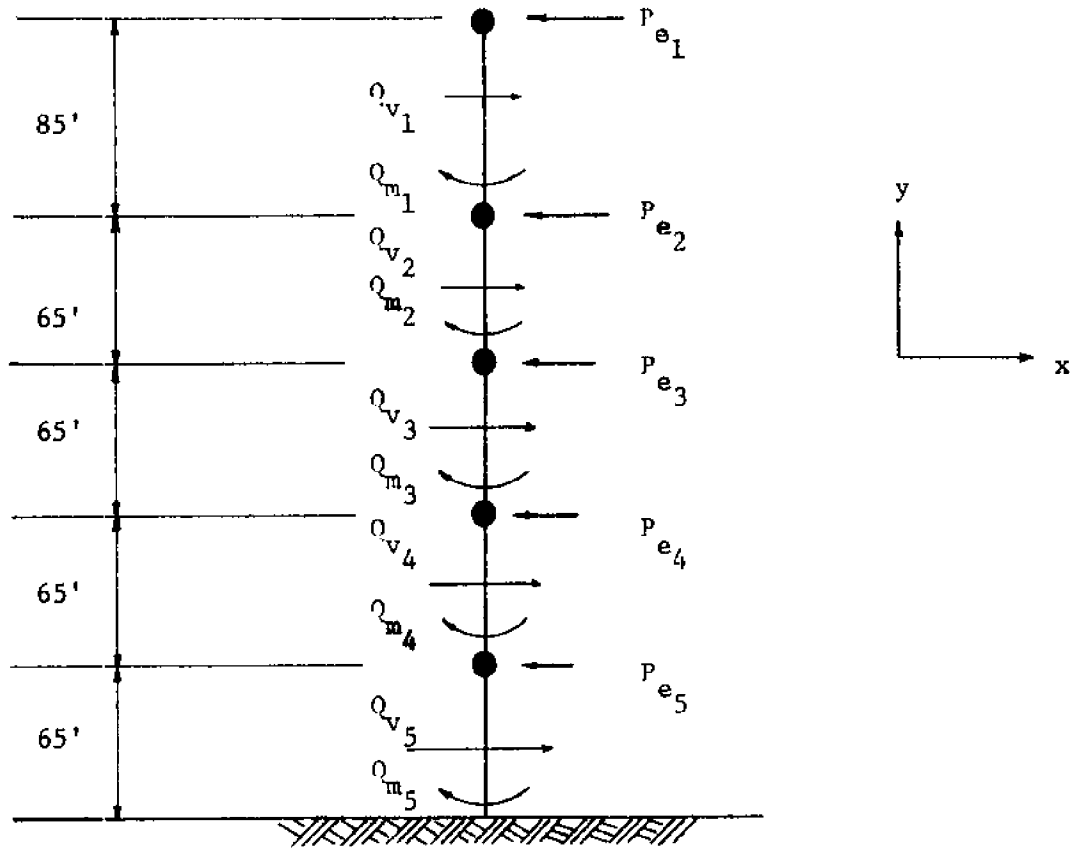


Figure 7.1. Total transverse forces on an independent coordinate system.

which corresponds to the idealized tower in Figure 3.2. If the independent displacement vector  $\{X\}$  is known, then an elastic force vector  $\{P_e\}$  acting at each independent coordinate, can be evaluated by the stiffness relation

$$\{P_e\} = [k^a] \{X\} \quad (7.18)$$

where  $[k^a]$  is the transformed structural stiffness matrix of the independent coordinate.

The total transverse shear vector is indicated by  $\{Q_v\}$ , of which the  $i^{\text{th}}$  element represents the total shear force across a tower section parallel to the ocean floor and at a level between the  $i^{\text{th}}$  and  $(i+1)^{\text{th}}$  coordinate.  $\{Q_v\}$  relates to the elastic force  $\{P_e\}$  through a dimensionless summing matrix

$$[\mu_{Q_v P_e}] = \begin{bmatrix} 1 & 0 & 0 & 0 & 0 \\ 1 & 1 & 0 & 0 & 0 \\ 1 & 1 & 1 & 0 & 0 \\ 1 & 1 & 1 & 1 & 0 \\ 1 & 1 & 1 & 1 & 1 \end{bmatrix} \quad (7.19)$$

which establishes the relation as

$$\{Q_v\} = [\mu_{Q_v P_e}] \{P_e\} \quad (7.20)$$

For example, the total transverse shear  $Q_{v2}$  is the sum of  $P_{e1}$  and  $P_{e2}$ , as can be seen from Figure 7.1.

The shear force and displacement relation matrix  $[\mu_{Q_v X}]$  can thus be constructed by substituting Equation (7.18) into Equation (7.20), which results in

$$[\mu_{Q_v X}] = [\mu_{Q_v P_e}] [k^a]. \quad (7.21)$$

Similarly, the total overturning moment vector is indicated by  $\{Q_m\}$ , of which the  $i^{\text{th}}$  element represents the total bending moment across the section just above the  $i^{\text{th}}$  coordinate. The overturning moment at the base of the structure becomes  $Q_{m_5}$  in this example.

The lever-arm matrix  $[\mu_{Q_m P_e}]$  relates  $\{Q_m\}$  and  $\{P_e\}$  by

$$\{Q_m\} = [\mu_{Q_m P_e}] \{P_e\} \quad (7.22)$$

in which

$$[\mu_{Q_m P_e}] = \begin{bmatrix} 85 & 0 & 0 & 0 & 0 \\ 150 & 65 & 0 & 0 & 0 \\ 215 & 130 & 65 & 0 & 0 \\ 280 & 195 & 130 & 65 & 0 \\ 345 & 260 & 195 & 130 & 65 \end{bmatrix} \quad (7.23)$$

For example, the total overturning moment  $Q_{m_2}$  is the sum of  $P_{e_2}$  acting through a 65-foot arm and  $P_{e_1}$  acting through a 150-foot arm.

Therefore, combining Equations (7.18) and (7.22), one obtains the bending moment and displacement relation matrix  $[\mu_{Q_m X}]$  as

$$[\mu_{Q_m X}] = [\mu_{Q_m P_e}] [k^a]. \quad (7.24)$$

## 7.3 Notation

[A]	transformation matrix
$A_p$	projected area of structural members
$B_k, B_r, B_s$	constant coefficients
[C]	structural damping matrix
$[C]$	optimal damping matrix
$[\bar{C}]$	equals to [C] - [C]
$[C^a]$	transformed optimal damping matrix
$[C_o]$	coupled damping matrix
$[C^*]$	optimized diagonal damping matrix in water
$[C']$	generalized structural damping matrix in air
$C_D$	drag coefficient
$C_M$	inertia coefficient
$[C_r]$	$r^{\text{th}}$ modal damping matrix
$\text{Cov}(X,Y)$	covariance of processes X and Y
D	diameter of cylinder
$E'_j$	error term
$E_i$	error term
$E[\cdot]$	expected (or mean) value of the quantity enclosed.
$\{F(t)\}$	force vector
$\{F'(t)\}$	generalized force vector

$H_k(\omega)$	complex frequency response function for the $k^{\text{th}}$ mode.
$[K]$	structural stiffness matrix
$[K^a]$	transformed structural stiffness matrix
$[K^*]$	generalized structural stiffness matrix in water
$[K']$	generalized structural stiffness matrix in air
$L$	wave length, or number of independent coordinate
$[M]$	structural mass matrix
$[M_s]$	matrix of structural and added mass
$[M^a]$	transformed mass matrix of $[M]$
$[M^*]$	generalized mass matrix in water
$[M']$	generalized mass matrix in air
$N$	number of dependent coordinate, or number of iterative cycles.
$N(\bar{n}_{\max})$	expected number of times that a peak $\bar{n}_{\max}$ is intercepted
$\{P\}$	vector of fluid forces at dependent coordinates
$\{P^a\}$	transformed fluid force vector
$\{P^*\}$	generalized fluid force vector
$P(\cdot)$	probability density function
$Q(\cdot)$	cumulative probability distribution function
$\{Q\}$	internal member force vector
$\{Q_v\}$	total transverse shear vector
$\{Q_m\}$	total overturning moment vector
$R_{XY}(\tau)$	cross-correlation function of processes X and Y

$S_{XY}(\omega)$	cross-spectral density function of processes X and Y
$S_{\eta\eta}(\omega)$	one-dimensional wave spectrum
T	wave period, or storm duration, or matrix transposition operation.
U(t)	structural nodal displacement
$\dot{U}(t)$	structural nodal velocity
$\ddot{U}(t)$	structural nodal acceleration
$\dot{V}(t)$	fluid particle velocity of wave motion
$\ddot{V}(t)$	fluid particle acceleration of wave motion
$V_c$	current velocity
W	mean wind speed
[W]	constant coefficient matrix in equation (3.83)
X(t)	displacement of independent coordinate, or a general random process
$\dot{X}(t), \ddot{X}(t)$	first and second derivatives of generalized coordinate, respectively.
Y(t)	generalized coordinate, or a general random process
$\dot{Y}(t), \ddot{Y}(t)$	first and second derivatives of generalized coordinate, respectively
Z(t)	response function

a	wave amplitude, or constant
b	constant
d	water depth
$dF(t)$	fluid force on element of cylinder
$\text{erf}(\cdot)$	error function
$f(t)$	effective forcing function
$f(\omega)$	arbitrary function
g	gravitational acceleration
$h_k(t)$	unit impulse response function for the $k^{\text{th}}$ mode
i	$i^{\text{th}}$ node, or a subscript represents the $i^{\text{th}}$ coordinate, or an imaginary unit
j	$j^{\text{th}}$ node, or a subscript represents the $j^{\text{th}}$ coordinate
k	generalized coordinate for mode k, or a subscript
m	dummy index
n	dummy index



r	dummy index, or subscript for the $r^{\text{th}}$ mode
$\dot{r}$	relative velocity between fluid particle velocity of wave motion and nodal velocity of structure
s	a subscript for the $s^{\text{th}}$ mode
t	time
u	dummy variable
v	dummy variable
x	horizontal coordinate, in direction of wave propagation
y	vertical coordinate, with origin at mean water level
z	horizontal coordinate, perpendicular to x, in the lateral direction

$\alpha$	constant
$\beta$	constant
$[\beta]$	matrix used in Equation (7.10)
$\delta(\omega)$	Dirac delta function
$\zeta_r$	modal damping ratio in air for the $r^{\text{th}}$ mode
$\eta$	surface displacement from mean water level
$\bar{\eta}$	variable
$\eta^t$	dummy variable
$\theta_1, \theta_2$	dummy variables
$[\theta]$	matrix used in Equation (7.9)
$\kappa$	wave number
$\lambda$	wave phase angle
$[\mu_{QX}]$	force and displacement relation matrix
$\nu$	quantity defined in Equation (3.100)
$\xi_k$	the $k^{\text{th}}$ modal damping ratio for optimized diagonal damping matrix
$\rho$	density of sea water
$\sigma_Z$	standard deviation of $Z$
$\sigma_Z^2$	variance of $Z$

$\tau$	time lag
$\phi$	velocity potential
$[\psi]$	matrix of mode shapes for structure in water
$[\psi']$	matrix of mode shapes for structure in air
$\{\psi_k\}$	the $k^{\text{th}}$ mode shape vector
$\psi_{ik}$	the $i^{\text{th}}$ element of the $k^{\text{th}}$ mode shape vector $\{\psi_k\}$
$\omega$	wave frequency, or frequency of the complex frequency response function
$\omega_k$	natural circular frequency of the $k^{\text{th}}$ mode
$\omega_{dk}$	damped natural circular frequency of the $k^{\text{th}}$ mode

## LIST OF RELATED WORK

1. Tung, C. C. and Huang, N. E. 1972. Wave-current force spectra. Report No. 72-2.
2. Tung, C. C. and Huang, N. E. 1973. Influence of current in some statistical properties of waves. Report No. 73-3.
3. Tung, C. C. 1974. Statistical properties of kinematics and dynamics of a random gravity wave field. Report No. 74-2.
4. Pajouhi, K. and Tung, C. C. 1975. Statistical properties of fluid motion and fluid force in a random wave field. Report No. 75-1.
5. Radwan, A. M., Huang, N. E. and Tung, C. C. 1975. Wave-current interactions in water of variable depth. Report No. 75-3.
6. Tung, Chi Chao and Huang, Norden E. 1973. Peak distribution of random wave-current force. Sea Grant Publication, UNC-SG-73-17.
7. Tung, C. C. 1974. On the statistical properties of wave force. Sea Grant Publication, UNC-SG-74-11.

Items 1 to 5 are available from the Center for Marine and Coastal Studies, 1204 Burlington Laboratories, North Carolina State University, Raleigh, North Carolina 27607. Items 6 and 7 are available from University of North Carolina Sea Grant Program, 1235 Burlington Laboratories, North Carolina State University, Raleigh, North Carolina 27607.

